Optimization of Droop Control Based Islanded Microgrid System under Load Variation

by

Nafiz Imtiaz Khan

MASTER OF SCIENCE

IN

ELECTRICAL AND ELECTRONIC ENGINEERING

Department of Electrical and Electronic Engineering
Islamic University of Technology (IUT)
Board Bazar, Gazipur-1704, Bangladesh
October, 2019.

©2019 Nafiz Imtiaz Khan
All Rights Reserved.

Certificate of Approval

The thesis titled, **"Optimization of Droop Control Based Islanded Microgrid System under Load Variation"** submitted by Nafiz Imtiaz Khan, St. No. 152622 of Academic Year 2015-16 has been found as satisfactory and accepted as partial fulfillment of the requirement for the Degree of Master of Science in Electrical and Electronic Engineering on October 30, 2019.

BOARD OF EXAMINERS:

.....

1.(Signature) Chairman
Name: Dr. Ashik Ahmed (Supervisor)
Designation: Associate Professor
Address: EEE Dept., IUT, Gazipur-1704, Bangladesh.

.....

2.(Signature) Member
Name: Prof. Dr. Md. Ruhul Amin (Ex-Officio)
Designation: Professor and Head
Address: EEE Dept., IUT, Gazipur-1704, Bangladesh.

.....

3.(Signature) Member
Name: Dr. Khondokar Habibul Kabir
Designation: Associate Professor
Address: EEE Dept., IUT, Gazipur-1704, Bangladesh.

.....

4.(Signature) Member
Name: Prof. Dr. Md. Fayzur Rahman (External)
Designation: Professor and Head
Address: EEE Dept., Green University, Dhaka.

Declaration

I hereby declare that this dissertation entitled **Optimization of Droop Control Based Islanded Microgrid System under Load Variation** was carried out by me for the degree of Master of Science in Electrical and Electronic Engineering, M.Sc. (Engg.) in EEE, under the guidance and supervision of Associate Prof. Dr. Ashik Ahmed, Islamic University of Technology, Gazipur, Dhaka, Bangladesh.

I also declare that this submission is my own work and to the best of my knowledge and belief, it contains no material previously published or written by another person, nor material which to a substantial extent has been accepted for the award of any other degree or diploma at EEE, IUT or any other educational institution, except where due acknowledgement is made in the thesis. Furthermore, the intellectual content of this thesis is the product of my own work, except to the extent that assistance from others in the project's design and conception or in style, presentation and linguistic expression is acknowledged.

Author

_____

Nafiz Imtiaz Khan
Student Id: 152622
Date: _____

Dedication

My respected Parents and Teachers

"Without whom none of my success would be possible"

Table of Contents

List of Figures

List of Tables

List of Abbreviations

Abbreviation	Meaning
DG	Distributed Generator
ES	Energy Source
APC	Active Power Conditioner
DERs	Distributed Energy Sources
PV	Photo voltaic
SVPWM	Space Vector Pulse Width Modulator
PLL	Phase Locked Loop
PI	Proportional Integral
PCC	Point of Common Coupling
GA	Genetic Algorithm
PSO	Particle Swarm Optimization
GWO	Grey Wolf Optimization
ACO	Ant Colony Optimization
LP	Linear Programming
NLP	Non Linear Programming
DP	Dynamic Programming
ES	Exhaustive Search
BF	Brute Force
IP	Interior Point
RWS	Roulette Wheel Selection
SUS	Stochastic Universal Sampling
KKT	Karush-Kuhn-Tucker
RAM	Random Access Memory

Nomenclature

Symbol	Meaning
θ	Angle difference between d-q frame of each inverter and common D-Q reference frame
δ	Phase angle
P, Q	Real, reactive power output from inverter
ω_c, ω_{cPLL}	Cut off frequency of the filters
v_{od}, v_{oq}	d,q axis output voltage of inverter
i_{od}, i_{oq}	d,q axis output voltage of inverter
ω_n, ω^*	Nominal frequency, reference frequency from droop
m, n	Droop co-efficient
$V_{oq,n}, V^*_{oq}$	Nominal voltage, reference voltage from droop
$v_{od,f}$	d axis filtered output voltage
ϕ_{PLL_i}	Input to the PLL
$k_{p,PLL}, k_{i,PLL}$	Integral and proportional gain of PLL
ω_{PLL}	Actual system frequency measured by PLL
$k_{pv,dq}, k_{iv,dq}$	Proportional,integral gain of voltage controller
ϕ_d, ϕ_q	Input to the voltage controller
i^*_{ld}, i^*_{lq}	Commanded filter inductor current
i_{ld}, i_{lq}	Measured filter inductor current
$k_{pc,dq}, k_{ic,dq}$	Proportional,integral gain of current controller
γ_d, γ_q	Input to the current controller
v^*_{id}, v^*_{iq}	Commanded voltage at the input of filter inductor
R_d	Damping resistor
i_{loadD}, i_{loadQ}	D, Q axis load current
i_{lineD}, i_{lineQ}	D, Q axis line current

Acknowledgment

First and foremost all the praise is paid to the Almighty, the most kind Allah for keeping alive and able, giving the knowledge, ability to think and for helping to successfully finish the thesis, with His inexhaustible kindness.

The author expresses wholehearted gratitude, indebtedness and appreciation to the honorable teacher and respected supervisor, Dr. Ashik Ahmed, Associate Professor, Department of Electrical Electronic Engineering, Islamic University of Technology (IUT), Board Bazar, Gazipur, Bangladesh, for the patient guidance, encouragement and advice throughout the period of the research work. The author is extremely lucky to have a supervisor who cared much about the work and responded to any questions promptly. In addition to being an admirable supervisor, he is a man of principles and has immense knowledge of research in general and his subject in particular. His commitment to excellence has been motivational now and in the future career.

The author would like to extend deep sense of gratitude to all of the respective teachers of the Department of Electrical Electronic Engineering, IUT, for their valuable suggestions, cooperation and best wishes. Thanks to all friends and colleagues for their support throughout the research work.

Finally, the author acknowledges that the work would be almost impossible to carry out successfully without inspiration from parents because of their moral support and optimistic encouragement throughout the research work.

Abstract

In an islanded microgrid, the system operating frequency and voltage is governed by the so-called droop based relationships due to the absence of conventional slack bus which necessitates incorporation of various controllers. The parameters of the controllers play a vital role ensuring stable and reliable supply of power to the connected consumers. In this work, a two-stage optimal tuning procedure is presented for controlling a two inverter based microgrid system under isolated mode of operation. At first, the key control parameters influencing the transient response of the system are identified. Next, an eigenvalue based optimization process has been adopted in which three population based search algorithms: Genetic Algorithm (GA), Particle Swarm Optimization (PSO) algorithm and Grey Wolf Optimization (GWO) algorithm are used in order to find out the initial range of controller parameters in an unbounded search space. In the second stage of optimization, Exhaustive Search (ES) and Interior Point (IP) based search algorithms are adopted to obtain the optimized value within the bounds provided by the population based search algorithms. At the end, time domain and comparative analyses among these combinational algorithms are presented to determine the most effective algorithm for the studied islanded microgrid system. The simulation results show that the performance of GA is inferior compared to other two algorithms: PSO and GWO. GWO provides better optimization in comparatively lesser amount of time than PSO in the first stage and in the second stage, IP yields better optimization than ES. Consequently, the two stage optimization process suggests that GWOIP could be chosen for the design problem.

Chapter 1

Introduction

In this chapter, a brief overview of the thesis has been provided along with the background and the motivation behind the work. Contemporary and previous research works regarding microgrid modeling and dynamic characteristic, control strategies, parameter's effect on stability and optimization as well as the shortcomings in those works have also been identified in this chapter. In section 1.1, background behind the research work has been discussed. Motivation of the work has been illustrated in section 1.2. Section 1.3 presents concurrent and previous works related to the thesis work and section 1.4 illustrates the research gap in those works . Thesis overview and objective have been discussed in section 1.5. Finally, the chapter comes to an end with the thesis organization in section 1.6.

1.1 Background

Nowadays, power system structure has been experiencing significant changes due to a lot of challenges such as load growth, new environmental policy with a demand of CO_2 emission reduction, and the economic stresses of marketplace. This has led to the increase of interest in the incorporation of the renewable energy sources at the distribution level. Microgrids are little electrical distribution system comprised of multiple distributed sources of generation and storage that connects multiple customers through the interface of power electronic inverters [1]. Microgrid can operate in two modes: islanded mode and grid connected mode [2]. In the grid connected mode, the control of the inverter is required to make the microgrid capable of regulating the active and reactive output currents, ensuring high power quality levels and achieving relative immunity to grid perturbation [3]. In the autonomous mode, the inverter is controlled with the predefined values of voltage and frequency according to specific control strategy [4] to feed the load. However, due to negligible physical inertia [5], they also make the system more prone to oscillation resulting from disturbances in the network [6]. Therefore, one of the significant issues in the consistent and reliable microgrids operation is small-signal stability. In either mode of operation, the stability of microgrids stability is very essential which is affected

by different parameters. In the autonomous mode operation, the microgrids stability can be highly influenced by controller parameters along with power sharing coefficients. In the grid connected mode of operation, filter and controller parameters are the key factors influencing the stability of microgrid. Generally, careful selection of the controller, filter, and power sharing parameters maintains power quality within the regulated range and enhances the system performance against load variation and unexpected disturbances. It is quite essential to select different parameters of controller or filter in order to maintain power quality within the regulated range and enhance the dynamic performance of microgrid system. In traditional power systems, stability analysis is well established and there are models for the different frequency ranges (or time horizons) of possible concern including appropriate characteristics. The characteristics have been well established on the base of decades of experience. As a result, there are various order standard models of synchronous machines, governors and excitation systems and they capture the significant modes for specific classes of problem. These types of models do not yet exist for microgrid which make complete small-signal dynamic modeling for microgrid difficult because of complex and diverse control strategies of DGs. As a result, small-signal modeling and performance analysis of microgrid have gradually become one of the concerning issues.

1.2 Motivation

Nowadays, microgrid, comprised of small generation unit, energy storage and load has gained popularity in the power engineering society [7] to meet up the growing demand of electrical energy. The concept of microgrid imposes significant control and management challenges compared to traditional centralized generating station [8]. Besides, at present microgrid needs to supply a wide variety of loads: static load, dynamic load, abnormal load [9]. This causes decrease in system damping property and makes the system more prone to oscillation [10]. Different types of load sharing strategies have been applied so far in microgrid [11]. Among different control strategies, droop control method is widely accepted as it does not require critical communication link for the coordination among DGs [12]. The droop controller mainly controls the real and reactive power sharing by controlling voltage and frequency magnitude [13]. But inverter interfaced droop controlled DG have relatively dynamic and complex properties. Moreover, poorly damped low frequency modes are mainly associated with droop controllers [4] and are very susceptible to instability. Besides, for regulation of voltage and current, proportional-integral (PI) based voltage and current controllers are widely used in microgrid [14]. PI controller is effective for inverter based microgrid system. But unwise selection of the controller parameters may significantly affect the performance and stability of microgrid and it is imperative to improve stability and transient behavior of microgrids to allow more effective utilization of the generation units without violating operational limits [15]. Thus, optimum selection of controller

parameters is necessary.

1.3 Literature review

The concept of microgrid was developed with an aim of integrating renewable energy sources in electricity generation and supply the surplus energy in the utility grid. Several microgrid models and control strategies have been developed so far to improve the stability of microgrid. In this section, previous works regarding microgrid modeling, effect of microgrid parameters, control strategies and optimization have been presented.

1.3.1 Microgrid modeling and dynamic characteristic

Sophisticated mathematical model depicting dynamic characteristics of microgrid is required to obtain an efficient control and power management strategy. However, because of the complexity inherent in higher order models, many studies have been performed based on various simulation software packages such as Power Systems Computer Aided Design (PSCAD)/Electromagnetic Transients including DC (EMTDC) and MATLAB/Simulink/Simpowersystem to select appropriate control parameters on a trial and error basis [16, 17]. These works finds that modeling based on simulation serves as a very powerful tool in investigating microgrid behavior. However, models based on simulation fail to provide an extensive prediction of all types of microgrid scenarios resulting in instability and poor power quality.

To this end, dynamic small signal model of a microgrid has been developed to give a more accurate representation of microgrid by optimizing the proper control strategies [18]. In that work, individual model representing each distributed generation source is at first obtained in its local dq0 reference frame and to form an integrated model of microgrid system, all the DGs' individual models are then transformed to the global dq0 frame. Small signal modeling and steady state analysis of an autonomous microgrid was investigated in [19]. A mathematical model for the microgrid was developed. Small signal results were verified with a time domain simulation. Howerver, the dynamics of the phase locked loop (PLL) were not discussed. A more detailed small-signal modeling was done by the authors in [20], in which the autonomous system was built with both conventional and electronically interfaced DGs' to study the system's stability and dynamic behavior. Besides, filter dynamics were ignored, though, which are an essential part of electronically interfaced DG systems. Although the filter components were included in [21] for modeling an inverter, line parameters, an important aspect of the network, were ignored for parallel inverter operation. A model including distribution line and filter dynamics was presented in [22], but only for a single inductor based filter, which does not always guarantee stability. A method for modeling a microgrid with all network components was

presented in [4], but the procedure for obtaining the small-signal model was rather complex. Also, the damping resistors of the LCL filters, which play a very important role in ensuring stability of the system, were ignored. Additionally, the model was designed such that a load current transient was used as a perturbation input, while in practice a change in impedance was observed during the transient analysis. This improper perturbation technique resulted in a significant reactive power mismatch between the experimental results and the results obtained from the model. Another small-signal model was derived in [23]. Again, the model did not include the passive damping properties of the filter. Results from this model were not validated against those from a hardware experiment. The models from the last two works did not include the dynamics of the PLL to verify system frequency during load perturbation. A small signal model was developed in [24] which included the PLL dynamics and a damping resistor in the filter. Once again, the model was not validated against the experimental results. Also, the input matrix was defined in such a way that it did not reflect the load perturbation in the system.

1.3.2 Microgrid control strategies

Generally, the control strategies associated with microgrid can be categorized in two distinct levels including primary (local) control level and secondary (power management) control level [25].

Primary control, which is also known as local or internal control, is simply based on local measurements. In this local control level, no communication is needed [26]. The deviation in the frequency and voltage of microgrid depends on the discrepancy between active and reactive power, the characteristics of load, and the droop model of the DG's. Therefore, f/V droop control and inverter output control strategies are the general methods being utilized in the primary level of control [27].

Unlike the primary control, the secondary control level approaches strongly need fast and reliable communication systems. Two control approaches: centralized and decentralized can be utilized in secondary control level [28]. Non model based fuzzy and neural network controllers [29, 30] and model based predictive controllers are the examples of centralized control approaches. Multi agent based control approaches [31, 32] are the examples of decentralized control methods in secondary control level of microgrid. Also, shaving of peak load, frugal discharge, state of charge set point, full power/minimum run time, and ideal predictive dispatch strategies [33] are other examples of secondary level control algorithms that have been proposed based on the main power management strategies.

1.3.3 Parameter's effect on microgrid stability

Stability is one of the major issues of microgrid due to backward flow of power from DGs', local oscillations, transient microgrid behavior, severe deviation of frequency in islanded/autonomous operation, and uncertainties associated with economical and supply demand of microgrid. To address these issues, several techniques have been suggested and developed [34, 35]. In Ref. [36], the stability constraints imposed by droop characteristics in an islanded microgrid are identified using a small signal approach. It was shown that microgrid stability and dynamic performance are greatly influenced by the droop gains. It is shown in Ref. [37] that the low frequency modes of microgrid are closely associated with the configuration of network and external power loop of inverter, whereas the high frequency modes are largely associated with the inverter inner loop, loads and network dynamic characteristics. In Ref. [38], an adaptive feed forward technique has been proposed to bring variation in the dynamic coupling between a DG unit and the host microgrid in such a way that the stability of the system becomes less sensitive as well as more robust to the coefficients of droop and network dynamics. The incompatible goals of proper sharing of loads and stability of an islanded microgrid have been well investigated in Ref. [39]. Specially under weak system conditions high values of angle droop is necessary for smooth sharing of load. However, overall stability of the system is negatively impacted by high droop gains. Effect of droop gains on the system stability has been shown in [40].Besides, how connecting lines with different X/R ratio can affect the stability of an autonomous microgrid has been shown in [19]. Stability analysis for active damper has been presented in [41]. Effect of filter dynamics on the stability has been shown in [42]. Apart from filter dynamics, the controller parameters also have impact on the stability [43]. Here, the authors illustrated only the effect of droop co-efficients, proportional gain of voltage controller and integral gain of current controller on system stability.

1.3.4 Microgrid optimization

The microgrid stability and controller parameters are greatly related with each other. The relationship between stability and various factors like droop gains was studied in [20] and [44]. However, the authors did not resort to any optimizing algorithm to find out the best possible performance of the incorporated controllers. It is to be noted that optimal selection of controller, filter and power sharing parameters ensures better power quality and improves the performance of the system against disturbances of various kinds [45]. Although different control strategies and control parameter selection approaches have been presented in [4, 46], most of those are time consuming due to their trial and error based nature. Computational intelligence algorithms have been applied to different problems associated with power system with an impressive success rate [47]. Recently, Genetic Algorithm (GA) [48] and Particle Swarm Optimization (PSO) [24, 49, 50] have been used in parameter selection and optimization process for

micro grid controllers. But the microgrid models used in those works lack fundamental microgrid components: LCL filter and coupling inductance [49] for removal of harmonics and PLL [48, 50] responsible for system frequency observation during transients. Besides, the objective function considered in [24] involve only real part of eigenvalue which would optimize only the damping property but not the oscillatory property of the system under disturbances. Moreover, [48]-[50] conducted the optimization process within a predefined search space, which may not provide the ultimate optimization due to the limited predefined search region and may result in sub-optimal conclusion. Moreover, these works did not present any comparative study between their adopted optimizer and any other well-established optimization tool. Furthermore, as most of these nature based optimization algorithms are stochastic in nature, it is always beneficial to execute the algorithms for multiple numbers of times and test the statistical significant differences among various optimizing algorithms for obtaining the best possible outcome [51, 52].

1.4 Existing research gap

From the literature review, the following research gaps could be inferred:

- Though different microgrid models have been developed, most of the models avoided fundamental components: filter, damping resistor, PLL to avoid complexity. As a result, analyses with those models do not depict the impact of those fundamental components.
- There are many parameters that affect microgrid stability. But the effect of the parameters, on the microgrid stability has not been analyzed thoroughly. Besides, since earlier works did not use PLL in their work for monitoring system frequency under disturbance, the effect of PLL parameters on microgrid system remained unanalyzed.
- Controller parameters have been selected on trial and error basis in previous works. In some works, optimization algorithms have been used for optimal selection of the parameters within a predefined search space, which might not provide the ultimate optimization due to the limited predefined search space and lead to sub-optimal conclusion.
- Randomness and probability are common nature of optimizing algorithms, earlier works did not resort to any further analysis to explore randomness and probabilistic nature of algorithms.
- Comparison study among the different algorithms for improving microgrid stability has not been accomplished yet.

1.5 Thesis overview and objective

To address the above mentioned problem, the main objective of this work is to employ a two stage optimization method to optimize a two inverter based islanded microgrid system along with comparative analyses to determine the better optimizer for the system. In this work, the controller parameters are optimized by a two-stage optimization process which involves GA (Genetic Algorithm), PSO (Particle Swarm Optimization) and GWO (Grey Wolf Optimization) algorithms in an open search space to find the bound of the parameters in first stage and another two sets of algorithm: ES (Exhaustive Search) and IP (Interior Point) are adopted to obtain the final optimized value of parameters in the second stage. Finally, the best combination of algorithm between first and second stage is being identified through various analyses: comparative analysis of fitness value and execution time, time domain analysis and statistical analysis namely Kolmogorov-Smirnov test and permutation test. The overview of the research is as follows

- Linearization of a dynamic microgrid model by using Taylor series expansion and discard the higher order terms.
- Identification of the key control parameters on the small signal stability of the studied microgrid system by using eigenvalue, participation factor and root locus analysis.
- Optimization of the identified parameters by two stage optimization method.
  - Stage 1: Determination of the bound of the parameters by using Genetic Algorithm (GA), Particle Swarm Optimization (PSO) and Grey Wolf Optimization (GWO).
  - Stage 2: Final optimization of parameters using Exhaustive Search (ES) and Interior Point (IP) algorithm.
- Study of the dynamics of power system followed by small perturbation in time domain simulation.
- Comparison of the performance of the optimizers using time domain simulation and statistical analysis: Kolmogorov-Smirnov test and permutation test

1.6 Thesis organization

The whole work is organized as follows:

- Chapter 1 signifies background, motivation, existing research and gap and lastly thesis objective and overview.

- Chapter 2 presents detailed mathematical model of studied microgrid system and linearization of the model.
- Chapter 3 describes the methodology of the thesis.
- Chapter 4 presents simulation and result containing time domain simulation and comparative analyses.
- Chapter 5 is the last part of this thesis work ending with an explanatory conclusion and direction towards future work.

Chapter 2

Mathematical modeling and linearization of the system

Microgrid system can operate in grid-connected or islanded mode. DGs act as a constant power source and are controlled to supply the demanded power in the network when microgrid operates in grid-connected mode. In islanded mode, DGs supply the demanded power as well as maintain the voltage and frequency within the allowable limit. To maintain the voltage and current, various controllers are incorporated resulting in complex structure of islanded microgrid unlike grid connected microgrid. This chapter represents the nonlinear and linearized dynamic model of studied microgrid system which is necessry for analyzing the small signal stability. In section 2.1 of the chapter, the detailed mathematical model of the Microgrid system has been discussed and in section 2.2 of the chapter, linearized model of the studied Microgrid system has been developed.

2.1 Mathematical model of microgrid system

In this work, a two-inverter interfaced DGs with a local load connected to each inverter bus is considered [53]. Two inverters are connected to each other with a line as shown in the Figure 2.1.The connection of switch at the PCC determines whether the microgrid operates in islanded or grid-connected mode. Here, the islanded operation of microgrid has been considered only. The whole system can be divided into three sub modules: energy source (ES), line, and load.

The components of energy source (ES), DG with interfacing inverter structure, have been shown in Figure 2.2. The inverter control techniques have been introduced based on local measurements. Control of inverter is performed in three loops: 1. Power control - responsible for controlling the real and reactive power by controlling the frequency and fundamental voltage magnitude using droop controller driven by droop equation, 2. Voltage control - responsible

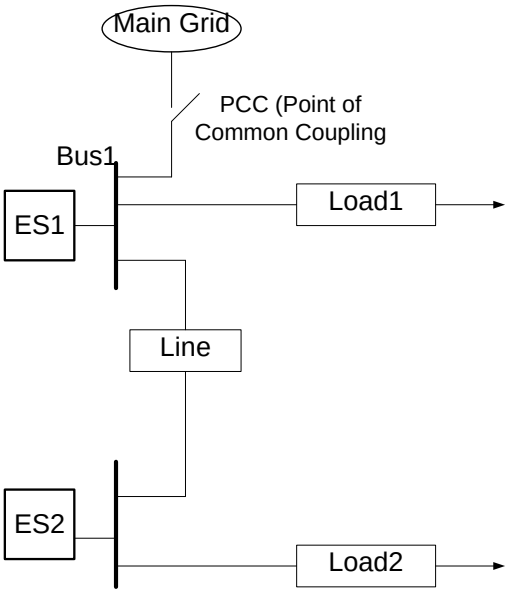

Figure 2.1: Studied microgrid structure

for controlling the voltage and sending current reference vector for the current controller and 3. Current control - responsible for generating voltage vector signal for pulse width modulator (PWM). The voltage controller and current controller yield sufficient damping for output LC filter and remove any high-frequency disturbances. Two assumptions have been made in this work. First, the DGs connected to the inverter is assumed to be ideal for neglecting dc bus dynamics. Second, the switching process of the inverter is neglected considering high switching frequencies. The output of the inverter contains high-frequency switching noise which is

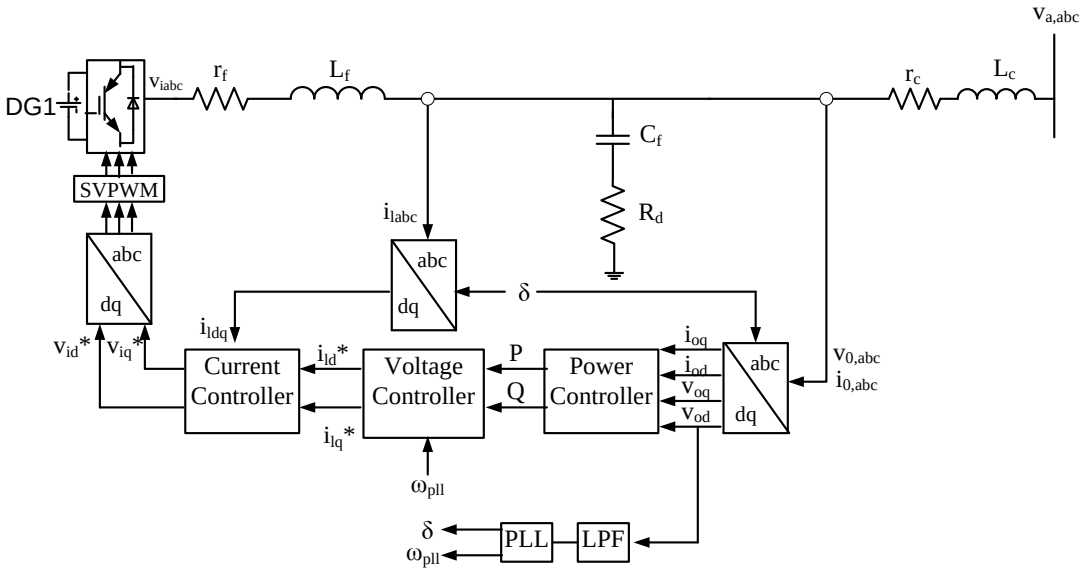

Figure 2.2: Inverter structure

removed by passing the inverter output through an LCL filter connected at the inverter output.

The output of the LCL filter is then converted to dq axis components for inverter output power calculation. This calculated power is passed to the droop equation driven droop controller followed by a low pass filter. Droop controller mimics the principle of the synchronous generator governor and sets the voltage and frequency reference. These voltage and frequency references are used to calculate the error signal which is fed to the proportional integral controller (voltage controller) to generate the current reference flowing through the inductor. Comparison of the current signal is again made with the measured value to generate the error signal which is again fed to another set of a proportional-integral controller (current controller) to produce the voltage reference signal available at the input of LCL filter. The inverter is connected to the bus through a coupling inductor and resistor along with a filter capacitor causing the damping of the resonant frequency related to the output filter. The equations of all controllers and filters are modeled in the individual local reference frame which is later transferred to the global reference frame which is the local reference frame of inverter 1. The various components of the inverter structure have been discussed in the following sections.

2.1.1 Power controller

The output of the inverter voltage and current is transformed to dq axis voltage, v_{od} and v_{oq} and current, i_{od} and i_{oq} which are used in the calculation of instantaneous average real power, P and reactive power, Q of the system as follows:

$$p = \frac{3}{2}(v_{od}i_{od} + v_{oq}i_{oq}) \tag{2.1}$$

$$q = \frac{3}{2}(v_{oq}i_{od} - v_{od}i_{oq}) \tag{2.2}$$

This instantaneous real and reactive power is passed through a low pass filter having cut off

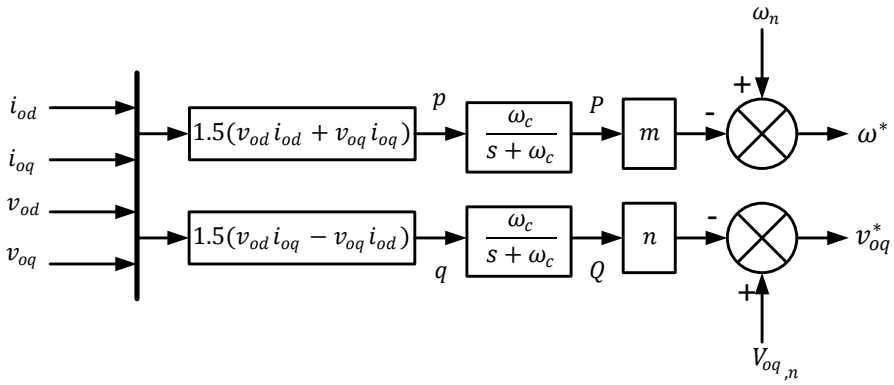

Figure 2.3: Power controller

frequency of ω_c, shown in Figure 2.3, in order to get the fundamental component of real and

reactive power.

$$P = \frac{\omega_c}{s+\omega_c} p \Rightarrow \dot{P} = -P\omega_c + 1.5\omega_c(v_{od}i_{od} + v_{oq}i_{oq}) \tag{2.3}$$

$$Q = \frac{\omega_c}{s+\omega_c} q \Rightarrow \dot{Q} = -Q\omega_c + 1.5\omega_c(v_{oq}i_{od} - v_{od}i_{oq}) \tag{2.4}$$

Here, s is the laplace operator.

The real and reactive power, P and Q are passed to the droop controller driven by the droop equation to generate voltage and frequency references, v^*_{oq} and ω^*.

2.1.2 Droop equation

When microgrid is connected to the utility grid, it follows the grid voltage and frequency [54]. But in the islanded operation of a microgrid, such reference voltage and frequency are not available. Thus, the inverters need to generate its own frequency reference, ω^* and a voltage reference, v^*_{oqi}. In this work, voltage and frequency based droop control, well established method and stated in IEEE 1547 standard [55], has been considered to generate those references. Droop equation imitates the synchronous generator governor system [56] which shares any increment of real power by decreasing the frequency according to $P - f$ droop equations and vice versa. Again, any increment of reactive power is balanced by decreasing the voltage following the $Q-V$ droop equation. The droop characteristic has been shown in the Figure 2.4.

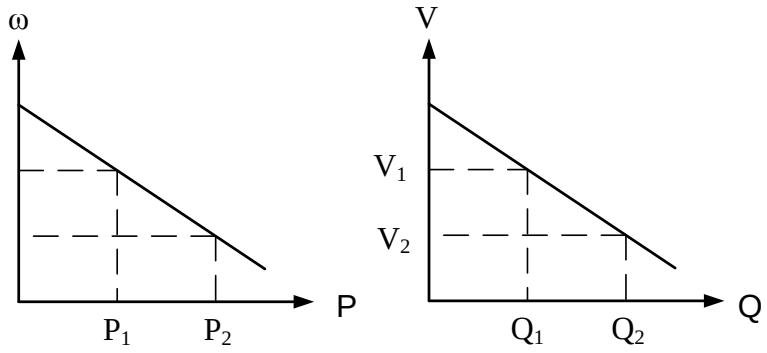

Figure 2.4: Droop characteristics

The droop equation representing the droop curve are

$$\omega^* = \omega_n - mP \tag{2.5}$$

$$v^*_{oq} = V_{oq,n} - nQ \tag{2.6}$$

Here, parameters n and m in above equations are the droop co efficients. These values determine the magnitude of the changes in frequency and bus voltage that will occur as a response to changes in complex power.

2.1.3 Phase locked loop

The phase-locked loop (PLL) has been proposed in [57] to track the frequency and phase angle of the system. The measurement strategy for phase lock loop is such that it takes either d or q axis component and phase is locked when either d or q axis component becomes zero i.e. $v_{od} = 0$ or $v_{oq} = 0$ respectively. Here, the phase lock loop is fed with the output d-axis component voltage of the filter capacitor as shown in Figure 2.5.

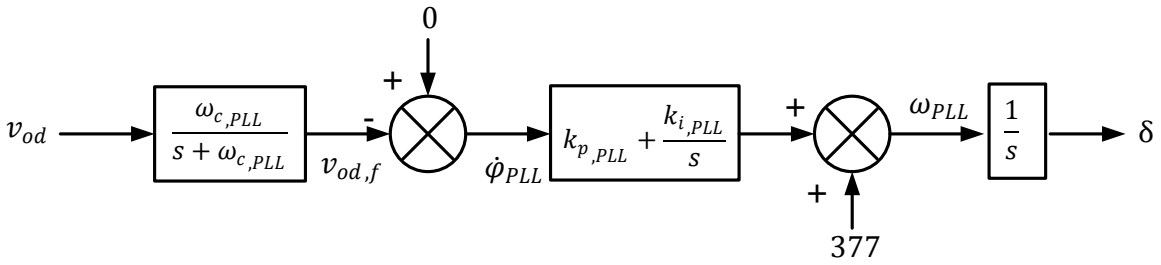

Figure 2.5: Phase locked loop

Thus, the phase is locked when $v_{od} = 0$. The q axis component could have also been considered. In that case, interchange of d and q axis quantities is required throughout the remainder of the work. There are three states in the PLL and state equations have been presented below:

$$\dot{v}_{od,f} = \omega_{c,PLL} v_{od} - \omega_{c,PLL} v_{od,f} \tag{2.7}$$

$$\dot{\phi}_{PLL} = -v_{od,f} \tag{2.8}$$

$$\dot{\delta} = \omega_{PLL} \tag{2.9}$$

$$\omega_{PLL} = 377 - k_{p,PLL} v_{od,f} + k_{i,PLL} \phi_{PLL} \tag{2.10}$$

Here, phase angle, δ is used in the reference frame transformation and ϕ_{PLL} is an integrator state.

The θ in Equation 2.11 - 2.12 represents the difference between the actual grid phase angle and the phase angle value calculated by the PLL. This difference must be accounted for in equations relating parameters calculated in the inverter's local reference frame to those in the global reference frame. In grid-tied operation, the global reference frame is set by the grid. But in islanded operation, an inverter is considered as reference. The transformation used to refer quantities derived in one reference frame to another is given by Equation 2.11 and 2.12. This

transformation is commonly used in modeling inverters and synchronous machines [4].

$$\begin{bmatrix} f_D \\ f_Q \end{bmatrix} = \begin{bmatrix} cos(\theta) & sin(\theta) \\ -sin(\theta) & cos(\theta) \end{bmatrix} \begin{bmatrix} f_d \\ f_q \end{bmatrix} \tag{2.11}$$

$$\begin{bmatrix} f_d \\ f_q \end{bmatrix} = \begin{bmatrix} cos(\theta) & -sin(\theta) \\ sin(\theta) & cos(\theta) \end{bmatrix} \begin{bmatrix} f_D \\ f_Q \end{bmatrix} \tag{2.12}$$

2.1.4 Voltage controller

The voltage controller consists of a proportional integral (PI) regulator and shown in Figure 2.6. The voltage and frequency references,v_{oq}^* and ω^* generated by the droop controller are compared

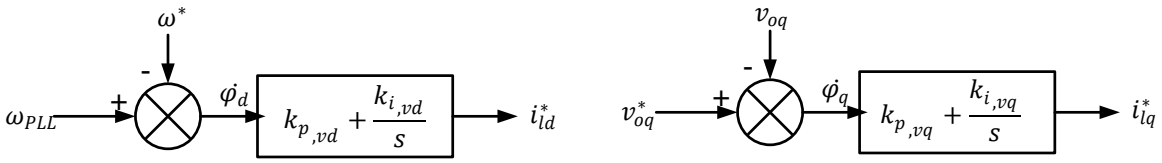

Figure 2.6: Voltage controller

with the q axis component of inverter output voltage, v_{oq} and system frequency, ω_{PLL} calculated by the PLL respectively and the error signal is fed to the PI controller. The output of the voltage controller is the filter inductor current,i_{ldq}^*. The equations describing the dynamics of the voltage controller are:

$$\dot{\phi}_d = \omega_{PLL} - \omega^* \tag{2.13}$$

$$\dot{\phi}_q = v_{oq}^* - v_{oq} \tag{2.14}$$

$$\dot{i}_{ld} = k_{iv,d}\phi_d + k_{pv,d}\dot{\phi}_d \tag{2.15}$$

$$\dot{i}_{lq} = k_{iv,q}\phi_q + k_{pv,q}\dot{\phi}_q \tag{2.16}$$

Here, $k_{pv,d}$ and $k_{pv,q}$ are proportional gains and $k_{iv,d}$ and $k_{iv,d}$ are integral gains of the PI controller.

2.1.5 Current controller

The current controller is perhaps the most generic aspect of the inverter model. The function of the controllers is to ensure that the filter current follows the reference current i_{ldq}^*. At the output of the controllers, cross-coupled terms are removed and the d- and q-axis voltage commands are sent to a space vector modulation (SVPWM) function, which calculates appropriate duty ratios. In this work, the averaged switch modeling technique is used to approximate the output of each phase leg as a continuous voltage source. This is a viable approximation as long as the

switching frequency is high compared to the dynamics of the control system and considerations are given to minimizing the effects of switch dead-time in the modulation strategy.The structure of current controller comprised of PI controller having a proportional and integral gain of $k_{pc,dq}$ and $k_{ic,dq}$ respectively is shown in Figure 2.7. In the current controller, the error signal fed to the

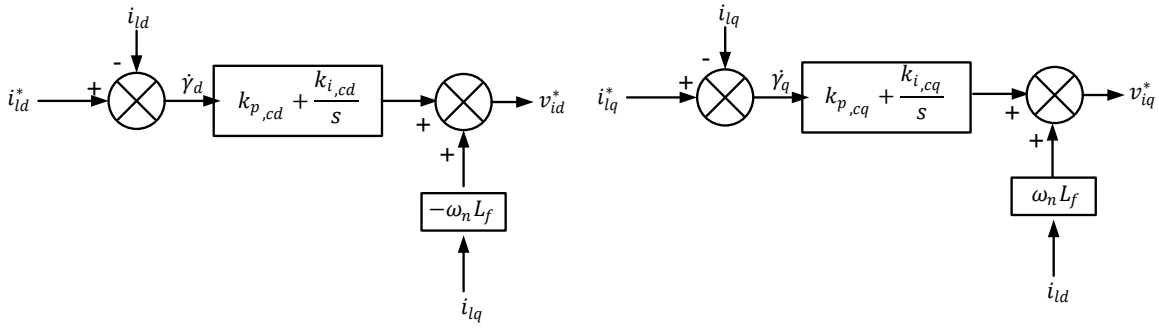

Figure 2.7: Current controller

PI controller is generated by comparing the reference filter inductor current, i^*_{ldq} and measured inductor filter current, i_{ldq}. The output of the controller is the output voltage of the inverter, v^*_{idq} prior to the LCL filter.

$$\dot{\gamma}_d = i^*_{ld} - i_{ld} \tag{2.17}$$

$$\dot{\gamma}_q = i^*_{lq} - i_{lq} \tag{2.18}$$

$$v^*_{id} = -\omega_n L_f i_{lq} + k_{ic,d}\gamma_d + k_{pc,d}\dot{\gamma}_d \tag{2.19}$$

$$v^*_{iq} = \omega_n L_f i_{ld} + k_{ic,q}\gamma_q + k_{pc,q}\dot{\gamma}_q \tag{2.20}$$

2.1.6 LC filter and coupling inductance

The LC filter and coupling inductance have been shown in the Figure 2.8. The LCL filter consists

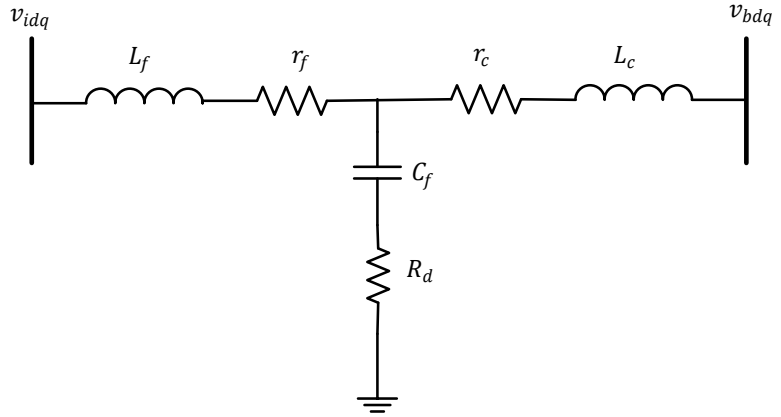

Figure 2.8: LCL filter

of filter inductor L_f, filter capacitor C_f, and coupling inductor L_c. The coupling inductor may

be a discrete component, or may represent the inductance of an isolating transformer. The model includes the series resistances of the filter and coupling inductors, r_f and r_c, respectively. The resonance of the filter is passively damped by resistor R_d. This resistor also represents the series resistance of the capacitors, which is much smaller than the damping resistance. Here, it is assumed that the inverter generates the voltage; $v_{idq} = v^*_{idq}$ by the current controller i.e. the losses in the diode and IGBT have been neglected. The state equations representing filter dynamics are

$$\dot{i}_{ld} = \frac{1}{L_f}(-r_f i_{ld} + v_{id} - v_{od}) + \omega_{PLL} i_{lq} \tag{2.21}$$

$$\dot{i}_{lq} = \frac{1}{L_f}(-r_f i_{lq} + v_{iq} - v_{oq}) - \omega_{PLL} i_{ld} \tag{2.22}$$

$$\dot{i}_{od} = \frac{1}{L_c}(-r_c i_{od} + v_{od} - v_{bd}) + \omega_{PLL} i_{oq} \tag{2.23}$$

$$\dot{i}_{oq} = \frac{1}{L_c}(-r_c i_{oq} + v_{oq} - v_{bq}) - \omega_{PLL} i_{od} \tag{2.24}$$

$$\dot{v}_{od} = \frac{1}{C_f}(i_{ld} - i_{od}) + \omega_{PLL} v_{oq} + R_d(\dot{i}_{ld} - \dot{i}_{od}) \tag{2.25}$$

$$\dot{v}_{oq} = \frac{1}{C_f}(i_{lq} - i_{oq}) - \omega_{PLL} v_{od} + R_d(\dot{i}_{lq} - \dot{i}_{oq}) \tag{2.26}$$

2.1.7 Line

The inverters are connected with each other through a line [4, 53] as shown in Figure 2.9. The line is represented by the series combination of resistor and inductor. The inductance,

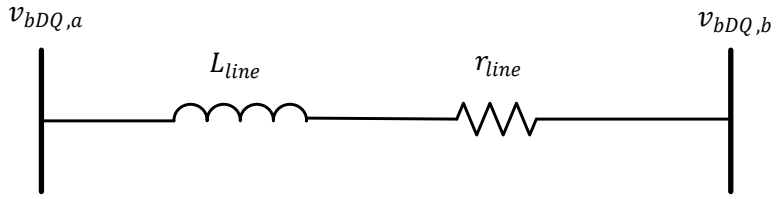

Figure 2.9: Line model

L_{line} represents the lumped inductance of the long transmission line and the resistance, r_{line} represents the resistive loss of the line.

$$\dot{i}_{lineDab} = \frac{1}{L_{line}}(r_{line} i_{lineD} + v_{bD,a} - v_{bD,b}) + \omega_{PLL} i_{lineQ} \tag{2.27}$$

$$\dot{i}_{lineQab} = \frac{1}{L_{line}}(r_{line} i_{lineQ} + v_{bQ,a} - v_{bQ,b}) - \omega_{PLL} i_{lineD} \tag{2.28}$$

2.1.8 Load

Various kinds of loads can be connected to a microgrid system. Here, RL load is considered as shown in the Figure 2.10. Loads are connected to inverter 1 and inverter 2 bus namely bus1

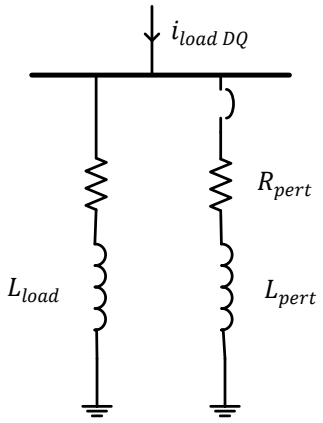

Figure 2.10: Static load model

and bus2 respectively. The load connected to the bus1 and bus2 is variable. The variation of the load at buses is brought by connecting a R_{pert} and L_{pert} with the fixed RL load through a switch. When the switch closes the R_{pert} and L_{pert} appear in parallel combination with the fixed RL load.

$$\dot{i}_{loadD} = \frac{1}{L_{load}}(-R_{load}i_{loadD} + v_{bD}) + \omega_{PLL}i_{loadQ} \tag{2.29}$$

$$\dot{i}_{loadQ} = \frac{1}{L_{load}}(-R_{load}i_{loadQ} + v_{bQ}) - \omega_{PLL}i_{loadD} \tag{2.30}$$

2.2 Linearized model of inverter operated islanded Microgrid

In this section, linearization of our above mentioned nonlinear mathematical model has been accomplished to develop the linearized form of each dynamic equations (i.e. Equation 2.1 - 2.30), since this linearized form is well suited for the study of small signal stability [58]. With this aim, Taylor-series expansion has been applied to these dynamic equations and higher order terms have been truncated in order to obtain corresponding linearized equations. Certainly, truncation of higher order term will introduce some inaccuracy, since nonlinearities associated with higher order terms are being ignored [59]. However, this error is insignificant for small signal analysis [60] and thus, can be neglected.. Now, after resorting to Taylor series expansion and considering the resulting first order term of dynamic system equations (Equation 2.1 - 2.30), the following linear equations are obtained. Since the system is very large containing 36

states equations, the linearized equations are arranged in matrix form which is later used in determining combined system model.

2.2.1 Linearized power controller model

The linearized equations of the power controller responsible for adjustment of any discrepancy in the voltage and frequency are

$$\Delta\dot{P}_i = -\omega_c\Delta P_i + 1.5\omega_c(v_{odi_0}\Delta i_{odi} + i_{odi_0}\Delta v_{odi} + v_{oqi_0}\Delta i_{oqi} + i_{oqi_0}\Delta v_{oqi}) \tag{2.31}$$

$$\Delta\dot{Q}_i = -\omega_c\Delta Q_i + 1.5\omega_c(v_{oqi_0}\Delta i_{odi} + i_{odi_0}\Delta v_{oqi} - v_{odi_0}\Delta i_{oqi} - i_{oqi_0}\Delta v_{odi}) \tag{2.32}$$

$$\begin{bmatrix}\Delta\dot{P}_i\\ \Delta\dot{Q}_i\end{bmatrix} = \begin{bmatrix}-\omega_c & 0\\ 0 & -\omega_c\end{bmatrix}\begin{bmatrix}\Delta P_i\\ \Delta Q_i\end{bmatrix} + \begin{bmatrix}1.5\omega_c v_{odi_0} & 1.5\omega_c v_{oqi_0} & 1.5\omega_c i_{odi_0} & 1.5\omega_c i_{oqi_0}\\ 1.5\omega_c v_{oqi_0} & -1.5\omega_c v_{odi_0} & -1.5\omega_c i_{oqi_0} & 1.5\omega_c i_{odi_0}\end{bmatrix}\begin{bmatrix}\Delta i_{odi}\\ \Delta i_{oqi}\\ \Delta v_{odi}\\ \Delta v_{oqi}\end{bmatrix} \tag{2.33}$$

2.2.2 Linearized droop equations

The discrepancy of voltage and frequency is adjusted by power controller using droop equations. The linearized droop equations are

$$\Delta\omega_i^* = -m\Delta P_i \tag{2.34}$$

$$\Delta V_{oqi}^* = -n\Delta Q_i \tag{2.35}$$

$$\begin{bmatrix}\Delta\omega_i^*\\ \Delta V_{oqi}^*\end{bmatrix} = \begin{bmatrix}-m & 0\\ 0 & -n\end{bmatrix}\begin{bmatrix}\Delta P_i\\ \Delta Q_i\end{bmatrix} \tag{2.36}$$

2.2.3 Linearized phase locked loop model

The PLL is mainly responsible for measurement of actual frequency of the system. In our system phase is locked when $v_{od,i} = 0$. The linearized equations describing the dynamics of PLL is given below

$$\Delta\dot{\phi}_{PLL_i} = -\Delta v_{odi,f} \tag{2.37}$$

$$\Delta\dot{v}_{odi,f} = \omega_{c,PLL}\Delta v_{odi} - \omega_{c,PLL}\Delta v_{odi,f} \tag{2.38}$$

$$\Delta\dot{\delta}_i = \Delta\omega_{PLL_1} - \Delta\omega_{PLL_i} \tag{2.39}$$

$$\Delta\omega_{PLL_i} = -K_{p,PLL}\Delta v_{odi,f} + K_{i,PLL}\Delta\phi_{PLLi} \tag{2.40}$$

$$\begin{bmatrix} \Delta\dot{\delta}_i \\ \Delta\dot{v}_{odi,f} \\ \Delta\dot{\phi}_{PLL_i} \end{bmatrix} = \begin{bmatrix} A_{PLL} \end{bmatrix} \begin{bmatrix} \Delta\delta_i \\ \Delta v_{odi,f} \\ \Delta\phi_{PLL_i} \end{bmatrix} + \begin{bmatrix} B_{PLL} \end{bmatrix} \begin{bmatrix} \Delta\delta_1 \\ \Delta v_{od1,f} \\ \Delta\phi_{PLL_1} \end{bmatrix} + \begin{bmatrix} 0 \\ \omega_{c,PLL} \\ 0 \end{bmatrix} \Delta v_{odi} \tag{2.41}$$

Here, $A_{PLL} = \begin{bmatrix} 0 & K_{p,PLL} & -K_{i,PLL} \\ 0 & -\omega_{c,PLL} & 0 \\ 0 & -1 & 0 \end{bmatrix}; B_{PLL} = \begin{bmatrix} 0 & -K_{p,PLL} & K_{i,PLL} \\ 0 & 0 & 0 \\ 0 & 0 & 0 \end{bmatrix}$

2.2.4 Linearized voltage controller model

The voltage controller maintains the output voltage with standard PI controller. After linearizing the dynamic equations of the voltage controller the following equations are obtained

$$\Delta i^*_{ldi} = k_{iv,d}\Delta\phi_{di} + k_{pv,d}\Delta\dot{\phi}_{di} \tag{2.42}$$

$$\Delta i^*_{lqi} = k_{iv,q}\Delta\phi_{qi} + k_{pv,q}\Delta\dot{\phi}_{qi} \tag{2.43}$$

$$\begin{bmatrix} \Delta\dot{\phi}_{di} \\ \Delta\dot{\phi}_{qi} \end{bmatrix} = \begin{bmatrix} 0 & 0 \\ 0 & 0 \end{bmatrix} \begin{bmatrix} \Delta\phi_{di} \\ \Delta\phi_{qi} \end{bmatrix} + \begin{bmatrix} m & 0 & 0 & -K_{p,PLL} & K_{i,PLL} \\ 0 & -n & -1 & 0 & 0 \end{bmatrix} \begin{bmatrix} \Delta P_i \\ \Delta Q_i \\ \Delta v_{oqi} \\ \Delta v_{odi,f} \\ \Delta\phi_{PLL_i} \end{bmatrix} \tag{2.44}$$

2.2.5 Linearized current controller model

The current filter controls the output filter inductor current. The linearized state equations of current controller are

$$\Delta v^*_{idi} = -\omega_n L_f \Delta i_{lqi} + k_{ic,d}\Delta\gamma_{di} + k_{pc,d}\Delta\dot{\gamma}_{di} \tag{2.45}$$

$$\Delta v^*_{iqi} = \omega_n L_f \Delta i_{ldi} + k_{ic,q}\Delta\gamma_{qi} + k_{pc,q}\Delta\dot{\gamma}_{qi} \tag{2.46}$$

$$\begin{bmatrix} \Delta\dot{\gamma}_{di} \\ \Delta\dot{\gamma}_{qi} \end{bmatrix} = \begin{bmatrix} 0 & 0 \\ 0 & 0 \end{bmatrix} \begin{bmatrix} \Delta\gamma_{di} \\ \Delta\gamma_{qi} \end{bmatrix} + \begin{bmatrix} B_{cc} \end{bmatrix} \begin{bmatrix} U_{cc} \end{bmatrix} \tag{2.47}$$

Here, $B_{cc} = \begin{bmatrix} mK_{pvd} & 0 & K_{ivd} & 0 & -1 & 0 & 0 & -K_{p,PLL}K_{pvd} & K_{i,PLL}K_{pvd} \\ 0 & -nK_{pvq} & 0 & K_{ivq} & 0 & -1 & -K_{pvq} & 0 & 0 \end{bmatrix}$;
$U_{cc} = \begin{bmatrix} \Delta P_i & \Delta Q_i & \Delta\phi_{di} & \Delta\phi_{qi} & \Delta i_{ldi} & \Delta i_{lqi} & \Delta v_{oqi} & \Delta v_{odi,f} & \Delta\phi_{PLL_i} \end{bmatrix}^T$

2.2.6 Linearized filter model

The purpose of the filter is to remove high frequency switching noise. Here, it is assumed that the inverter produces the required voltage $v_{idq,i} = v^*_{idq,i}$ The linearized state equations governing the filter dynamics are

$$\Delta\dot{i}_{ldi} = \frac{1}{L_f}(-r_f\Delta i_{ldi} + \Delta v_{idi} - \Delta v_{odi}) + \omega_{PLL}\Delta i_{lqi} + i_{lqi_0}\Delta\omega_{PLL} \tag{2.48}$$

$$\Delta\dot{i}_{lqi} = \frac{1}{L_f}(-r_f\Delta i_{lqi} + \Delta v_{iqi} - \Delta v_{oqi}) - \omega_{PLL}\Delta i_{ldi} - i_{ldi_0}\Delta\omega_{PLL} \tag{2.49}$$

$$\Delta\dot{i}_{odi} = \frac{1}{L_c}(-r_c\Delta i_{odi} + \Delta v_{odi} - \Delta v_{bdi}) + \omega_{PLL}\Delta i_{oqi} + i_{oqi_0}\Delta\omega_{PLL} \tag{2.50}$$

$$\Delta\dot{i}_{oqi} = \frac{1}{L_c}(-r_c\Delta i_{oqi} + \Delta v_{oqi} - \Delta v_{bqi}) - \omega_{PLL}\Delta i_{odi} - i_{odi_0}\Delta\omega_{PLL} \tag{2.51}$$

$$\Delta\dot{v}_{odi} = \frac{1}{C_f}(\Delta i_{ldi} - \Delta i_{odi}) + \omega_{PLL}\Delta v_{oqi} + v_{oqi_0}\Delta\omega_{PLL} + R_d(\Delta\dot{i}_{ldi} - \Delta\dot{i}_{odi}) \tag{2.52}$$

$$\Delta\dot{v}_{oqi} = \frac{1}{C_f}(\Delta i_{lqi} - \Delta i_{oqi}) - \omega_{PLL}\Delta v_{odi} - v_{odi_0}\Delta\omega_{PLL} + R_d(\Delta\dot{i}_{lqi} - \Delta\dot{i}_{oqi}) \tag{2.53}$$

Here, the phase angle of inverter 1 is considered as reference frame which necessitates the new phase angle derivation.

$$\Delta\dot{\delta}_1 = \Delta\omega_{PLL1} - \Delta\omega_{PLL1} = 0 \tag{2.54}$$

$$\Delta\dot{\delta}_2 = \Delta\omega_{PLL1} - \Delta\omega_{PLL2} \tag{2.55}$$

To connect an individual inverter with the rest of the system, transformation of the output variables of that inverter is required. The linearized equations for the transformation of variable are

$$\Delta i_{oD} = (\cos\theta_0)\Delta i_{od} + (\sin\theta_0)\Delta i_{oq} - (i_{od_0}\sin\theta_0)\Delta\theta + (i_{oq_0}\cos\theta_0)\Delta\theta \tag{2.56}$$

$$\Delta i_{oQ} = (-\sin\theta_0)\Delta i_{od} + (\cos\theta_0)\Delta i_{oq} - (i_{od_0}\cos\theta_0)\Delta\theta - (i_{oq_0}\sin\theta_0)\Delta\theta \tag{2.57}$$

$$\Delta v_{bd} = (\cos\theta_0)\Delta v_{bD} - (\sin\theta_0)\Delta v_{bQ} - (v_{bD_0}\sin\theta_0)\Delta\theta - (v_{bQ_0}\cos\theta_0)\Delta\theta \tag{2.58}$$

$$\Delta v_{bq} = (\sin\theta_0)\Delta v_{bD} + (\cos\theta_0)\Delta v_{bQ} + (v_{bD_0}\cos\theta_0)\Delta\theta - (v_{bQ_0}\sin\theta_0)\Delta\theta \tag{2.59}$$

After substituting v_{bdq} from the above equations in eq. (2.48)-(2.53) , the filter equations can be written in matrix form as follows

$$\left[\dot{x}_{filter1}\right] = \left[A_{filter}\right]\left[u_{filter}\right] + \left[B_{filter}\right]\left[x_{filter}\right] \tag{2.60}$$

$$\text{Where, } A_{filter} = \begin{bmatrix} \frac{-r_f - K_{pcd}}{L_f} & \omega_{PLL} - \omega_n & 0 & 0 & -\frac{1}{L_f} & 0 \\ \omega_n - \omega_{PLL} & \frac{-r_f - K_{pcq}}{L_f} & 0 & 0 & 0 & \frac{-1 - K_{pcq}K_{pvq}}{L_f} \\ 0 & 0 & -\frac{r_c+2}{L_c}; & \omega_{PLL} & \frac{1}{L_c} & 0 \\ 0 & 0 & -\omega_{PLL} & -\frac{r_c+2}{L_c} & 0 & \frac{1}{L_c} \\ V_{od8_i} & V_{od9_i} & V_{od12_i} & V_{od13_i} & V_{od10_i} & V_{od11_i} \\ V_{oq8_i} & V_{oq9_i} & V_{oq12_i} & V_{oq13_i} & V_{oq10_i} & V_{oq11_i} \end{bmatrix}$$

$$x_{filter} = \begin{bmatrix} \Delta\delta_i, \Delta P_i, \Delta Q_i, \Delta\phi_{di}, \Delta\phi_{qi}, \Delta\gamma_{di}, \Delta\gamma_{qi}, \Delta\phi_{PLL_i}, \Delta v_{odi,f}, \Delta i_{loadD_i}, \Delta i_{loadQ_i}, \dots \\ \Delta i_{lineD_{ij}}, \Delta i_{lineQ_{ij}} \end{bmatrix}^T_{1x13}$$

$$u_{filter} = \begin{bmatrix} \Delta i_{ldi} & \Delta i_{lqi} & \Delta i_{odi} & \Delta i_{oqi} & \Delta v_{odi} & \Delta v_{oqi} \end{bmatrix}^T$$

Here, the upper and lower subscript denotes the variable in global and local reference frame respectively.

2.2.7 Linearized load model

In our system, RL load is connected to each inverter bus. The linearized state equations describing the load dynamics are

$$\begin{bmatrix} \Delta\dot{i}_{loadDi} \\ \Delta\dot{i}_{loadQi} \end{bmatrix} = \begin{bmatrix} -\frac{R_{loadi}}{L_{loadi}} - \frac{r_N}{L_{loadi}} & \omega_{PLL} \\ -\omega_{PLL} & -\frac{R_{loadi}}{L_{loadi}} - \frac{r_N}{L_{loadi}} \end{bmatrix} \begin{bmatrix} \Delta i_{loadDi} \\ \Delta i_{loadQi} \end{bmatrix} + \begin{bmatrix} B_{load} \end{bmatrix} \begin{bmatrix} \Delta\delta_i \\ \Delta iod_i \\ \Delta ioq_i \\ \Delta\phi_{PLL_i} \\ \Delta v_{odi,f} \\ \Delta i_{lineD_{ij}} \\ \Delta i_{lineQ_{ij}} \end{bmatrix} \tag{2.61}$$

$$\begin{bmatrix} B_{load} \end{bmatrix} = \begin{bmatrix} \frac{r_N(i_{oqi_0}\cos\delta_{i0} - i_{odi_0}\sin\delta_{i0})}{L_{loadi}} & \frac{r_N\cos\delta_{i0}}{L_{loadi}} & \frac{r_N\sin\delta_{i0}}{L_{loadi}} & K_{i,PLL}i_{loadQi_0}\cdots \\ & -K_{p,PLL}i_{loadQi_0} & \frac{r_N}{L_{loadi}} & 0 \\ -\frac{r_N(i_{oqi_0}\sin\delta_{i0} + i_{odi_0}\sin\delta_{i0})}{L_{loadi}} & -\frac{r_N\sin\delta_{i0}}{L_{loadi}} & \frac{r_N\cos\delta_{i0}}{L_{loadi}} & -K_{i,PLL}i_{loadDi_0}\cdots \\ & K_{p,PLL}i_{loadDi_0} & 0 & \frac{r_N}{L_{loadi}} \end{bmatrix}_{2x7}$$

2.2.8 Linearized line model

The line parameter consists of resistance and inductance. The linearized line equations connected between i^{th} and j^{th} bus are

$$\begin{bmatrix} \Delta\dot{i}_{lineDij} \\ \Delta\dot{i}_{lineQij} \end{bmatrix} = \begin{bmatrix} \frac{r_{lineij}}{L_{lineij}} & \omega_{PLL} \\ -\omega_{PLL} & \frac{r_{lineij}}{L_{lineij}} \end{bmatrix} \begin{bmatrix} \Delta i_{lineDij} \\ \Delta i_{lineQij} \end{bmatrix} + \begin{bmatrix} B_{line} \end{bmatrix} \begin{bmatrix} u_{line} \end{bmatrix} \tag{2.62}$$

Here,

$$u_{line} = \begin{bmatrix} \Delta\delta_i, \Delta\delta_j, \Delta i_{od_i}, \Delta i_{oq_i}, \Delta i_{od_j}, \Delta i_{oq_j}, \Delta\phi_{PLL_i}, \Delta v_{odi,f}, \Delta i_{loadD_i}, \Delta i_{loadQ_i}, \Delta i_{loadD_j}, ... \\ \Delta i_{loadQ_j} \end{bmatrix}^T_{1x12}$$

2.2.9 Linearized combined system model

There are 15 states in each inverter and the linearized equations of two inverters are

$$\begin{bmatrix} \dot{x}_{inv1} \\ \dot{x}_{inv2} \end{bmatrix} = A_{Inverter} \begin{bmatrix} x_{inv1} \\ x_{inv2} \end{bmatrix} + B_{Inverter} \begin{bmatrix} \Delta v_{bDQ1} \\ \Delta v_{bDQ2} \end{bmatrix} \tag{2.63}$$

$$x_{inv_1} = \begin{bmatrix} \Delta\delta_1 \ \Delta P_1 \ \Delta Q_1 \ \Delta\phi_{d1} \ \Delta\phi_{q1} \ \Delta\gamma_{d1} \ \Delta\gamma_{q1} \ \Delta i_{ld1} \ \Delta i_{lq1} \ \Delta v_{od1} \ \Delta v_{oq1} \ \Delta i_{od1} \ \Delta i_{oq1} ... \\ \Delta\phi_{PLL1} \ \Delta v_{od1,f} \end{bmatrix}_{15x1} \tag{2.64}$$

$$x_{inv_2} = \begin{bmatrix} \Delta\delta_2 \ \Delta P_2 \ \Delta Q_2 \ \Delta\phi_{d2} \ \Delta\phi_{q2} \ \Delta\gamma_{d2} \ \Delta\gamma_{q2} \ \Delta i_{ld2} \ \Delta i_{lq2} \ \Delta v_{od2} \ \Delta v_{oq2} \ \Delta i_{od2} \ \Delta i_{oq2} ... \\ \Delta\phi_{PLL2} \ \Delta v_{od2,f} \end{bmatrix}_{15x1} \tag{2.65}$$

To complete the linearized dynamic model of our studied microgrid system, the bus voltages need to be included in the system matrix. This can be easily accomplished by assuming a virtual resistance with high resistive value connecting at the inverter bus. The linearized bus voltages using virtual resistor are

$$\Delta v_{bDi} = r_N(\Delta i_{oD,i} + \Delta i_{lineD,ij} - \Delta i_{loadD,i}) \tag{2.66}$$

$$\Delta v_{bQi} = r_N(\Delta i_{oQ,i} + \Delta i_{lineQ,ij} - \Delta i_{loadQ,i}) \tag{2.67}$$

Using eq. (2.66) and (2.67) the bus voltages v_{bDQi} are eliminated from our representation

$$\begin{bmatrix} \dot{x}_{inv} \\ \dot{x}_{loadDQ} \\ \dot{x}_{lineDQ} \end{bmatrix} = A_{system} \begin{bmatrix} x_{inv} \\ x_{loadDQ} \\ x_{lineDQ} \end{bmatrix} \tag{2.68}$$

The system matrix, A_{system} is a $36x36$ matrix represented in subsection A.1.1 of appendix A. This matrix is evaluated around steady state operating point and the resultant matrix is used in further analyses: eigenvalue analysis, participation factor analysis and root locus analysis of the studied microgrid system.

Chapter 3

Methodology

In this chapter, basic methodology has been discussed to optimize a droop control based islanded microgrid system. In this work, crucial controller parameters have been optimized using different algorithms and a comparative analyses among the applied algorithm have been carried out in optimizing the parameters. To begin the optimization, the key parameters need to be identified first which has been discussed in section 3.1. In section 3.2, the problem of optimization has been formulated with an eigenvalue based objective function. The procedure of parameter optimization has been presented in section 3.3. Lastly, comparison methods among the applied algorithms have been discussed in section 3.4.

3.1 Determination of key parameters affecting stability

Eigenvalue analysis of the system matrix at an operating condition is one of the effective methods to investigate small signal stability of a system. By inspecting the nature of the eigenvalues, the characteristic of the system oscillation can be identified. The oscillation frequency and damping ratio calculated from the eigenvalue help in identification of the eigenvalues crucial for system stability. Moreover, the participation factors derived from the left and right eigen vectors corresponding to the eigenvalues of the system matrix indicates the contribution of a mode to the response of a particular eigenvalue. The eigenvalue, oscillation frequency, damping and participation factor analyses determine key parameters critical to system stability and root locus analysis of the parameters validates the selection of the parameters affecting stability.

3.1.1 Determination of steady state operating point

In order to analyze the system, the system matrix, A_{system} is linearized around steady state operating point which can be found by setting the nonlinear state equations to zero i.e. $\dot{x} = 0$ or by power flow solution of the system. In the conventional power system, the system frequency is known and fixed at grid frequency. But in droop controlled islanded microgrid, the concept of

constant frequency is violated because of its droop characteristics. The variation of frequency affects the power-sharing between the different generating units as well as voltage drop in the reactive component of the network unlike the conventional power system. As a result, traditional methods of determining steady-state power system operating points are not applicable to droop controlled microgrids. In droop controlled islanded microgrid system, it is not possible to obtain the steady state operating point by directly setting the state equations zero without determining the frequency and voltage through appropriate procedure. The following section 3.1.1.1-3.1.1.6 represents the method [61] that has been adopted in this work to determine the operating voltage and frequency and ultimately the operating point of the studied microgrid system.

3.1.1.1 Initialization

From the steady state equations of the PLL, it is found that the d axis component of the output voltage, $v_{od} = 0$. So, to start the power flow solution, the initial value of the q axis component of output voltage, v_{oq} is assumed to be equal to the nominal q axis voltage, $V_{oq,n}$. Again, since the phase angle of inverter 1 is considered as the reference, the phase angle, δ_1 of inverter 1 is considered zero. The phase angle of inverter 2 is also considered zero for the initial start. The system frequency, ω_{PLL} is assumed to be equal to nominal frequency, ω_n. So, the initial conditions are:

$$v_{od1} = 0, v_{od2} = 0 \tag{3.1}$$

$$v_{oq1} = v_{oq2} = V_{oq,n} \tag{3.2}$$

$$\delta_1 = \delta_2 = 0 \tag{3.3}$$

It is assumed that the inverter1 bus serves as the system's reference and consequently is labeled the global reference frame. The inverter operates in its own local reference frame and its equations are derived in terms of that reference. A transformation is required to go from local to global reference frame and vice-versa. For single inverter single bus system, the inverter's local reference frame can be set to the same as that of the global reference frame. Mathematically this is done by setting the angle difference between the local and global reference frame (θ) to zero. This transformation between reference frame have greater significance here as multiple inverters are added in the system.

Here, the voltages of the inverter are in its local reference frame. So, they need to transferred to the global reference frame and this transformation is accomplished using the Equation 2.11.

$$V_{od,i} = \sin(\delta_i) v_{oq,i} \tag{3.4}$$

$$V_{oq,i} = \cos(\delta_i) v_{oq,i} \tag{3.5}$$

$$V_{o,i} = V_{od,i} + jV_{oq,i} \tag{3.6}$$

Here, subscript i represents the i^{th} inverter.

3.1.1.2 Calculation of injected current

Since there are no PQ loads, the microgrid model consists of only inverters and constant impedance loads. The voltage source and coupling inductance of the inverter may be converted to a Norton equivalent circuit as follows:

$$I_{sc,i} = \frac{V_{o,i}}{Z_c(\omega)} \tag{3.7}$$

$$Z_c(\omega) = r_c + j\omega L_c \tag{3.8}$$

The main advantage of this conversion is that the equivalent current source injects current directly into the local bus. This simplifies the process of calculating the bus voltages, which are needed to determine the load and line currents.

3.1.1.3 Construction of bus impedance matrix

The bus voltages can be calculated from this injected current and system bus matrix, Z_{bus}. This bus impedance matrix is a well-known concept in power system analysis. Here, since ω changes in every iteration, the bus impedance matrix must be updated at each iteration. This is the key difference between microgrids and conventional power systems. When the system contains a slack bus, it is capable of sourcing sufficient power to keep frequency constant, or near enough to justify a constant-frequency approximation. The assumption of constant frequency leads to constant system level admittance and impedance matrices, which are central components of conventional power flow analysis. Islanded microgrids do not contain a slack bus, and are therefore unable to utilize a constant admittance or impedance matrix. The bus impedance matrix $Z_{bus}(\omega)$ is formed of load, line and inverter coupling impedance. The virtual resistance r_n is also added to the matrix to omit the error due to the inclusion of the virtual resistance.

3.1.1.4 Calculation of bus voltages

Once the bus impedance is calculated for a particular system frequency ω, this bus impedance matrix can be used to calculate the bus voltages as given by the Equation 3.9. Once V_b has been

determined, it may be broken into synchronous reference frame quantities using Equation 3.10 - 3.11.

$$V_b = Z_{bus}(\omega)I \tag{3.9}$$

$$V_{bD} = real(V_b) \tag{3.10}$$

$$V_{bQ} = imag(V_b) \tag{3.11}$$

3.1.1.5 Calculation of inverter output current

The inverter output current $I_{o,i}$ can be calculated using Equation 3.12 once the bus voltages, $V_{b,i}$ are calculated.

$$I_{o,i} = \frac{V_{o,i} - V_{b,i}}{Z_c(\omega)} \tag{3.12}$$

$$I_{od,i} = real(I_{o,i}) \tag{3.13}$$

$$I_{oq,i} = imag(I_{o,i}) \tag{3.14}$$

3.1.1.6 Calculation of power mismatch

Here, the unknowns of the iterative solution are

$$y = [\omega_{PLL}, \delta_2, v_{oq,1}, v_{oq,2}]^T \tag{3.15}$$

The power mismatch equation of the inverter is the difference between the calculated inverter output power and the power provided by the drop equations

$$\Delta P_i = 1.5(v_{od,i}i_{od,i} + v_{oq,i}i_{oq,i}) - \frac{\omega_n - \omega_{PLL}}{m_i} \tag{3.16}$$

$$\Delta Q_i = 1.5(v_{oq,i}i_{od,i} - v_{od,i}i_{oq,i}) - \frac{V_{oq,n} - v_{oq,i}}{n_i} \tag{3.17}$$

The complete set of power mismatch equations is

$$F(y) = [\Delta P_1, \Delta Q_1, \Delta P_2, \Delta Q_2] \tag{3.18}$$

The quantities in the above equations contain all the information necessary to evaluate the power mismatch function, F(y).Here, the solution from the power flow is the vector y for which $F(y) < \varepsilon$. Here, ε is the pre-specified error tolerance which has been considered 10^{-7} in the work. The solution is obtained numerically using the standard multivariate Newton Raphson / quasi-Newton method. The equation used to update the values of the variable in each iteration

is

$$y^{j+1} = y^j - [B(y^j)]^{-1} F(y^j) \tag{3.19}$$

In the equation above j is the current iteration and matrix B(y) can be alternative to Jacobean matrix or standard Jacobean matrix. The iterative solution continues and the values are updated using Equation 3.19 unless

$$F(y^k) < \varepsilon \tag{3.20}$$

Using the above procedure, the q axis inverter output voltage, $v_{oq,i}$, system frequency, ω_{PLL} and phase angle other than reference phase, δ_i are calculated. Once these quantities are calculated, by equating dynamic equations to zero, the operating point can be calculated. Based on the system parameters shown in appendix A, Table A.1, operating point has been determined and listed in appendix A, Table A.2.

3.1.2 Eigenvalue and participation factor analysis

The number of state and eigenvalue are dependent on the dimension of system matrix, A_{system}. By observing the system matrix it is easy to inspect the nature of steady state stability or small signal stability around the operating point [62].

$$[A - \lambda I]\phi_r = 0 \tag{3.21}$$

$$[A - \lambda I]\phi_l = 0 \tag{3.22}$$

Here, λ represents eigenvalue and ϕ_r represents right eigenvector and ϕ_l represents left eigen vector. For non-trivial solution, determinant of $[A - \lambda I]$ equals to zero and the eigenvalues can be calculated using Equation 3.21-3.22.

The right eigen vector is called the mode shape as it provides information about how each of the system state is influenced by the oscillatory mode or in other word, the modal observability of the system. Again, the left eigen vector provides information on the amplitude of the mode obtained from system's initial state. Moreover, information related to controllability is also obtained by left eigen vector. Eigen vectors are important in finding mode sensitivity, transfer function residues and participation factors. Mode sensitivity, transfer function residues and participation factor plays vital role in planning of controller design and analysis of system states. It is to be mentioned that all the eigen values of the system matrix should lie in the left half plane to make the system stable i.e. the position of the real part of complex conjugate must

reside in the left half plane. In case of system instability, real part of atleast one eigenvalue always lies in the right half plane with its complex conjugate.[63].

The natural frequency of oscillation (f) and damping ratio (ζ) can be calculated using expressions given in Equation 3.23-3.24.

$$\zeta = \frac{-\sigma}{\sqrt{(\sigma^2 + \omega^2)}} \tag{3.23}$$

$$f = \frac{\omega}{2\pi} \tag{3.24}$$

Here, σ and ω are real and imaginary part of eigenvalue respectively.

Participation factors are scalars intended to measure the relative contribution of system modes to system states. A participation factors can be positive, zero, or negative. A positive participation factor associated with a particular state means that state is contributing to the oscillation of the system. A negative participation factor indicates a state that is dampening the system oscillation [53]. The participation factor matrix can be calculated by combining the left and right eigenvectors [64] as shown below.

$$P = [P_1, P_2, ...P_n] \tag{3.25}$$

with

$$P_i = \begin{bmatrix} P_1 \\ P_2 \\ \\ .... \\ P_n \end{bmatrix} \begin{bmatrix} \phi_{1i}\psi_{i1} \\ \phi_{2i}\psi_{i2} \\ \\ .... \\ \phi_{ni}\psi_{in} \end{bmatrix}$$

Ultimately, the participation factor matrix is represented as

$$P_{ki} = \Phi_{ki}\psi_{ik} \tag{3.26}$$

Here, right eigen vector and left eigen vector of the i^{th} mode are expressed as Φ_{ki} and ψ_{ik} respectively.

By applying the above mentioned method, the eigenvalue of the studied system has been calculated. To determine the relative contribution of the system modes to system states, participation factor has also been calculated. The eigenvalue of the system is depicted in the figure

3.1. From the figure, it is seen that a wide range of frequency components exist in the eigenvalues. Table 3.1 contains the real and imaginary component of eigenvalues, natural frequency, damping ratio and the states having more than 80% participation.

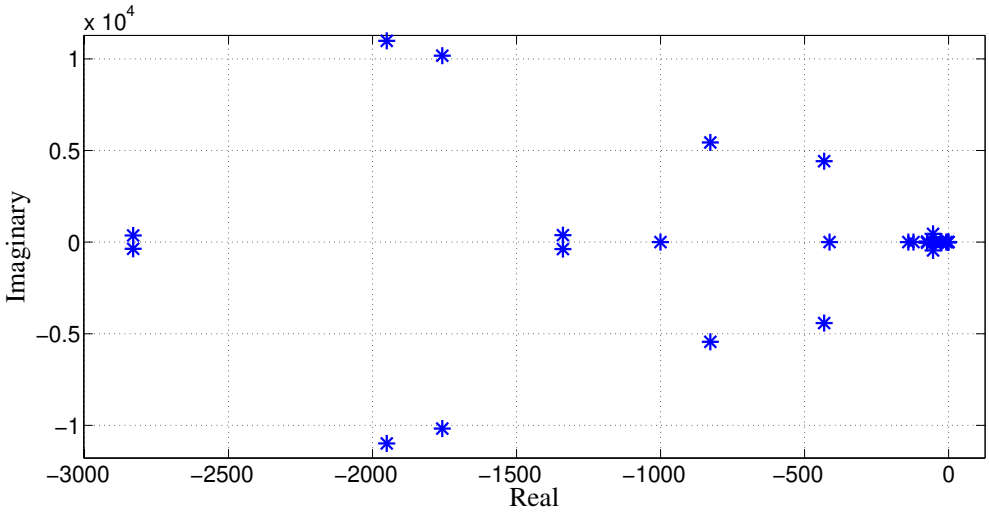

Figure 3.1: Eigenvalue of the system

Based on the frequency components, the Eigen values can be categorized into two categories: i) oscillatory modes and ii) non-oscillatory modes. The table shows there are 14 oscillatory modes and 8 non-oscillatory modes in the system. The analysis of the participation factor was carried out to determine the major participating states in those modes. The states of the PLL, voltage, current and power controller are the major participants in the non-oscillatory modes. Among the non-oscillatory modes, the PLL dominated 17 and 18 modes are the closest to the origin and the mode 22 lies exactly at the origin. These modes are very much crucial in determining stability of the system. Again, among the 11, 12, 13, 19 and 20 modes, voltage and power controller dominated 19 and 20 modes are more closer to origin and lie close to each other than the current controller based 11, 12 and 13 mode. The current controller based 12 and 13 mode is closer to the origin in comparison with the current dominated 11 mode.

The oscillatory modes of the eigenvalues can be categorized into three types: i) High frequency oscillatory mode (3, 4, 5, and 6), ii) Medium frequency oscillatory mode (1, 2, 7, 8, and 10) and iii) Low frequency oscillatory mode (14, 15, 16 and 21). Among the oscillatory frequency modes, modes 1, 2 and 21 are highly damped. All the $v_{odq,i}$ dominated high-frequency oscillatory modes (3-6) are less damped and will highly affect the performance of the system under disturbance. Among medium frequency oscillatory modes, load current dominated mode 7 and 8 are highly damped compared to the PLL dominated mode 10. Among the low-frequency oscillatory modes, voltage and current controller dominated mode 16 is less damped than mode 14 and 15. From the discussion above it can be said that, the proportional and integral gains of voltage controller,

Table 3.1: Eigenvalue of system matrix, A_{system}

Index	Eigenvalue $\lambda = \sigma \pm j\omega$	Natural Freq. $f = \frac{\omega}{2\pi}$	Damping Ratio $\zeta = -\frac{\sigma}{\sqrt{\sigma^2+\omega^2}}$	Mode	Participation Factor
$1, 2$	$-7.1017x10^6 \pm 376.63j$	$7.1017x10^6$	100	1	i_{lineDQ}
$3, 4$	$-2.1039x10^6 \pm 377.26j$	$2.1038x10^6$	100	2	$i_{odq1},\ i_{odq2}$
$5, 6$	$-1950.65 \pm 10987.89j$	11159.70	17.4795	3	v_{oq1}, v_{oq2}
$7, 8$	$-1757.92 \pm 10178.32j$	10329.0228	17.0193	4	v_{od1}, v_{od2}
$9, 10$	$-827.31 \pm 5439.92j$	5502.5214	15.0351	5	v_{oq1}, v_{oq2}
$11, 12$	-432.06 ± 4420.024j	4441.0919	9.7288	6	v_{od1}, v_{od2}
$13, 14$	$-2831.1 \pm 365.92j$	2854.6569	99.1750	7	$i_{loadDQ2}$
$15, 16$	$-1338.91 \pm 381.0371j$	1392.0832	96.1810	8	$i_{loadDQ1}$
17	-1000.23 ± 0	1000.2303	100	9	$v_{od1,f}, v_{od2,f}$
$18, 19$	$-53.8185 + 450.8854j$	454.0859	11.852	10	δ_2
20	$-413.1548 + 0j$	413.1548	100	11	i_{ldq1}, i_{ldq2}
21	$-139.58 \pm 0j$	139.5823	100	12	γ_{d2}
22	$-121.7934 + 0j$	121.7934	100	13	γ_{d1}
$23, 24$	$-74.7013 + 33.5242j$	81.8790	91.2339	14	γ_{q1}, γ_{q2}
$25, 26$	$-25.3199 \pm 31.1291j$	40.1263	63.1005	15	$\varphi_{q1,2}, \gamma_{q1,2}$
$27, 28$	$-1.8833 \pm 4.7142j$	5.0765	37.0975	16	$\varphi_{dq1}, \varphi_{dq2}$
29	$-7.9968 \pm 0j$	7.9968	100	17	$\varphi_{PLL1},\ \varphi_{PLL2}$
30	$-8.006 + 0j$	8.0006	100	18	$\varphi_{PLL1},\ \varphi_{PLL2}$
31	$-48.6515 + 0j$	48.6515	100	19	$\varphi_{d1},\ \varphi_{d2}$
$32, 33$	$-50.1738 \pm 0j$	50.1738	100	20	P_1, P_2
$34, 35$	-50.2594 ± 0.0012j	50.2594	100	21	P_1, P_2, Q_1, Q_2
36	$0 + 0j$	0	∞	22	δ_1

current controller and PLL play a vital role in the crucial states of the system. Thus, their proportional and integral gain needs to be selected suitably for ensuring the optimum stability of the system.

3.1.3 Root locus analysis

To study the effect of controller gains on the stability root locus study has been performed. The root locus of controller gain has been shown in figure 3.2-3.7. As stated in [53], eigenvalues closest to the imaginary axis with low-frequency mode are the most dominant and crucial for the stability of system and eigenvalues close to the real axis affects the damping and dynamic properties of the system. It is seen that as the k_{pv} increases, the eigenvalues moves away from the imaginary axis improving the damping performance and away from real axis making the system more oscillatory and ultimately becomes unstable. Again, as the k_{iv} and k_{ic} increases, eigenvalues move away from real axis decreasing the system damping ratio. For the increase in k_{pc} system moves from stable to unstable region and then again moves back to the stable region with higher oscillatory property. Again, as the $k_{p,PLL}$ increases, dominant eigenvalues

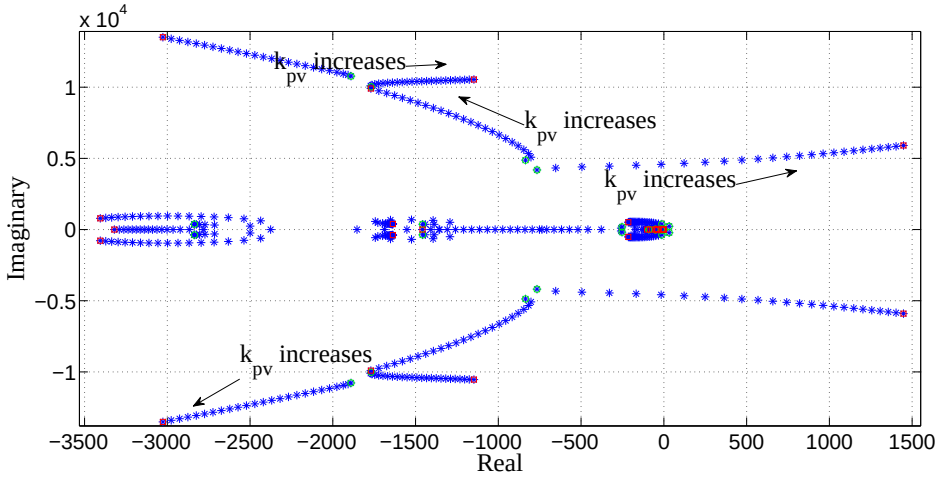

Figure 3.2: Root locus of the system as $k_{pv}\epsilon[0.005, 5]$

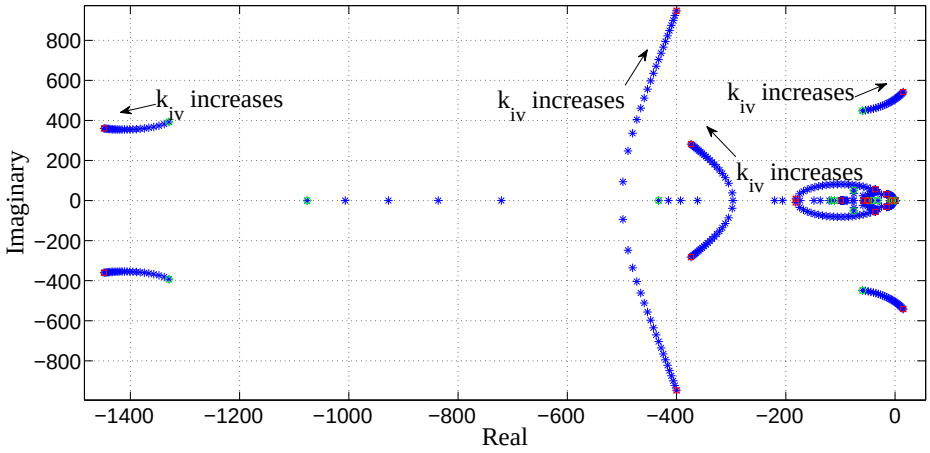

Figure 3.3: Root locus of the system as $k_{iv}\epsilon[2.5, 500]$

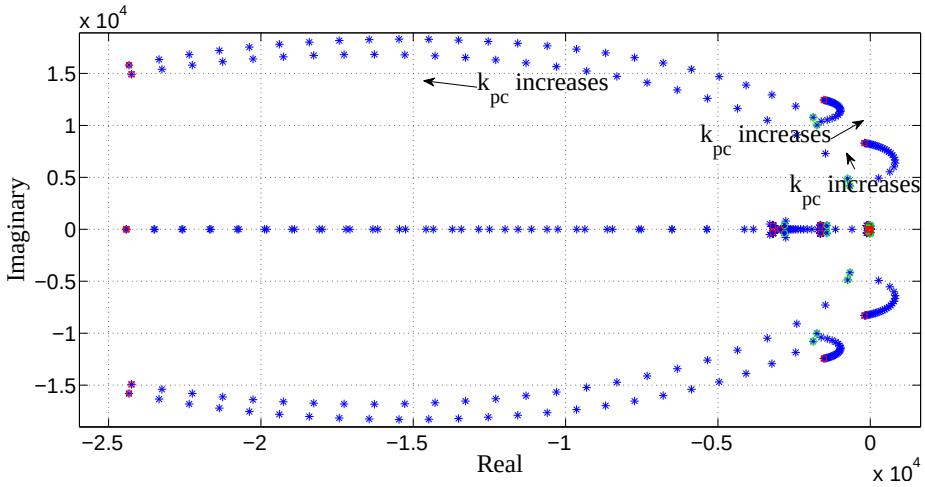

Figure 3.4: Root locus of the system as $k_{pc}\epsilon[0.01, 100]$

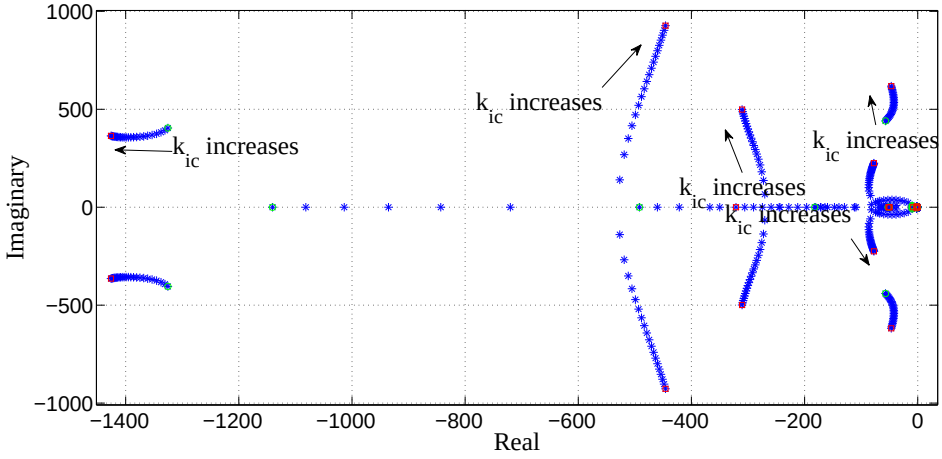

Figure 3.5: Root locus of the system as $k_{ic}\epsilon[10, 1000]$

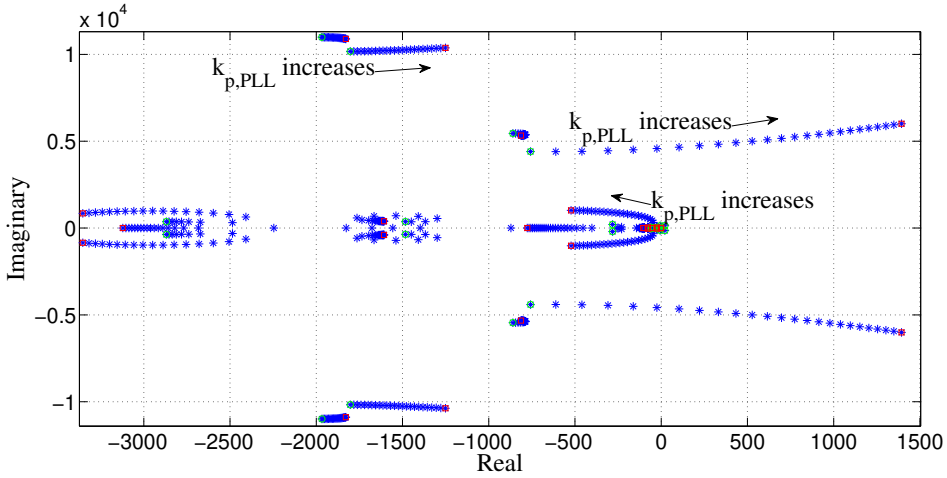

Figure 3.6: Root locus of the system as $k_{p,PLL}\epsilon[0.025, 2.5]$

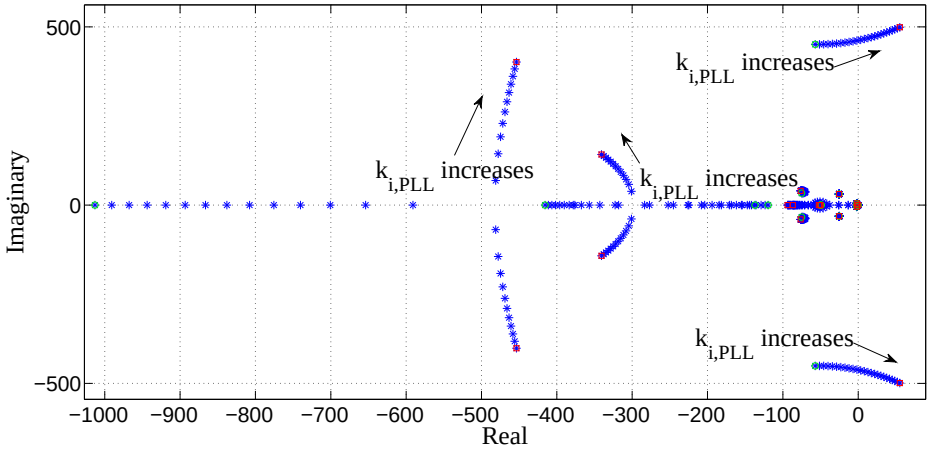

Figure 3.7: Root locus of the system as $k_{i,PLL}\epsilon[0.2, 75]$

move closer to imaginary axis which decrease the damping ratio of the system and become unstable. The integral gain of the PLL also affects the dominant root significantly and may lead to instability. So, it is seen that the integral and proportional gain of the controller play a vital role in the system stability and proper selection of these parameters can provide better stability of the system.

3.2 Objective function

From the root locus analysis, it has been found that integral and proportional gains of the controllers have significant effect on the damping and oscillation of the system. Here, the objective is to increase the damping of the system and decrease the oscillation of the system. To increase the damping of the system, the real part of eigenvalue $|\sigma|$ need to be increased or in other words $-\sigma$ need to be decreased. Again, to make the system less oscillatory the imaginary part of eigenvalue, ω need to be decreased. So, the objective function for this work need to be defined in such a way that optimization of that objective function improves system damping but impairs oscillation. In this work, the controller design problem is formulated as the minimization of an eigenvalue based objective function [52]. The objective function for this work is defined as

$$f_{\min} = -\sum_{i=1}^{n} \frac{\sigma_i}{(\sigma_i^2 + \omega_i^2)^{\frac{1}{2}}} \tag{3.27}$$

Here, σ_i and ω_i are the real and imaginary part of the i^{th} eigenvalues obtained from the system matrix, A_{system}.

3.3 Optimization of parameters

Earlier works reported in [24],[50] proposed PSO and GA for optimizing the controller parameters of islanded microgrids. However, they performed the optimization within a limited search space finding the solution variables. Hence, the algorithm could not exploit the entire search space. Moreover, they did not compare their designed controller performance against other optimizing algorithms which could lead to better outcome. Furthermore, in [24], the objective function for the optimization involved only the real part of Eigen value which would optimize only the damping property of the system but not the oscillatory property under disturbances. This work eliminates the shortcoming of the previous mentioned works by exploiting the entire search space and incorporating oscillatory part in the objective function as shown in Equation 3.27. Here, the optimization of the parameters have been accomplished in two stages-stage I: determination of parameter bound by exploiting the entire search space and Stage II:

determination of ultimate optimized parameter within the bound found in stage I.

3.3.1 Stage I: Determination of the parameter bound

As mentioned earlier, previous works have optimized the parameters within a predefined search space. As a result, ultimate optimization could not achieved in those works [24, 50]. Here, instead of putting arbitrarily chosen bounds on the optimizer search space, the bounds are found by applying nature inspired optimization algorithms: Genetic algorithm (GA), Particle Swarm Optimization Algorithm (PSO) and Grey Wolf Optimization algorithm (GWO). A key characteristic of these algorithms is that they converge quickly to the near-optimal solution.

3.3.1.1 Genetic Algorithm

Genetic algorithm (GA) [65] is stochastic search technique used to find approximate solutions to optimization and search problems. A genetic or evolutionary algorithm implements the idea of evolution technique found in nature to the issue or problem of determining an optimal solution to a problem. In genetic algorithm, the given problem is encoded in a series of genes or bit strings which the algorithm manipulates. These bit strings are coded representation of input variables. The main concept of GA is to simulate the process in natural system which is required for evolution, specially for those following the concept first invented by Charles Darwin. Genetic algorithm is widely used in engineering problems.

As a preparation to start the optimization process, a GA requires a group of initial solutions as the first generation. The generation no. 1 or the first generation is usually a group of arbitrarily generated solutions created by an arbitrary number generator. The generation or population size species how many individuals there are in each generation. With a large population size, the genetic algorithm searches the solution space more thoroughly and gives more possibility to return the global optimum. As a result, the population size in genetic algorithm should be big enough so that there could be a reasonable amount of genetic diversity in the population. Besides, the number of generation or population specifies the highest number of iteration for the genetic algorithm to perform. If this number is too low, the genetic algorithm is not able to converge to the global solution.

The fitness function assessment is performed to measure how close that individuals fit the desired result. A fitness function could be either complex or simple depending on the optimization problem addressed. In the situation when the minimization is required, the most fitted individual solution owns the lowest numerical value of the corresponding fitness function.

In genetic algorithm, individuals are selected in accordance to a fitness based process. The

operator of selection is made up of ranking and selection progress by which more copies of the individuals that fit the optimization problem better will be produced in the upcoming generation. In GA, there are basically two ways using which a new population can be selected. They are: Roulette Wheel Selection (RWS) and Stochastic Universal Sampling (SUS).

The individuals will be recombined (crossover) after the selection. This operation is to produce two new individuals from two existing individuals selected by the operator of selection by cutting them at one or more position and exchanging the parts following the cur. The new individuals therefore can inherit some parts of both parents' genetic material. There are various ways of doing this : arithmetic crossover,one point crossover, two point crossover, cycle crossover and uniform crossover.

Mutation is another operator to produce latest individuals. The dissimilarity is that the new individual is generated from an old single one. In this operation, the individual bit values are arbitrarily reversed according to a specified feature. A mutation can also helps the GA to avoid local optimums and find the global best solution The group of individuals produced after the mutation is the second generation. The fitness value of each individual in the second generation is computed again and the cycle does not stop until the result is close enough or after a certain generation.

Steps of GA algorithm

- Step 1: Generate random population.
- Step 2: Evaluate the fitness of each individual in the population.
- Step 3: Generate a new population through repetition of the following steps until the new population is complete.
  - Selection: Select two parent from a population according to their fitness (the better the fitness, the bigger the chance to be selected).
  - Crossover: With a probability of cross over, cross over the parents in order to form new offspring.
  - Mutation: With a mutation probability, mutate new offspring at each locus.
- Step 4: Use the new population obtained from step 3.
- Step 5: Repeat step 2 - step 4 until stopping criteria is fulfilled.

3.3.1.2 Particle Swarm Optimization

The particle swarm optimization (PSO) is a novel population based metahuristic algorithm invented by Kennedy and Eberhart in 1995 [66]. PSO uses the social manners for instance, fish schooling and birds flocking to provide alternative solution to optimization problem from a given system, generally non-linear in nature. The procedure that PSO follows is about sharing individual knowledge of fishes or birds originated from group communication during the period of migration or food searching. However, it is very common that the finest path of food searching will not be known to all and once it is identified by one member, the rest of the group follow that path.

In PSO, every individual from the population is known as a particle and the entire population is named as swarm. The algorithm begins with an arbitrarily introduced population and moves in arbitrarily selected route. Each particle remembers the previous best records of its own and neighbors during the period of crossing in the searching space. Particles of a swarm learn better positions to one another as well as progressively alter their very own position and speed originated from the best position of whole particles. At whatever points every one of the particles have finished their development to another position, the subsequent stage starts. All particles in this manner will in general fly towards better positions over the searching procedure until the swarm go to an ideal position of the objective function.

Consider a search space of N-dimensional shape at the starting (N denotes the number of particle that needs to be optimized) and x_i^o s are produced within the boundary limit $x_{min} < x_i^o < x_{max}$ where x_{min} and x_{max} are denoted as lower and upper boundary limit of the search region. Current fitness value are calculated from the initial fitness of x_i^o. It is to be mentioned that minimum current fitness values are recorded as personal best $j_{ind,i}^o$ whereas the lowest value of personal best is termed as global best j_{best}^0. The position of particle corresponding to pbest and gbest is recorded as p_{best}^0 and g_{best}^0 respectively.

In the event that x_i^t indicates the position vector of particle i in the N-dimensional search space at time step t. At that point, the situation of every particle is modified from time to time in the search space according to equation 3.28-3.29.

$$v_i^{t+1} = v_i^t + c_1(pbest_i^t - x_i^t) + c_2(gbest_i^t - x_i^t) \tag{3.28}$$

$$x_i^{t+1} = x_i^t + v_i^{t+1} \tag{3.29}$$

with $x_{mini} < x_i^0 < x_{maxi}$

Here, v_i^t is the velocity vector of particle i that drives the advancement procedure and reflects both individual and social experience information from every one of the particles; x_{min} and x_{max}

are the lowest and highest points of confinement of the search space, separately.

In this way, in a PSO strategy, all particles are started arbitrarily and assessed to process fitness together with finding the individual (best estimation of every particle) and global (best estimation of particle in the whole swarm). After that, a loop begins to locate an ideal position. Advancing first, the particles' speed is modified by the individual and global bests, and afterward every particle's position is updated by the present velocity. The loop is finished with a stopping criteria determined beforehand.

Steps of PSO algorithm

- Step 1: Define the problem space and set the boundaries.
- Step 2: Initialize an array of particles with random positions and velocities.
- Step 3: Evaluate the fitness of each particle.
- Step 4: Compare the current fitness value with the particle's previous best value (pbest). If the current fitness value is better, assign the current value to pbest update the current coordinates.
- Step 5: Determine the current global minimum among the molecule's best position (gbest).
- Step 6: If the current global minimum is superior to gbest, employ the present value to gbest and update the current global best positions.
- Step 7: Update the velocity as per Equation 3.28.
- Step 8: Move every particle to the new position as per Equation 3.29 and go back to Step 3.
- Step 9: Repeat Step 3 to Step 8 until the stopping criteria is fulfilled.

3.3.1.3 Grey Wolf Optimization

Grey Wolf Optimization (GWO) algorithm is one of the recently (2014) invented algorithms inspired by grey wolf belonging to canidae family. According to position, Grey wolves are placed in the highest rank as predators, implying that they are at the top of the natural way of life. For the most of the time, grey wolves like to live in a pack. The bunch estimate is 5 $\sim$12 by and large. In the bunch, they have a severe social predominant pack order.

The pioneers are a male and a female, called alphas.The alpha is in the charge of decision making about chasing, time to wake, sleeping place etc for the most part. The alpha's choices are

managed to the pack. However, some sort of popularity based conduct has too been watched, in which an alpha trails other members of the pack. In social occasions, the whole pack recognizes the alpha by holding their tails down. The alpha wolf is likewise called the predominant wolf since his/her requests ought to be trailed by the pack. The alpha wolves are just permitted to mate in the pack. Strangely, the alpha isn't really the most grounded individual from the pack in any case, rather, the best regarding dealing with the pack. This demonstrates the association and order of a pack is remarkably significant than its quality.

The second position in the hierarchy system of grey wolves is beta. The subordinate wolves are the betas that assist the alpha in basic leadership or the other pack activities. The beta wolf most likely the best contender to be the alpha in the event that one of the alpha wolves passes away or turns out to be old. The beta fortifies the alpha's directions all through the pack and offers criticism to the alpha.

The most minimal positioning dim wolf is omega. The omega plays the job of substitute. Omega wolves dependably need to submit to all the other prevailing wolves. They are the last wolves that are permitted to eat. It might appear the omega isn't a significant individual in the pack, yet it has been seen that the entire pack face inner battling and issues if there should be an occurrence of losing the omega.

If a wolf is no longer alpha, beta, or omega, he/she is known as subordinate (or delta in some references). Delta wolves are inferior to alphas and betas, however, they are superior to the omega. Scouts, sentinels, elders, hunters, and caretakers belong to this category [67].

In order to model mathematically the social hierarchy of wolves at the time of designing GWO, the most fit solution are regarded as the alpha (α). Consequently, the second best solutions are named beta (β) and the third best solutions are named delta (δ). The remaining of the candidate solutions are regarded as to be omega (ω). In the GWO algorithm, the optimization is dictated by α, β, and δ. The ω wolves just follow these three wolves[68].The location of omega wolf is updated using the following equation

$$X_{ij}(t+1) = \frac{X_{\omega\alpha ij} + X_{\omega\beta ij} + X_{\omega\delta ij}}{3} \tag{3.30}$$

Here, $X_{ij}(t+1)$ is the new location of j^{th} element of i^{th} omega location.
$X_{\omega\alpha ij}$ is the new location of j^{th} element of omega's location vector, X_i based on the j^{th} element of alpha's location vector, X_α.
$X_{\omega\beta ij}$ is the new location of j^{th} element of omega's location vector, X_i based on the j^{th} element of beta's location vector, X_β.

$X_{\omega\delta ij}$ is the new location of j^{th} element of omega's location vector, X_i based on the j^{th} element of delta's location vector, X_δ.

$X_{\omega\alpha ij}, X_{\omega\beta ij}, X_{\omega\delta ij}$ are calculated using the following equation

$$\begin{aligned} X_{\omega\alpha ij} &= X_{\alpha j} - A_{\omega\alpha ij}.(D_{\omega\alpha ij}) \\ X_{\omega\beta ij} &= X_{\beta j} - A_{\omega\beta ij}.(D_{\omega\beta ij}) \\ X_{\omega\delta ij} &= X_{\delta j} - A_{\omega\delta ij}.(D_{\omega\delta ij}) \end{aligned} \tag{3.31}$$

Here, $X_{\alpha j}, X_{\beta j} and X_{\delta j}$ are the location of the j^{th} element of alpha, beta and delta respectively. $A_{\omega ij}, A_{\beta ij} and A_{\delta ij}$ are the j^{th} element of t^{th} omega's randomization co-efficient vectors, $A_{\omega\alpha}, A_{\omega\beta}$ and $A_{\omega\delta}$.
$D_{\omega\alpha ij}, D_{\omega\beta ij} and D_{\omega\delta ij}$ is the distance between j^{th} element of omega's location vector, X_i and j^{th} element of alpha, beta and delta's location vector, $X_\alpha, X_\beta and X_\delta$.

$A_{\omega\alpha}, A_{\omega\beta} and A_{\omega\delta}$ are calculated using following equations

$$\begin{aligned} A_{\omega\alpha ij} &= 2ar - a \\ A_{\omega\beta ij} &= 2ar - a \\ A_{\omega\delta ij} &= 2ar - a \end{aligned} \tag{3.32}$$

Here, $r = rand[0, 1]$ is a random number in the interval $[0, 1]$ and a is called decision variable which is uniformly decreased from 2 to 0 during course of iteration which is used to model the exploration and encircling behavior of wolves.

Steps of GWO algorithm

- Step 1: **Initialization:** Initialize the main population of grey wolf randomly, figure their fitness and discover the best wolf as alpha, second best as beta and third best as delta. The remainder of wolf expected as omega.
- Step 2: **Updating the position of grey wolf:** The situation of the wolf is modified time to time on the basis of the location of three wolfes (alpha, beta and delta).
- Step 3: **Replacing the present position with the better one:** Update the position of alpha, beta or delta if new position of wolf have better fitness.
- Step 4: **Checking the stopping criterion of the algorithm:** If end criterion is fulfilled, return the alpha as the best solution for given issue. Again if find something different, back to refresh wolf position steps.

3.3.2 Stage II: Determination of ultimate optimized parameter

In the second stage, two algorithms namely, Exhaustive Search (ES) and Interior Point (IP) algorithm have been used to find the ultimate optimal solution within the bound defined by the three nature inspired algorithms stated above.

3.3.2.1 Exhaustive Search

The algorithm that tries every possible solution is known as exhaustive search [69], also known as brute force (BF) method. It is a straightforward method used to solve problems of combinatorial problems. It produces each and every element of the domain of the problem depending on the satisfaction of constraints of the problem and then find a desired element. The main advantage of this algorithm is that it is widely applicable, particularly to search-oriented problems. It provides optimum result, given correct generation and checking.

Steps of Exhaustive search Method

- Step 1: Generate possible combination of solution
- Step 2: Evaluate the fitness of each combination of solution.
- Step 3: Determine the combination that optimizes the fitness function the most.

3.3.2.2 Interior Point

Interior point methods are a type of algorithm that are used in solving both linear and nonlinear convex optimization problems that contain inequalities as constraints. From a geometric standpoint, interior point methods approach a solution from the interior or exterior of the feasible region, but are never on the boundary. The Interior-Point method relies on having a linear programming model with the objective function and all constraints being continuous and twice continuously differentiable. In general, a problem is assumed to be strictly feasible, and will have a dual optimal that will satisfy Karush-Kuhn-Tucker (KKT). The problem is solved either by iteratively solving for KKT conditions or to the original problem with equality instead of inequality constraints, and then applying Newton's method to these conditions.

There are two important interior point algorithms: the barrier method and primal-dual IP method. The primal-dual method is usually preferred due to its efficiency and accuracy. Major differences between the two methods are that there is only one loop/iteration in primal-dual because there is no distinction between outer and inner iterations as with the barrier method. In this work, primal dual interior point method [70] has been used.

3.4 Comparison of performance of algorithms

To make a fair comparison of the algorithms, the complete analyses have been performed in the same platform, 2.5 GHz Intel Core i5 processor with 8 GB RAM (Random Access Memory) using MATLAB 2013b and IBM SPSS 16 software. For comparison among the algorithms, time domain simulation and statistical analysis have been accomplished.

3.4.1 Time domain analysis

One of the most effective ways to depict the response of the system subjected to disturbance is the time domain analysis. In time domain analysis, mode is perturbed and the behavior of state variable is calculated by solving differential equations using some numerical integration techniques with the known initial values [71]. In this case, the initial values are the steady state operating point. It is to be noted that dynamic characteristics of the state such that rise time, settling time and percentage overshoot can be perceived easily from time domain analysis. When a system is subjected to small disturbance it experiences transient reaction with a oscillation that may sustain or decay. The certain behavior of the system relies on the parameters of the system. Since any system can be modeled with a direct differential condition, the arrangement of this direct differential condition gives the reaction of the system. The depiction of a system by direct differential condition of elements of time and its outcome is called time domain simulation. From the time domain simulation it is seen that transient response is started from steady state operating point and oscillates for a specific period and afterward turns out to be consistent after transient disappears.

3.4.2 Statistical analysis

In this work, statistical analyses such as Kolmogorov-Smirnov test and Permutation test have been employed to identify the significant differences among the algorithms. For that purpose, algorithms have been executed several times (30) in MATLAB to obtain corresponding fitness values. These fitness values have been analyzed in IBM SPSS software. Here, Kolmogorov-Smirnov test is performed with the null hypothesis, H_0 and alternate hypothesis, H_1. The null hypothesis assumes that the data sample fits the normal distribution whereas alternative hypothesis assumes that the data sample does not fit normal distribution with 5% significant level. Besides, permutation test has been performed with null hypothesis, H_0 assuming mean data sample does not differ significantly and alternate hypothesis, H_1 assuming difference in mean in the data sample obtained from 30 individual run with 5% significance.

Chapter 4

Simulation and Results

In this chapter, the simulation and result of the work have been discussed. In section 4.1, value of various parameters, number of iteration, stopping criteria have been discussed. The results obtained from two step parameter optimization along with comparison of fitness value, time domain analysis and statistical analysis have been presented in section 4.2.

4.1 Simulation setup

Various parameters such as population size (= 500), the number of iterations (= 100) and stopping criteria (terminates when generation/iteration (=100) exceeds) are kept constant for each of the GA, PSO and GWO algorithm to perform the comparative study of these algorithms. Since randomness is an integral part of these algorithms, these algorithms are run 10 times to find the upper bound and lower bound of the parameters.

Firstly in GA, the selection function is chosen as roulette selection in which a random number is used to select one of the sections with a probability equal to its area [72]. Arithmetic crossover function has been chosen such that the created children become the weighted average of the parents and uniform mutation with the rate of the vector entries to be mutated being 0.001 [73].

In PSO, there are two parameters: cognitive parameter (C_1) and social parameter (C_2). The cognitive parameter aids the particles to learn from their neighboring swarm members and the social parameter helps the particle to learn in a global perspective. Here, $C_2(= 2) > C_1(= 1.5)$ implies greater learning of swarm particle to set its position from a global perspective in the successive iteration [74].

Grey Wolf Optimization (GWO) is a recently developed meta heuristic optimization technique based on the effect of leadership hierarchy and hunting mechanism of wolves in nature [75]. GWO only requires defining population size and a maximum number of iteration for its

functionality. Here, 500 populations and 100 maximum iterations have been used.

4.2 Results of 2-step parameter optimization

The bound of the parameters obtained from 10 individual run of these algorithms has been listed in table 4.1. These values are used as upper bound and lower bound in the Exhaustive Search (ES) and Interior Point (IP) algorithm to find the optimized value listed in table 4.2. From the table, it is seen that the range of the values obtained using PSO is very high compared to the values obtained from the GWO and GA. Among the values obtained from GA and GWO, the range of the values from GWO is higher than the values from GA.

Table 4.1: Controller parameter bounds obtained from GA, PSO and GWO

Controller	Genetic Algorithm		Particle Swarm		Grey Wolf	
Parameters	Max	Min	Max	Min	Max	Min
$k_{pv,d}$	0.6119	0.1477	31.0545	7.8654	22.5543	0.5584
$k_{pv,q}$	0.1919	0.0036	0.3344	0.2151	27.6498	0.0258
$k_{iv,d}$	0.9579	0.3587	1822.998	14.2178	2004.7935	0.2875
$k_{iv,q}$	0.9072	0.3003	36.2125	0.1539	29.6252	0.0381
$k_{pc,d}$	0.999	0.3876	639125.766	22451.0196	23607.4398	41.0677
$k_{pc,q}$	0.993	0.7992	15735.7698	112.4195	112.8294	0.3427
$k_{ic,d}$	0.6255	0.0105	28413.379	11.2431	303126	1.8111
$k_{ic,q}$	0.5621	0.0659	1472.2957	38.5605	113.3055	0.6606
$k_{p,PLL}$	0.0912	0.0274	64.8856	3.6744	2.7225	0.0001
$k_{i,PLL}$	0.9948	0.1422	1369.6193	2.7637	47.3522	0.0001

Table 4.2: Controller parameter values obtained from Exhaustive Search (ES) and Interior Point (IP) algorithm

	Genetic Algorithm		Particle Swarm		Grey Wolf	
Parameters	ES	IP	ES	IP	ES	IP
$k_{pv,d}$	0.2661	0.332	8.295	10.1469	15.5172	6.1832
$k_{pv,q}$	0.052	0.018	0.3264	0.3313	0.8815	1.3124
$k_{iv,d}$	0.368	0.639	31.9227	367.8557	1296.6123	416.2484
$k_{iv,q}$	0.6568	0.578	23.2659	0.2575	1.7029	0.0958
$k_{pc,d}$	0.976	0.9466	508813.379	132315.357	17430.8797	4730.0277
$k_{pc,q}$	0.9639	0.9658	8338.1594	3169.6468	111.0871	103.7645
$k_{ic,d}$	0.0154	0.3456	8284.4852	5685.7272	2.8661	2.9965
$k_{ic,q}$	0.3805	0.3454	939.4172	302.2426	84.5742	49.4008
$k_{p,PLL}$	0.0503	0.0371	29.7178	13.4388	1.5775	1.5512
$k_{i,PLL}$	0.2394	0.2121	749.5731	274.611	44.934	43.6685

In general, the values of the parameter for a particular algorithm differ very less in exhaustive search and interior point algorithm as seen from table 4.2. For some parameters ($k_{pc,d}$), there is

Table 4.3: Fitness value (FV) and execution time (ET) of GA, PSO and GWO for finding the bound

	Best			Average			Worst		
	GA	PSO	GWO	GA	PSO	GWO	GA	PSO	GWO
FV	-0.1656	-0.9775	-0.9777	-0.1641	-0.9772	-0.9772	-0.1623	-0.9765	-0.2123
ET	232.97	232.64	228.38	237.571	235.62	229.46	264.23	241.68	230.47

a significant amount of variation in values obtained from the interior point and the exhaustive search algorithm. However, this variation is seen in the values from each of the algorithms for a particular parameter.

As stated earlier, to make a fair comparison among different algorithms, various parameters have been kept similar while the algorithms have been executed in MATLAB. Table 4.3 lists fitness value and execution time categorized by the best, average and worst of GA, PSO and GWO for finding the upper and lower bound of the parameters.

From table 4.3, it is observed that the fitness value of objective function obtained from the algorithms is not close to each other. The PSO and GWO algorithm give the best minimized value $(-0.9775(PSO) and -0.9777(GWO))$ of the objective function whereas the GA gives the worst minimized value (-0.1656) of the objective function. In the best and average case, the fitness value obtained from GWO and PSO do not differ much. However, in worst case scenario, the difference between GWO and PSO fitness value is significant. Again, there is a significant amount of variation in the execution time of these algorithms. The difference in the execution time is the highest in the worst case scenario and the least in the worst case scenario between GA and GWO. In all the cases, GWO takes the least amount of time and GA takes the highest amount of time in execution.

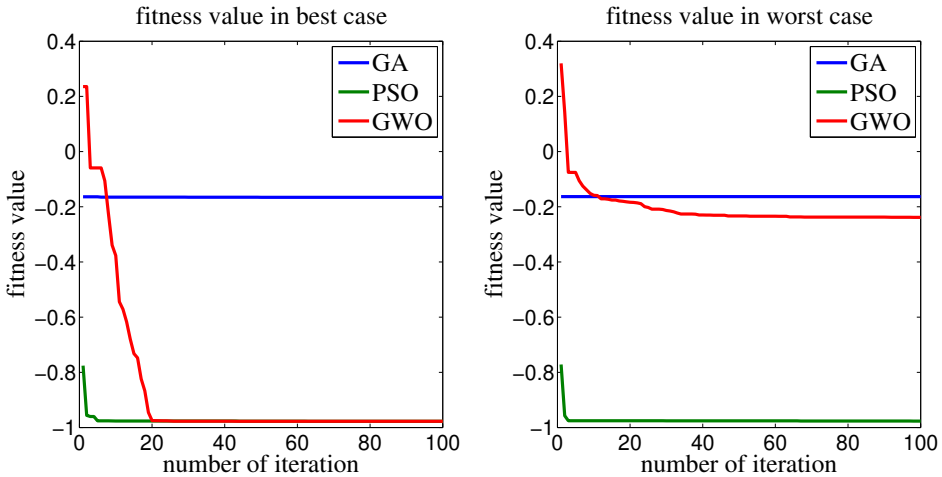

Figure 4.1: Locus of the fitness value from GA, PSO and GWO

Again, from the trajectory of the locus shown in figure 4.1, it is observed that in GWO, the

locus of the fitness value reaches to its optimum value a little slower than PSO in both best case and worst case while the locus of the fitness value for GA remain almost a straight line.

4.2.1 Comparative analysis regarding fitness value and execution time

Table 4.4: Comparison of Interior Point (IP) and Exhaustive Search (ES) algorithm

		GAES	GAIP	PSOES	PSOIP	GWOES	GWOIP
Fitness Value	Best	-0.1663	**-0.1642**	**-0.9768**	-0.9766	-0.9762	-0.9702
	Avg.	-0.1654	**-0.1642**	-0.9679	**-0.9766**	-0.9673	-0.9702
	Worst	**-0.1622**	-0.1642	-0.9679	**-0.9766**	-0.9468	-0.9702
Execution Time	Best	6.2490	6.4314	6.1782	**6.7544**	6.1639	**4.5336**
	Avg.	6.4412	6.5668	6.2757	**6.9235**	6.2543	**4.7586**
	Worst	6.8131	6.6867	6.3651	**7.3360**	6.7819	**5.4351**

Since randomness and probability is the characteristic of all optimization algorithms, here, the comparative performance among the adopted algorithms from a statistical point of view is presented. Table 4.4 shows the best, average and worst case of the fitness values and execution times obtained from 30 individual runs for all the six combinations between the first stage algorithms: GA, PSO , GWO and the second stage algorithms: ES and IP. It can be seen from the table that, the fitness values obtained from GAES ($bestcase$: -0.1663) and GAIP ($bestcase$: -0.1642) are the worst whereas the fitness values obtained from PSOES ($bestcase$: -0.9768), PSOIP ($bestcase$: -0.9766), GWOES ($bestcase$: -0.9762) and GWOIP ($bestcase$: -0.9702) are almost identical. However, considering the average fitness value from 30 individual runs, PSOES (-0.9679) and PSOIP (-0.9766) returns slightly better performance compared to the average fitness values obtained from GWOES (-0.9673) and GWOIP (-0.9702), respectively. Considering the algorithm execution time, from table 4.4 it is found that on an average, GWOIP ($4.7586sec.$) takes the minimum amount of time for completing an individual run while PSOIP ($6.9235sec.$) consumes the maximum amount of time. In the best case, the execution time for GWOIP ($4.5336sec.$) is found to be the smallest whereas the PSOIP ($-6.7544sec.$) execution time is found to be the largest. From these results, it can be inferred that GAES and GAIP performance is relatively poor and on an average, PSOIP provides better optimization than GWOIP but takes a larger amount of time than GWOIP. However, considering only the minimum fitness value, the best optimization is obtained with PSOES.

4.2.2 Time domain analysis

In order to have better insight into the comparative performances among the optimizing algorithms, nonlinear time domain analysis of the system has been performed. The system

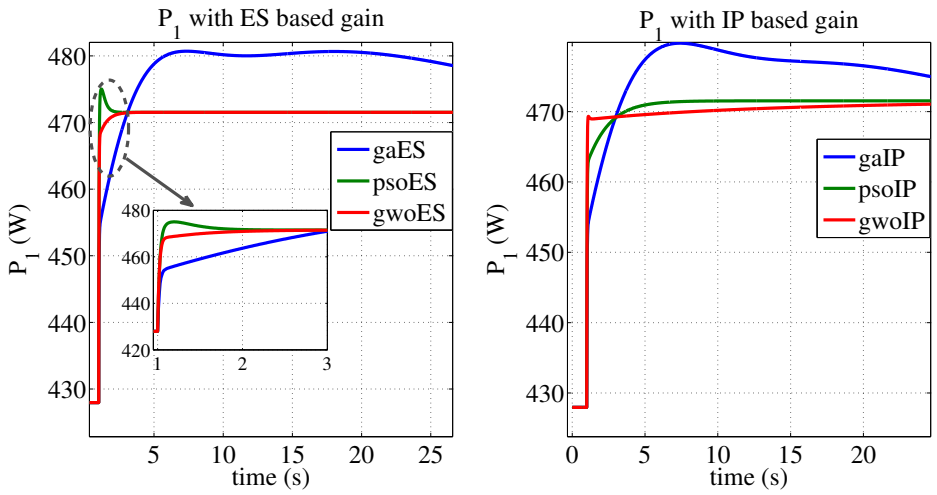

Figure 4.2: Response of real power output of inverter 1, P_1

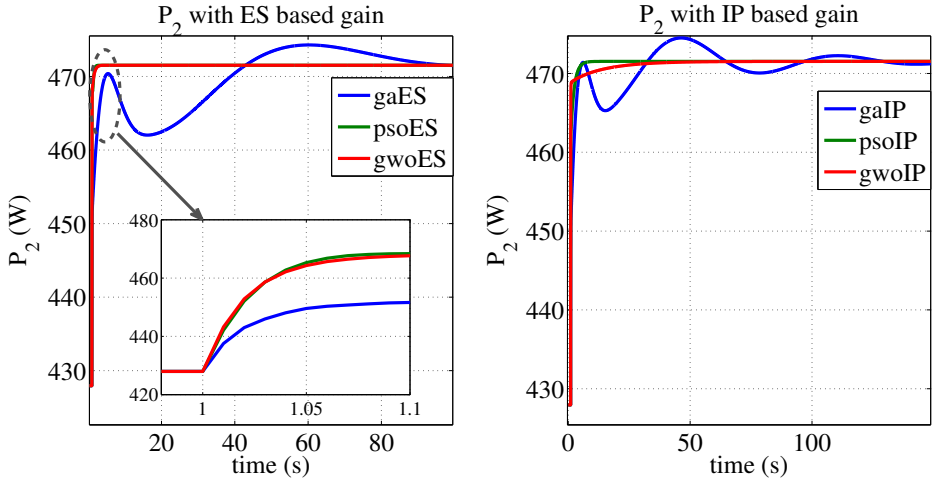

Figure 4.3: Response of real power output of inverter 2, P_2

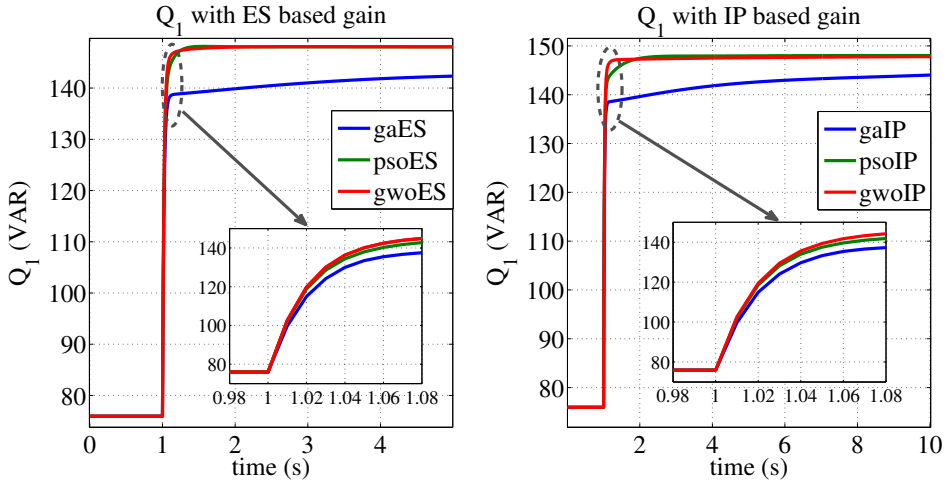

Figure 4.4: Response of reactive power output of inverter 1, Q_1

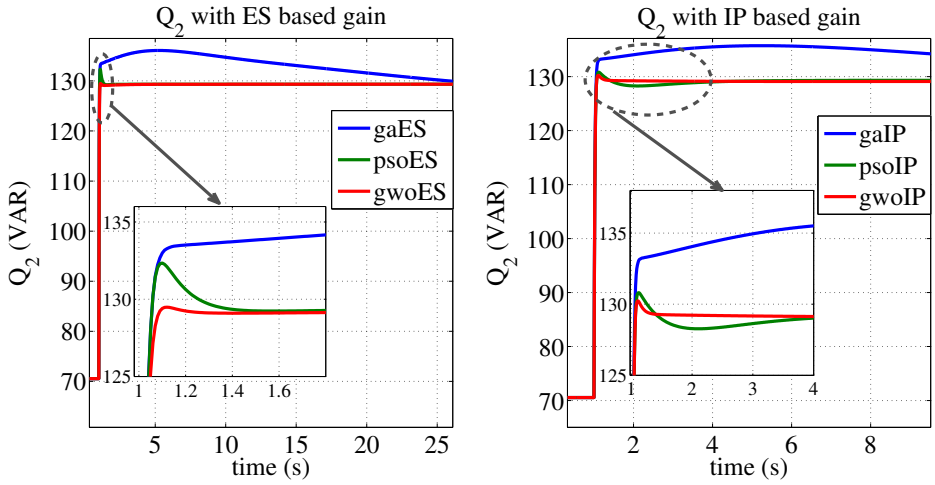

Figure 4.5: Response of reactive power output of inverter 2, Q_2

dynamics is initiated by applying step load changes (1000 unit) at all the load buses at time 1.0 sec. The rise time, settling time and percentage overshoot of system variable have been recorded. The Figure 4.2-4.5 shows real power, P and reactive power, Q response of the system and the table 4.5 lists the rise time, settling time and percentage overshoot for P and Q.

Table 4.5: Rise time (R.T), settling time (S.T) and % overshoot (O.S) for P and Q of inverters

		GA		PSO		GWO	
		ES	IP	ES	IP	ES	IP
P_1	R.T(s)	4.8389	3.9209	4.5178	**2.0492**	4.53012	9.101
	S.T(s)	83.5112	88.6951	**1.6597**	4.4439	1.8153	16.095
	% O.S	1.9487	1.7396	0.7425	$9.17\text{x}10^{-5}$	$7.53\text{x}10^{-4}$	**0**
Q_1	R.T(s)	1.8211	1.9785	0.0610	0.0661	**0.0504**	0.0535
	S.T(s)	**1.1908**	69.5022	**1.1908**	1.6198	1.1287	1.1679
	% O.S	0.0650	2.1037	0.0650	0.0013	0.0355	**0**
P_2	R.T(s)	2.4106	2.5642	**0.0611**	1.1244	0.0809	0.0738
	S.T(s)	83.5237	88.7008	**1.6602**	4.4342	1.8195	16.0954
	% O.S	0.5831	0.6289	$1.44\text{x}10^{-6}$	$9.37\text{x}10^{-5}$	$8.68\text{x}10^{-4}$	**0**
Q_2	R.T(s)	**0.0353**	0.0354	0.0359	0.0396	0.0418	0.0387
	S.T(s)	56.8790	73.1413	1.2092	1.1793	1.0689	**1.0597**
	% O.S	124.6758	4.9576	2.3272	1.1509	**0.1216**	0.7006

It is seen that the response with GA base gains is the worst. For real power output of inverter 1, rise time is minimum with PSO IP based gains and maximum with GWO IP based gains. The settling time is maximum with GA IP gains and minimum with PSO ES gains but the maximum and minimum overshoot of P_1 occurs with GA ES and GWO IP based gains respectively. The minimum rise time and settling time for inverter 1 reactive power output, Q_1 is obtained with GWO ES and PSO ES gains respectively but the minimum overshoot of Q_1 is obtained with GWO IP gains. The rise time of inverter 2 real power output, P_2 is minimum

with PSO ES gains. Although the settling time of P_2 is minimum for PSO ES gains, minimum overshoot is obtained with GWO IP gains. Again, rise time of inverter 2 reactive power output, Q_2 is minimum with GA ES gains and it is maximum with GWO ES gains.

Again, it is seen that the output current response in figure 4.6 - 4.9 of both inverter 1 and inverter 2 has the worst rise time, settling time and percentage overshoot for GA based gains as shown in table 4.6. Except q axis output current of inverter 2, all the remaining inverter output currents has similar rise time for PSO and GWO based gain. D axis output current of

Table 4.6: Rise time (R.T), settling time (S.T) and % overshoot (O.S) for i_{odq1} and i_{odq2} of inverters

		GA		PSO		GWO	
		ES	IP	ES	IP	ES	IP
i_{od_1}	R.T(s)	1.1099	1.3031	0.0083	0.0083	**0.0081**	0.0082
	S.T(s)	51.9201	69.4224	1.1687	1.4515	**1.0705**	1.1180
	% O.S	2.2278	4.3089	0.1325	0.1455	0.0865	**0**
i_{oq_1}	R.T(s)	0.6572	0.7994	0.0084	0.0088	0.0082	**0.0080**
	S.T(s)	83.3445	88.5088	1.6354	3.4252	**1.4199**	6.3780
	% O.S	0.0846	0.0595	0.0325	$1.84\text{x}10^{-6}$	$1.37\text{x}10^{-5}$	**0**
i_{od_2}	R.T(s)	**0.0075**	**0.0075**	0.0078	0.0078	0.0079	0.0078
	S.T(s)	1.1876	73.1004	1.1876	1.2605	**1.0460**	**1.1026**
	% O.S	7.6673	10.5542	7.6673	4.8925	**2.2788**	4.3087
i_{oq_2}	R.T(s)	2.0294	2.0945	0.0086	0.1983	**0.0084**	**0.0084**
	S.T(s)	83.3707	88.5240	1.6363	3.397	**1.4344**	6.4473
	% O.S	0.0253	0.0273	$3.52\text{x}10^{-8}$	$2.18\text{x}10^{-6}$	$2.18\text{x}10^{-5}$	**0**

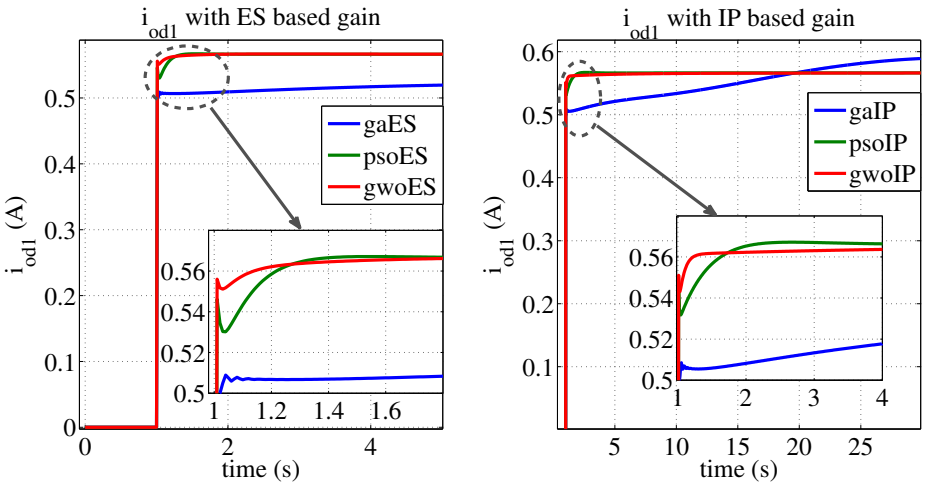

Figure 4.6: Response of d axis output current of inverter 1, i_{od1}

inverter 1 has maximum settling time for GA IP gains and minimum settling time for GWO ES. The q axis output current of both the inverters has maximum and minimum settling time and

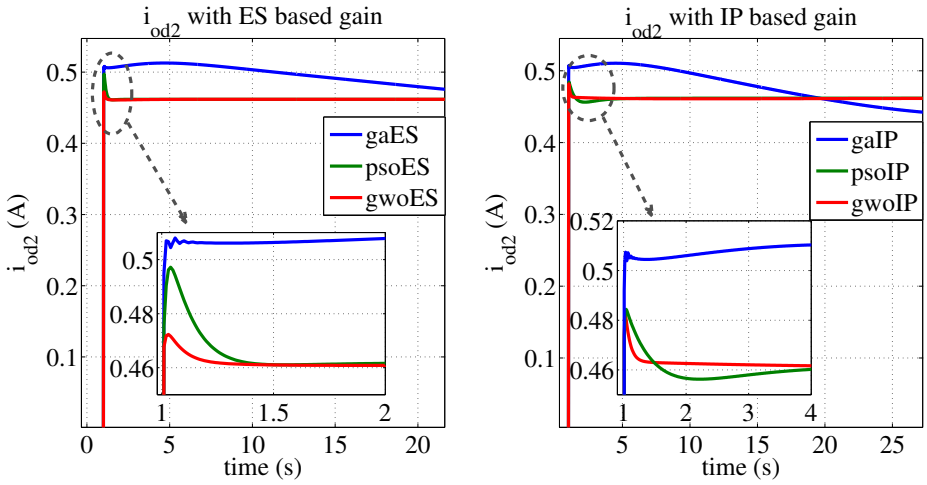

Figure 4.7: Response of d axis output current of inverter 2, i_{od2}

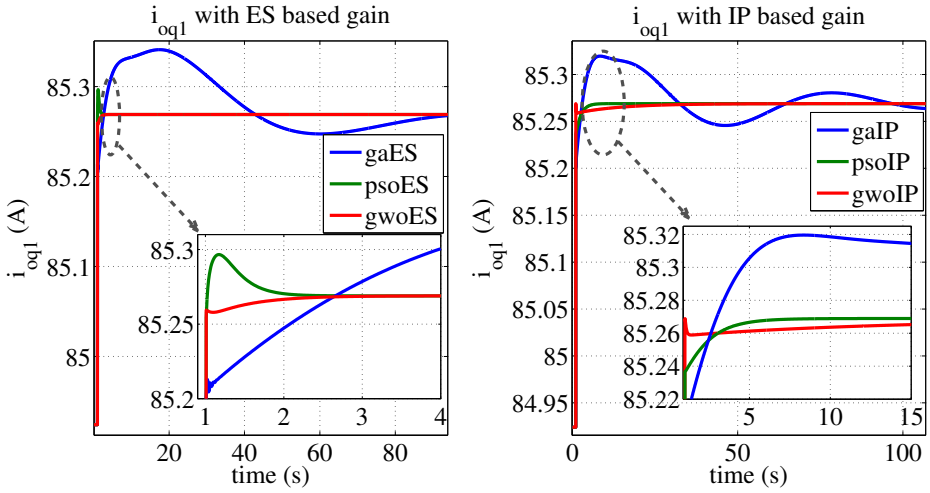

Figure 4.8: Response of q axis output current of inverter 1, i_{oq1}

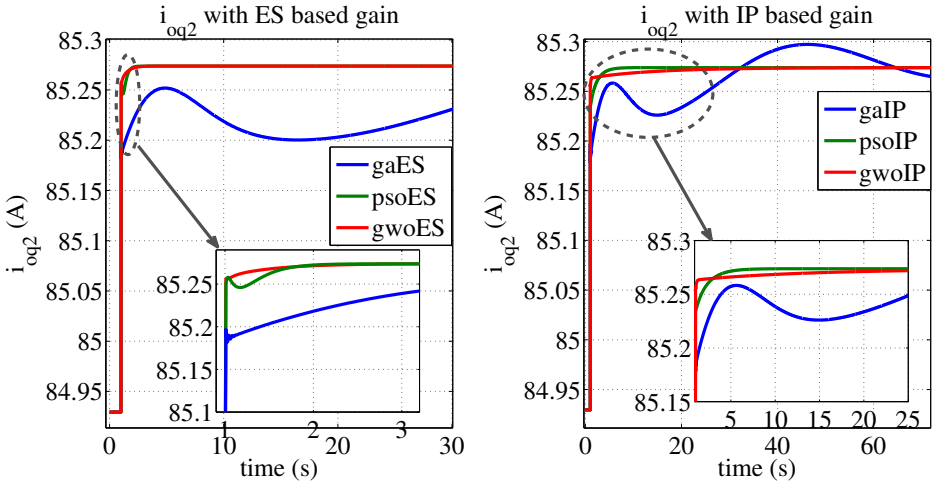

Figure 4.9: Response of q axis output current of inverter 2, i_{oq2}

rise time for GA-IP and GWO-ES gains respectively. The inverter 2 d axis output current has minimum and maximum value of settling time for GWO IP and GA IP based gains respectively. The q axis output current of both inverters has minimum overshoot for GWO IP gains. The d axis output current of both the inverter has maximum overshoot with GA based gain and minimum overshoot with GWO based gain.

The response of output voltage of inverter 1 and inverter 2 has been shown in figure 4.10 - 4.13 and the table 4.7 shows the rise time, settling time and %overshoot of the inverter output voltage, v_{odq1} and v_{odq2}. The rise time of v_{odq1} is maximum (0.99 sec) with PSOES gain and

Table 4.7: Rise time (R.T), settling time (S.T) and % overshoot (O.S) for v_{odq1} and v_{odq2} of inverters

		GA		PSO		GWO	
		ES	IP	ES	IP	ES	IP
v_{od1}	R.T(s)	$2.48x10^{-12}$	$6.21x10^{-15}$	**0.99**	$4.33x10^{-13}$	$2.13x10^{-14}$	$1.28x10^{-14}$
	S.T(s)	**1.4491**	1.3773	1.0685	1.1787	1.1418	**1.1303**
	% O.S	5.979	**8.0592**	**0.0019**	0.0047	0.0348	0.0716
v_{oq1}	R.T(s)	$3.01x10^{-4}$	$2.92x10^{-4}$	**0.0011**	$5.99x10^{-4}$	0.0014	0.0019
	S.T(s)	11.2345	12.2712	**1.0784**	6.6655	3.0173	**55.3406**
	% O.S	10.9310	**11.5292**	**2.1927**	**2.1927**	**2.1927**	**2.1927**
v_{od2}	R.T(s)	1.88^{-12}	$5.99x10^{-15}$	0.99	0.99	**1.0223**	0.99
	S.T(s)	**1.4425**	1.3750	**1.0734**	1.1878	1.1470	1.1374
	% O.S	6.266	**8.3073**	**0.0015**	0.0042	0.0323	0.0622
v_{oq2}	R.T(s)	$2.51x10^{-4}$	$2.44x10^{-4}$	$8.96x10^{-4}$	$4.99x10^{-4}$	0.0012	**0.0017**
	S.T(s)	11.2901	12.3001	**1.0625**	6.6904	3.0420	**55.6223**
	% O.S	11.3150	**11.91**	**1.7810**	3.3593	**1.7810**	**1.7810**

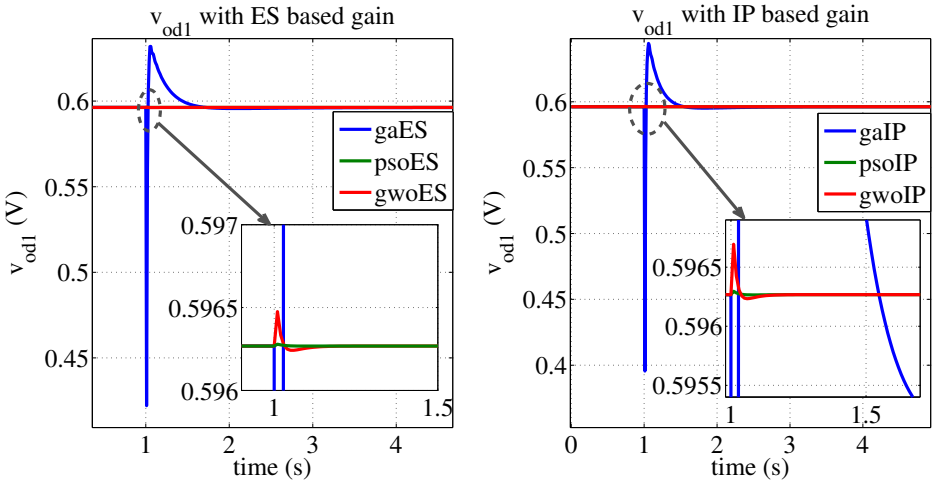

Figure 4.10: Response of d axis output voltage of inverter 1, v_{od1}

minimum ($6.21x10^{-15}$ sec) with GAIP gain. But the maximum and minimum rise time of v_{od2} is

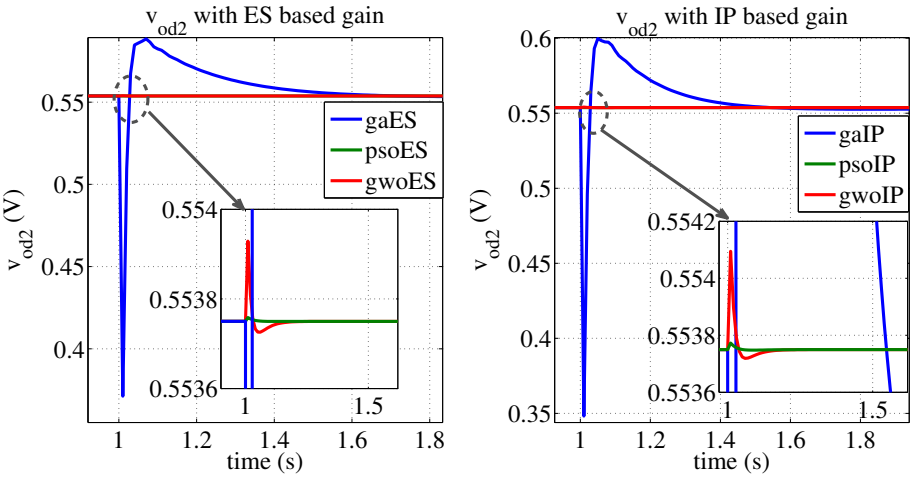

Figure 4.11: Response of d axis output voltage of inverter 2, v_{od2}

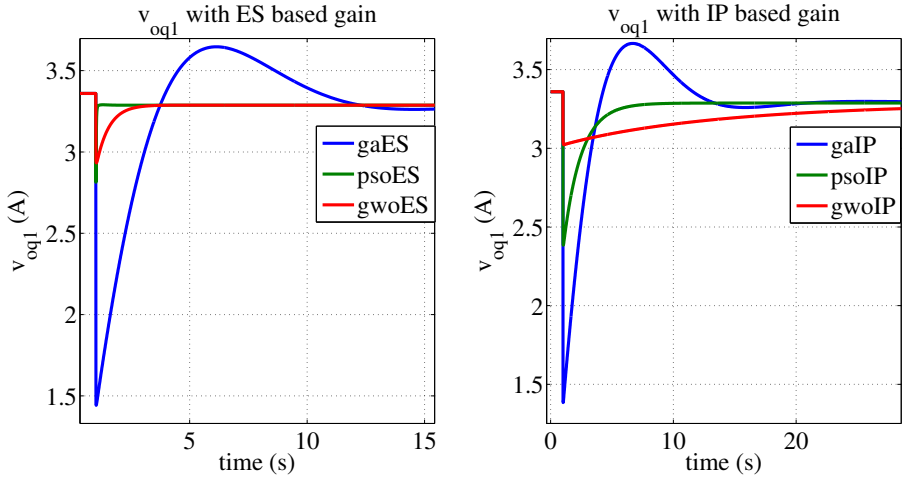

Figure 4.12: Response of q axis output voltage of inverter 1, v_{oq1}

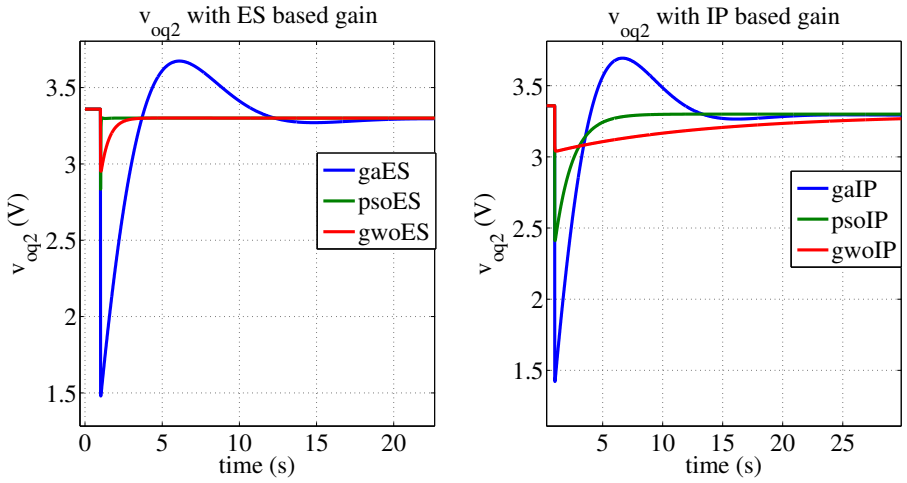

Figure 4.13: Response of q axis output voltage of inverter 2, v_{oq2}

obtained respectively with GWOES (1.023 sec) and GAIP ($5.99x10^{-15}$ sec) gains and the same is obtained for $voq2$ with GWOIP (0.0017 sec) and PSOES ($8.96x10^{-4}$ sec) gain respectively. For both $vod_1 and vod_2$ the maximum settling time is obtained with GAES (1.4491 sec (vod_1) and 1.4425 sec (vod_1)) gain. But minimum settling time for v_{od1} and v_{od2} is obtained with GWOIP gains (1.1303 sec) PSOES gains (1.0734 sec). The maximum and minimum settling time for $v_{oq1} and v_{oq2}$ is obtained with GWOIP gains and PSOES gains respectively. The % overshoot is maximum with GAIP gains and minimum with PSOES gains for both v_{od1} and v_{od2}. Maximum overshoot of v_{oq1} and v_{oq2} obtained with GAIP gains and and minimum overshoot is achieved with PSOES,GWOES, GWOIP gains.

The response of filter currents has been illustrated in figure 4.14 - 4.17. From the table 4.8, showing the rise time, settling time and overshoot of filter currents, it is seen that the maximum

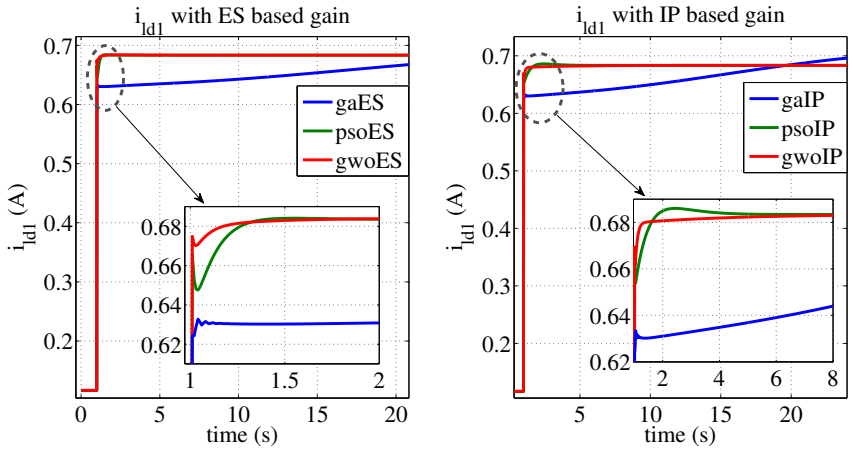

Figure 4.14: Response of d axis filter current of inductor 1, i_{ld1}

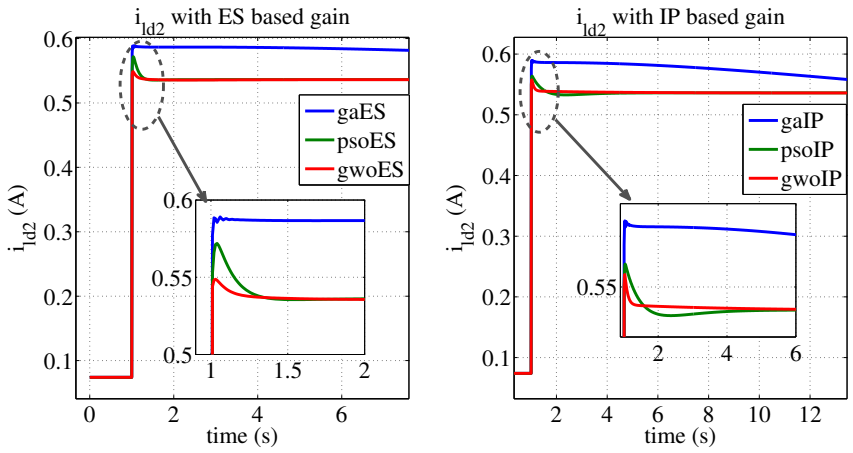

Figure 4.15: Response of d axis filter current of inductor 2, i_{ld2}

rise and settling time for i_{ld1} and i_{lq1} is obtained with GAIP based gains whereas minimum rise time and settling time for i_{ld1} and i_{lq1} is achieved with GWOES gains. The overshoot of i_{ld1} is

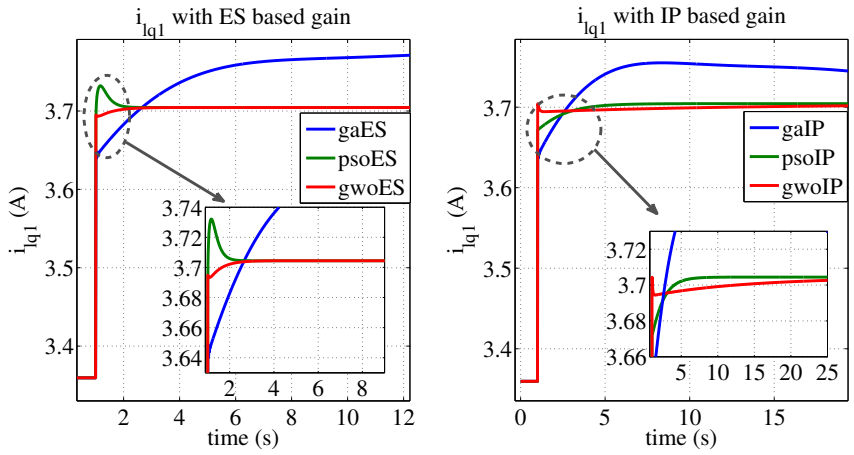

Figure 4.16: Response of q axis filter current of inductor 2, i_{lq1}

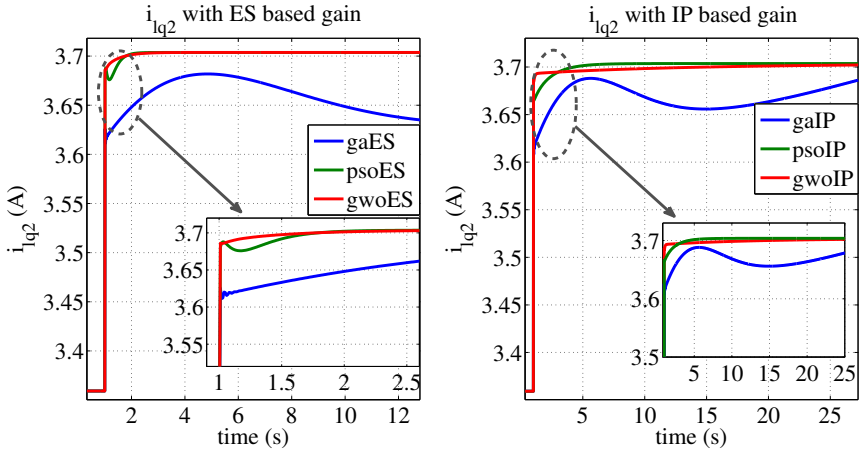

Figure 4.17: Response of q axis filter current of inverter 2, i_{lq2}

Table 4.8: Rise time (R.T), settling time (S.T) and % overshoot (O.S) for i_{ldq1} and i_{ldq2} of inverters

		GA		PSO		GWO	
		ES	IP	ES	IP	ES	IP
i_{ld1}	R.T(s)	0.0242	**0.028**	0.0083	0.0082	**0.0081**	0.0082
	S.T(s)	51.9029	**69.3706**	1.1690	1.3468	**1.0521**	1.1022
	% O.S	1.8452	**3.5661**	0.1071	0.3818	0.0873	**0.0103**
i_{lq1}	R.T(s)	0.6568	**0.7992**	0.0083	0.0088	0.0082	**0.008**
	S.T(s)	83.3445	**88.5088**	1.6354	3.4248	**1.4195**	6.3776
	% O.S	**1.9478**	1.3690	0.7481	$4.24x10^{-5}$	$3.16x10^{-4}$	**0**
i_{ld2}	R.T(s)	**0.0073**	0.0074	0.0077	0.0078	**0.0079**	0.0078
	S.T(s)	56.8208	**73.0807**	1.1872	1.3579	**1.0646**	1.1180
	% O.S	9.8615	**9.9776**	6.6498	5.1433	**2.3265**	3.9639
i_{lq2}	R.T(s)	2.029	**2.0941**	0.0086	0.19820	**0.0084**	**0.0084**
	S.T(s)	83.3707	**88.528**	1.6363	3.3953	**1.4341**	6.4470
	% O.S	0.5816	**0.6276**	$8.11x10^{-7}$	$5.04x10^{-5}$	$5.03x10^{-4}$	**0**

maximum with GAIP (3.5661) and minimum with GWOIP (0.0103) gains. The maximum and minimum overshoot of i_{lq1} is obtained with GAES (1.9478) and GWOIP (0) respectively. The maximum and minimum rise time and settling time for i_{ldq2} is obtained with GA and GWO based gains. The maximum overshoot of o_{ldq2} is achieved with GAIP (9.9776 (i_ld2) and (0.6276 (i_{lq2})). For i_{ld2} minimum overshoot is obtained with GWOES (2.3265) but minimum overshoot is obtained with GWOIP (0) for i_{lq2}.

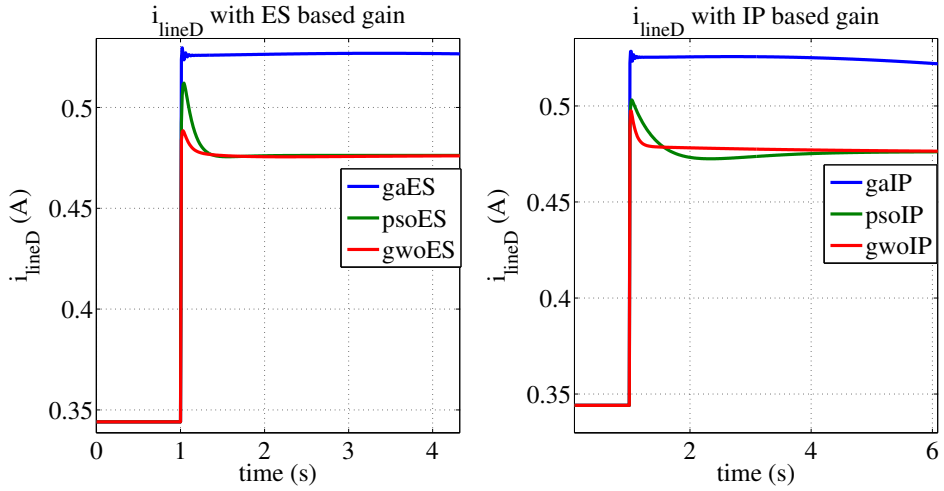

Figure 4.18: Response of D axis line current, i_{lineD}

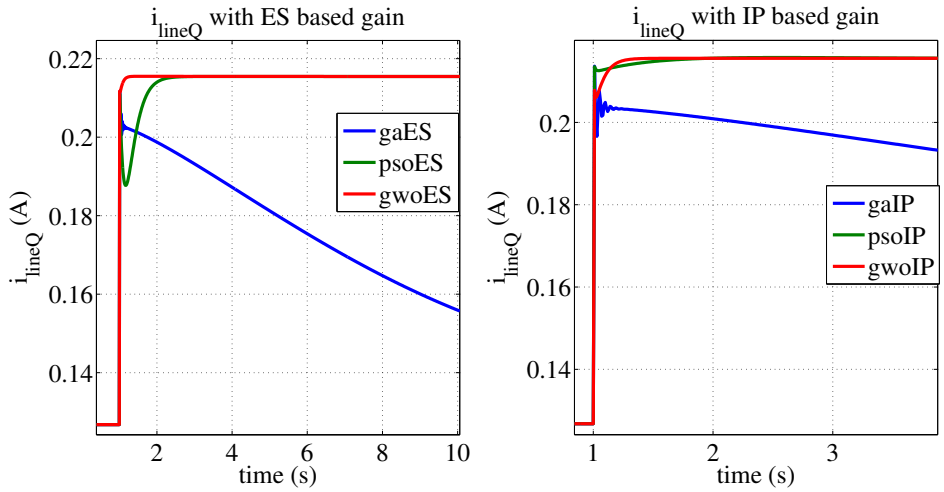

Figure 4.19: Response of Q axis line current, i_{lineQ}

The figure 4.18 - 4.19 shows the response of the line currents. From the table 4.9, it is seen that the maximum rise time, settling time and % overshoot for line current, i_{lineDQ} is obtained with GAIP based gains. The minimum settling time, rise time and overshoot is achieved with GWO based gain, either with GWOIP or GWOES. From the table, it is also found that the settling time and rise time of i_{lineD} is significantly higher than settling and rise time of i_{lineQ}.

Table 4.9: Rise time (R.T), settling time (S.T) and % overshoot (O.S) for the i_{lineDQ} of inverters

		GA		PSO		GWO	
		ES	IP	ES	IP	ES	IP
i_{lineD}	R.T(s)	2.029	**2.0941**	0.0086	0.198	**0.0084**	**0.0084**
	S.T(s)	83.3707	**88.5280**	1.6363	3.3953	**1.4341**	6.447
	% O.S	0.5816	**0.6276**	$8.11x10^{-7}$	$5.04x10^{-5}$	$5.03x10^{-4}$	**0**
i_{lineQ}	R.T(s)	0.0084	**0.0082**	0.0084	0.0082	0.0084	**0.0088**
	S.T(s)	92.2216	**152.6513**	1.9562	1.2272	**1.0865**	1.1599
	% O.S	9.9894	**10.7846**	**$2.72x10^{-6}$**	0.1421	0.0197	0.0557

Table 4.10: Rise time (R.T), settling time (S.T) and % overshoot (O.S) for $i_{loadDQ1}$ and $i_{loadDQ2}$ of inverters

		GA		PSO		GWO	
		ES	IP	ES	IP	ES	IP
i_{loadD_1}	R.T(s)	0.0082	0.0083	**0.008**	0.0081	**0.008**	**0.008**
	S.T(s)	1.0184	1.0233	1.0099	1.0099	1.0098	**1.0085**
	% O.S	0.2256	0.2301	0.0193	2.18x10-5	$1.84x10^{-4}$	**0**
i_{loadQ_1}	R.T(s)	0.8078	0.9265	**0.0082**	0.0087	0.9265	**0.0082**
	S.T(s)	8.4389	9.3733	**1.2812**	3.0135	9.3733	2.8161
	% O.S	0.3833	0.4049	$4.15x10^{-4}$	$4.71x10^{-5}$	0.4049	**0**
i_{loadD_2}	R.T(s)	0.0083	0.0084	**0.008**	0.0081	**0.008**	**0.008**
	S.T(s)	1.0209	1.0258	1.0099	1.0099	**1.0098**	**1.0098**
	% O.S	0.2978	0.2905	0.0631	$1.15x10^{-5}$	8.01x10-5	**0**
i_{loadQ_2}	R.T(s)	1.439	1.6301	0.0086	0.511	0.0084	**0.0083**
	S.T(s)	9.6314	10.6319	**1.03**	3.8307	1.582	10.3874
	% O.S	0.4028	0.4257	$7.59x10^{-7}$	$4.77x10^{-5}$	$4.15x10^{-4}$	0

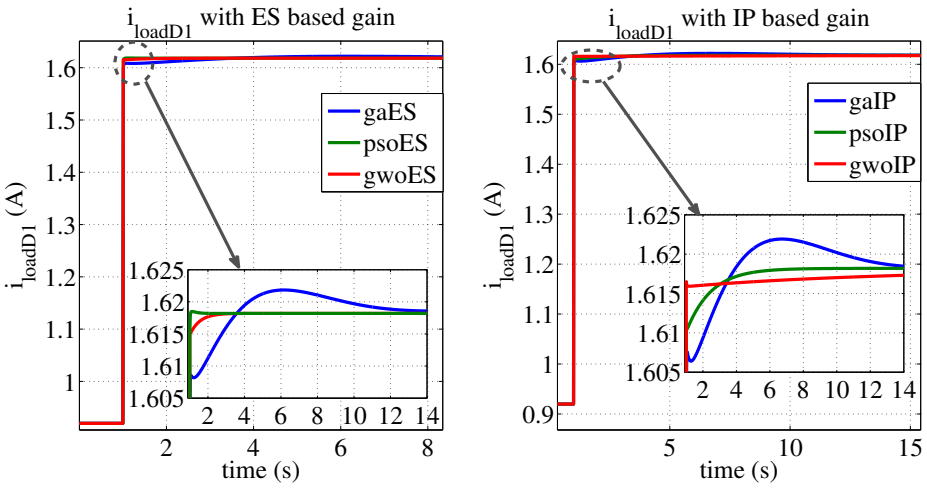

Figure 4.20: Response of D axis load1 current, i_{loadD1}

The d axis load currents, $i_{loadD,i}$ in figure 4.20-4.23 have similar minimum rise time for all PSO and GWO based gains but maximum rise time for GA IP gains as shown in table 4.10. The settling time and overshoot of d axis output currents,$i_{loadD,i}$ of both inverters are minimum for

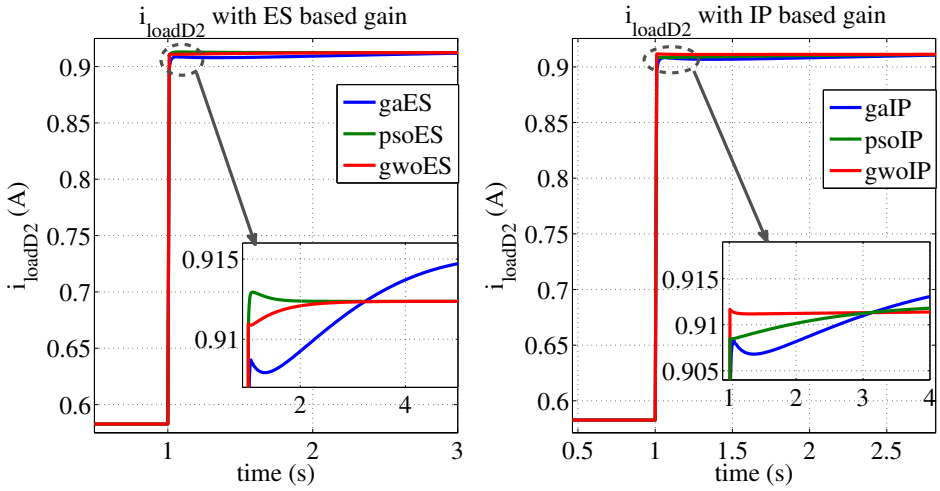

Figure 4.21: Response of D axis load2 current, i_{loadD2}

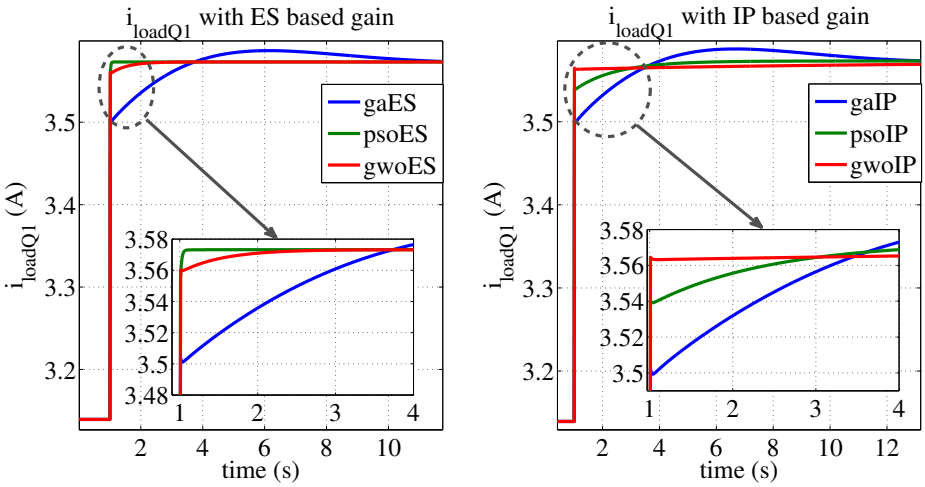

Figure 4.22: Response of Q axis load1 current, i_{loadQ1}

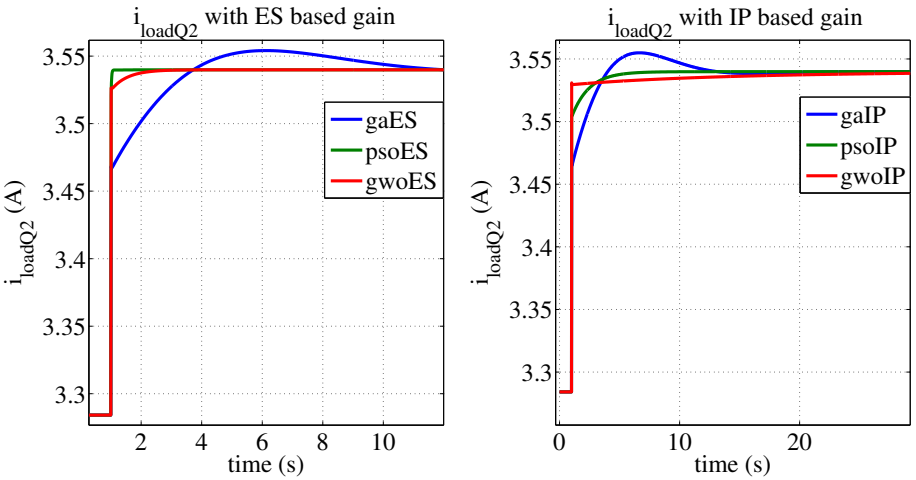

Figure 4.23: Response of Q axis load2 current, i_{loadQ2}

GWO IP gains. The q axis output currents, $i_{loadQ,i}$ have minimum settling time and overshoot for PSO ES and GWO IP gains, respectively.

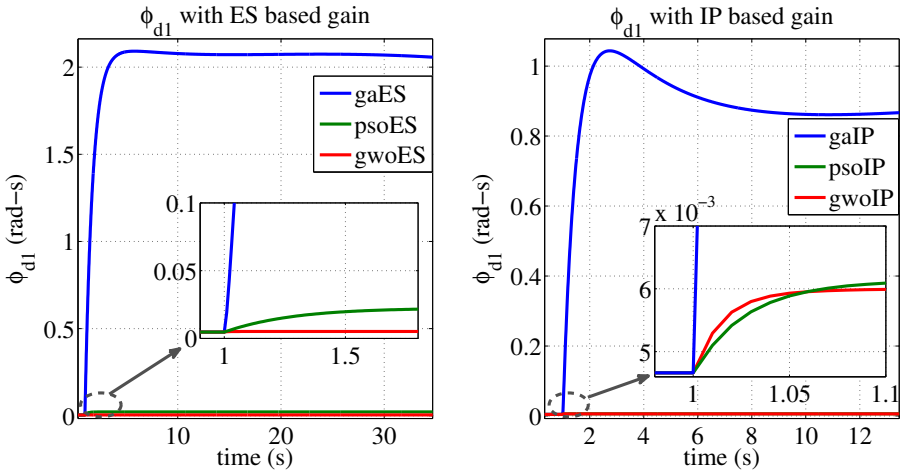

Figure 4.24: Response of d axis differential input to voltage controller 1, ϕ_{d1}

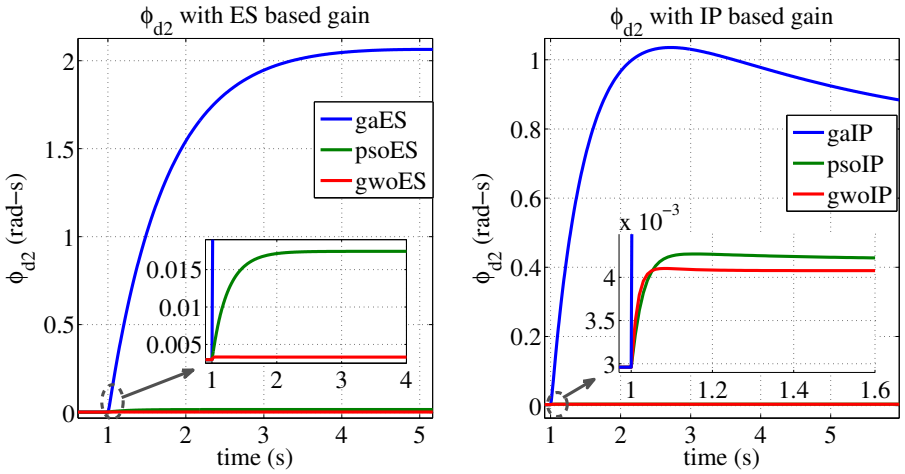

Figure 4.25: Response of d axis differential input to voltage controller 2, ϕ_{d2}

The response of ϕ_{dq1} and ϕ_{dq2} has been shown in figure 4.24 - 4.27. The rise time of ϕ_{d1} is maximum (0.7547 sec) with GAES gain and minimum (0.0292 sec) with GWOES gain. The maximum and minimum settling time for ϕ_{d1} is achieved with GAES (194.6742 sec) and PSOES (1.0749 sec). For % overshoot, the maximum is obtained with GAES (34.7623) and minimum is achieved with PSOES ($9.1x10^{-5}$). The maximum rise time for $\phi_{q1,2}$ is achieved with GWOIP. However, minimum rise time for ϕ_{q1} and ϕ_{q2} is achieved with PSOES (0.0316 sec) and GWOES (1.0926 sec) respectively. The maximum settling time for both ϕ_{q1} (1.6574 sec) and ϕ_{q1} (1.6445 sec) is achieved with PSOES gains. For overshoot of ϕ_{q1} and ϕ_{q2}, maximum value (258.68 (ϕ_{q1}) and 244.3321 (ϕ_{q2})) and minimum value (0) is obtained with GAIP and GWOIP gains respectively.

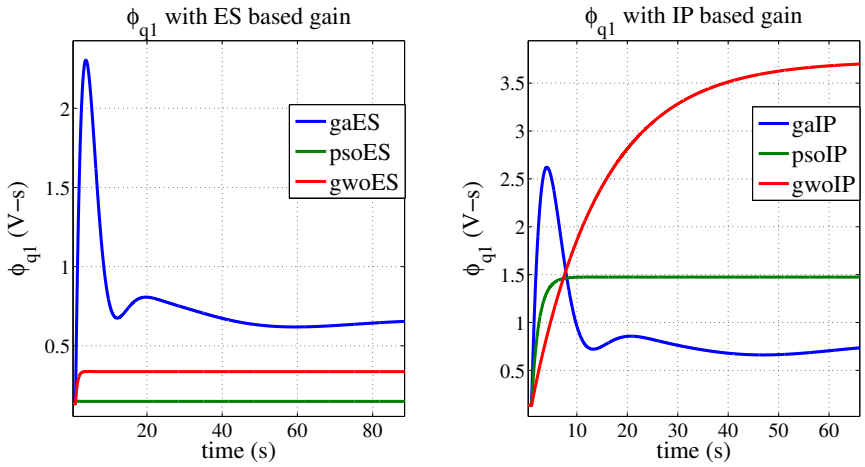

Figure 4.26: Response of q axis differential input to voltage controller 1, ϕ_{q1}

Table 4.11: Rise time (R.T), settling time (S.T) and % overshoot (O.S) for ϕ_{dq1} and ϕ_{dq2} of inverters

		GA		PSO		GWO	
		ES	IP	ES	IP	ES	IP
ϕ_{d1}	R.T(s)	**0.7547**	0.5569	0.5807	0.0776	**0.0292**	1.0749
	S.T(s)	**194.6742**	69.5785	2.022	1.3753	**1.0749**	1.1198
	% O.S	**34.7623**	17.0272	**9.10x10^{-5}**	0.1143	0.009	0.0032
ϕ_{q1}	R.T(s)	0.2417	0.2661	**0.0316**	3.1464	1.0714	**30.7775**
	S.T(s)	68.8327	57.7360	**1.6574**	6.5513	**2.7464**	55.8625
	% O.S	249.4697	**258.68**	0.8013	0.0465	0.3124	**0**
ϕ_{d2}	R.T(s)	0.5327	0.3807	**0.5577**	0.0506	**0.0251**	0.0283
	S.T(s)	**193.4465**	72.7293	2.0107	1.3865	**1.0386**	1.1337
	% O.S	**63.2008**	42.5944	**5.60x10^{-5}**	1.2606	0.1949	0.7761
ϕ_{q2}	R.T(s)	0.2473	0.2721	0.0397	3.1521	**1.0926**	**30.8104**
	S.T(s)	**70.2293**	58.1660	**1.6445**	6.5627	2.8022	55.9087
	% O.S	235.1259	**244.3321**	0.0041	0.0385	0.2418	**0**

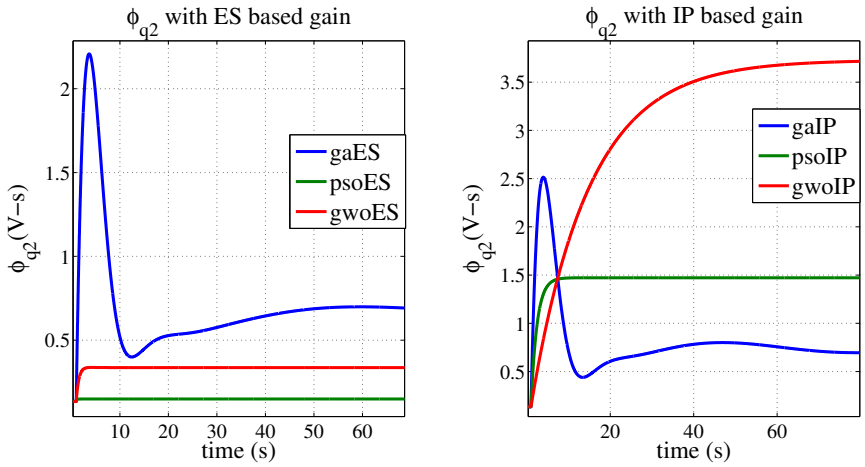

Figure 4.27: Response of q axis differential input to voltage controller 2, ϕ_{q2}

Table 4.12: Rise time (R.T), settling time (S.T) and % overshoot (O.S) for γ_{dq1} and γ_{dq2} of inverters

		GA		PSO		GWO	
		ES	IP	ES	IP	ES	IP
γ_{d1}	R.T(s)	**133.8614**	**8.9426**	130.8925	51.1292	239.1881	238.9293
	S.T(s)	225.7693	**70.6157**	221.6363	92.0356	**293.8735**	293.4302
	% O.S	**0**	**4.1083**	**0**	**0**	**0**	**0**
γ_{q1}	R.T(s)	4.7150	5.0528	19.5020	**23.3292**	**3.0092**	12.0073
	S.T(s)	48.5356	**69.4322**	35.7332	42.8265	**6.2782**	32.0335
	% O.S	1.9929	**3.6928**	$1.11x10^{-13}$	**0**	$4.44x10^{-14}$	**0**
γ_{d2}	R.T(s)	134.7727	**4.3865**	130.8936	51.1377	**239.1887**	238.9567
	S.T(s)	226.0811	**75.2409**	221.6239	92.028	**293.8737**	293.4295
	% O.S	**0**	**5.6460**	**0**	**0**	**0**	**0**
γ_{q2}	R.T(s)	3.5733	3.8938	19.5027	**23.3822**	**3.0501**	13.1739
	S.T(s)	52.3627	**73.07**	35.7268	42.98	**6.3378**	34.7916
	% O.S	13.5757	**13.6772**	**0**	**0**	**0**	**0**

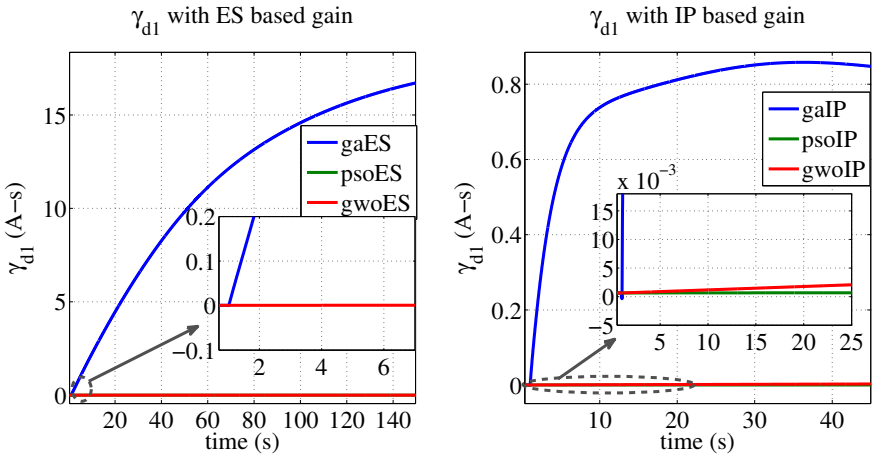

Figure 4.28: Response of d axis differential input to current controller 1, γ_{d1}

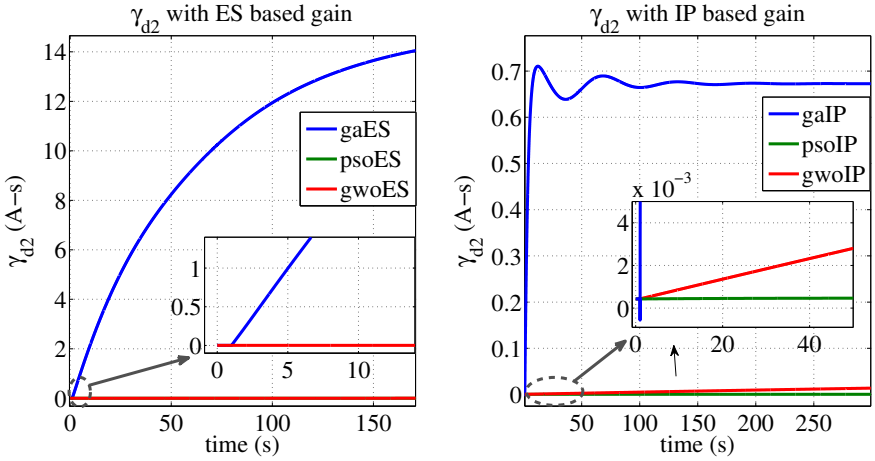

Figure 4.29: Response of d axis differential input to current controller 2, γ_{d2}

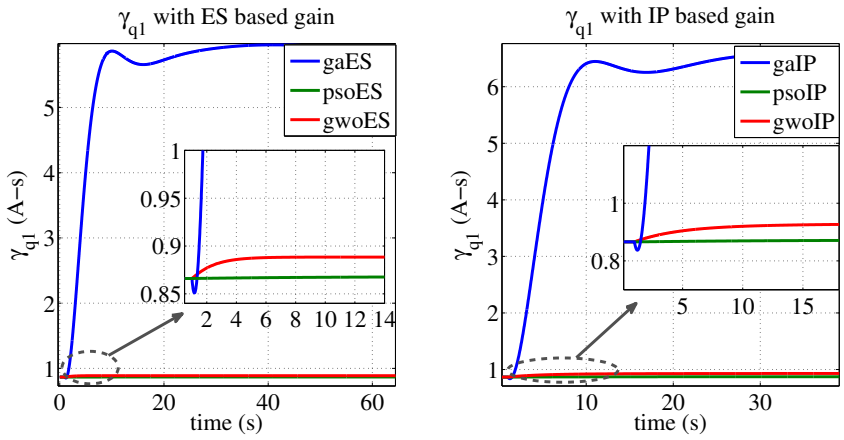

Figure 4.30: Response of q axis differential input to current controller 1, γ_{q1}

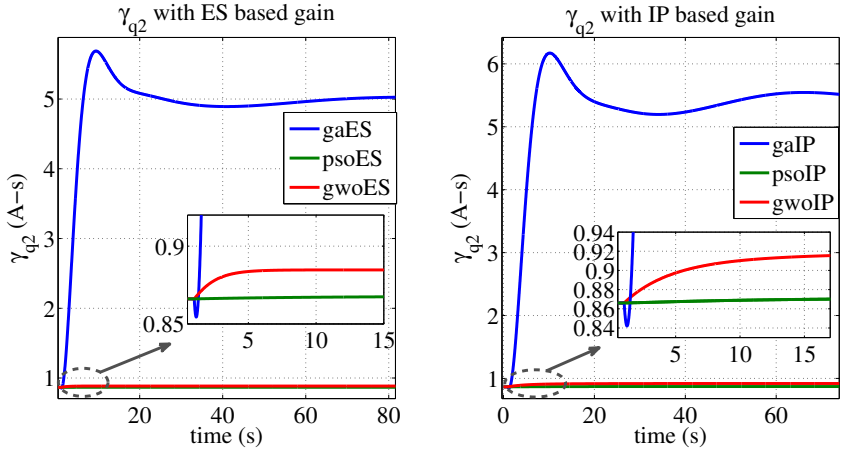

Figure 4.31: Response of q axis differential input to current controller 2, γ_{q2}

The figure 4.28 - 4.31 illustrates the response of γ_{dq1} and γ_{dq2} of the inverters. From table 4.12, it is seen that the minimum rise time, settling time and maximum % overshoot is obtained with GAIP based gain for both γ_{d1} and γ_{d2}. For γ_{dq1} and γ_{dq2}, the % overshoot is minimum (0) with all the gains except GAIP. The minimum rise time and settling time for $\gamma_{q1,2}$ is obtained with GWOES based gain.

Table 4.13: Rise time (R.T), settling time (S.T) and % overshoot (O.S) for the δ_1 and δ_2 of inverters

		GA		PSO		GWO	
		ES	IP	ES	IP	ES	IP
δ_1	R.T(s)	0	0	0	0	0	0
	S.T(s)	0	0	0	0	0	0
	% O.S	∞	∞	∞	∞	∞	∞
δ_2	R.T(s)	1.2519	0.9773	0.5040	0.2781	**0.2634**	**3.9264**
	S.T(s)	154.5990	**177.5012**	**2.1282**	4.2490	3.5072	5.4003
	% O.S	**182.7282**	143.5418	77.2759	42.7482	**24.8160**	47.3139

The figure 4.32 - 4.33 represents the response of the reference angle, $\delta_{1,2}$ of the inverters and table 4.13 enlists the rise time, settling time and % overshoot of δ_1 and δ_2. Since inverter 1 is considered as the reference, there is no variation in the δ_1 but with δ_2.

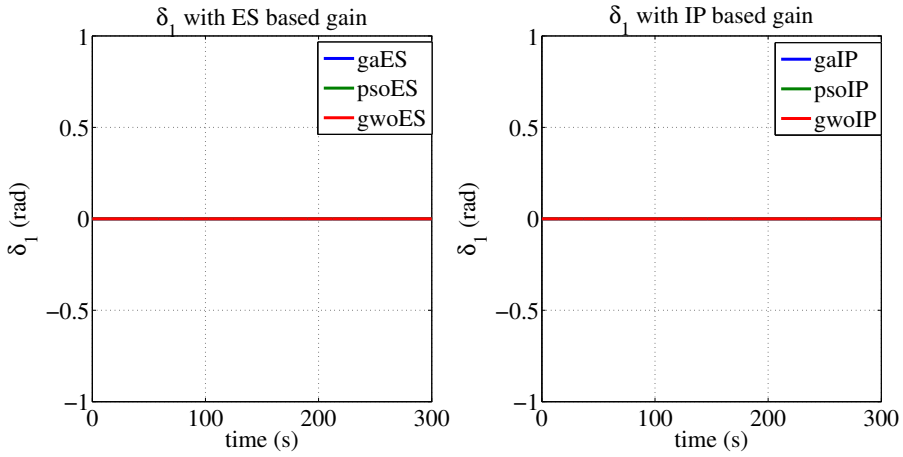

Figure 4.32: Response of phase angle of inverter 1, δ_1

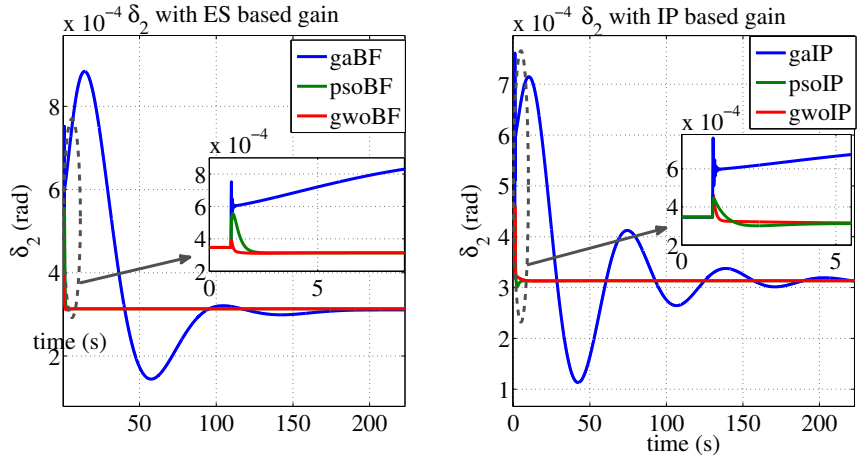

Figure 4.33: Response of phase angle of inverter 2, δ_2

Table 4.14: Rise time (R.T), settling time (S.T) and % overshoot (O.S) for $v_{od1,f}$ and $v_{od2,f}$

		GA		PSO		GWO	
		ES	IP	ES	IP	ES	IP
$v_{od1,f}$	R.T(s)	$1.36x10^{-9}$	$3.13x10^{-12}$	$3x10^{-12}$	$1.36x10^{-12}$	**$6.45x10^{-6}$**	**$4.18x10^{-13}$**
	S.T(s)	**3.3643**	2.7783	1.7007	1.3218	1.2074	**1.1952**
	% O.S	**$7.05x10^{8}$**	$3.16x10^{11}$	$2.67x10^{11}$	$5.65x10^{11}$	$3.58x10^{6}$	**$1.91x10^{12}$**
$v_{od2,f}$	R.T(s)	$1.38x10^{-9}$	$1.7x10^{-10}$	$3.62x10^{-12}$	$4.33x10^{-12}$	**$3.76x10^{-6}$**	**$4.89x10^{-13}$**
	S.T(s)	**3.3585**	2.7733	1.7532	1.3358	1.2188	**1.2064**
	% O.S	$7.11x10^{8}$	$4.47x10^{10}$	$2.96x10^{11}$	$2x10^{11}$	**$6.23x10^{6}$**	**$1.51x10^{12}$**

The figure 4.34 - 4.35 illustrates the $v_{od1,f}$ and $v_{od2,f}$ response and the table 4.14 shows the rise time, settling time and %overshoot of $v_{od1,f}$ and $v_{od2,f}$. For $v_{od1,f}$ and $v_{od2,f}$, the minimum

rise time, settling time and % overshoot is obtained with GWOIP gains. The rise and settling time for $v_{od1,f}$ and $v_{od2,f}$ is maximum with GWOES and GAES gains.

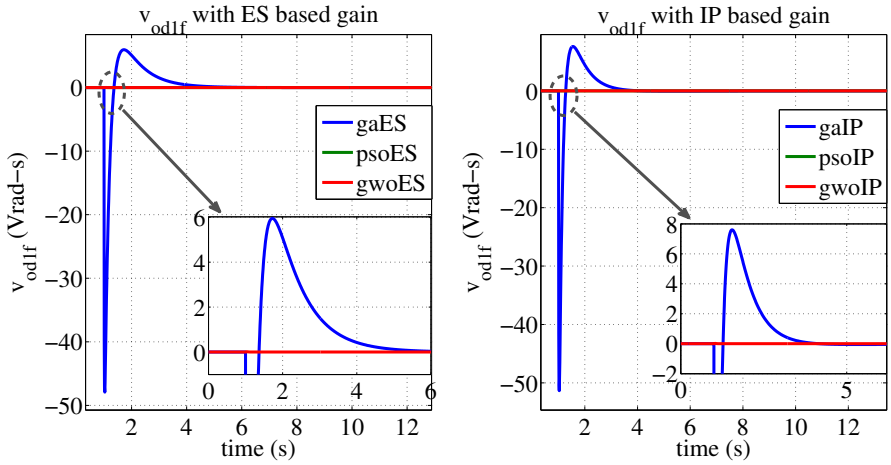

Figure 4.34: Response of , $v_{od1,f}$

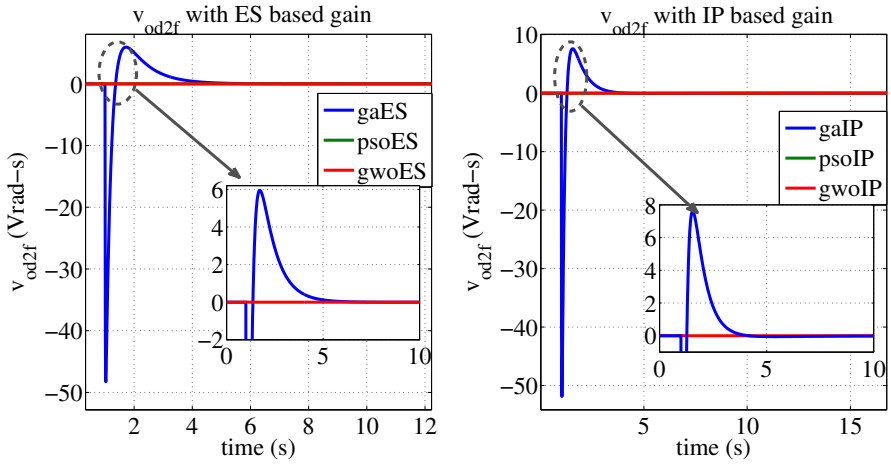

Figure 4.35: Response of , $v_{od2,f}$

Table 4.15: Rise time (R.T), settling time (S.T) and % overshoot (O.S) for ϕ_{PLL1} and ϕ_{PLL2}

		GA		PSO		GWO	
		ES	IP	ES	IP	ES	IP
ϕ_{PLL1}	R.T(s)	0.8322	0.1882	0.5648	**1.1136**	0.1285	**0.1112**
	S.T(s)	4.3917	7.0785	2.0456	4.2508	**1.8101**	**12.4490**
	% O.S	13.6565	**61.4715**	$3.29x10^{-9}$	$7.41x10^{-7}$	$3.75x10^{-5}$	**0**
ϕ_{PLL2}	R.T(s)	0.8314	0.1882	0.5720	**1.211**	0.1369	**0.1225**
	S.T(s)	4.3912	7.0807	2.0632	4.2885	**1.8233**	**13.0335**
	% O.S	13.6837	**61.4929**	$3.63x10^{-9}$	$7.48x10^{-7}$	$4.16x10^{-5}$	**0**

The response of ϕ_{PLL1} and ϕ_{PLL2} is represented in figure 4.36 - 4.37. From the table 4.15 it is found that, the maximum and minimum rise time of ϕ_{PLL1} and ϕ_{PLL2} is obtained with

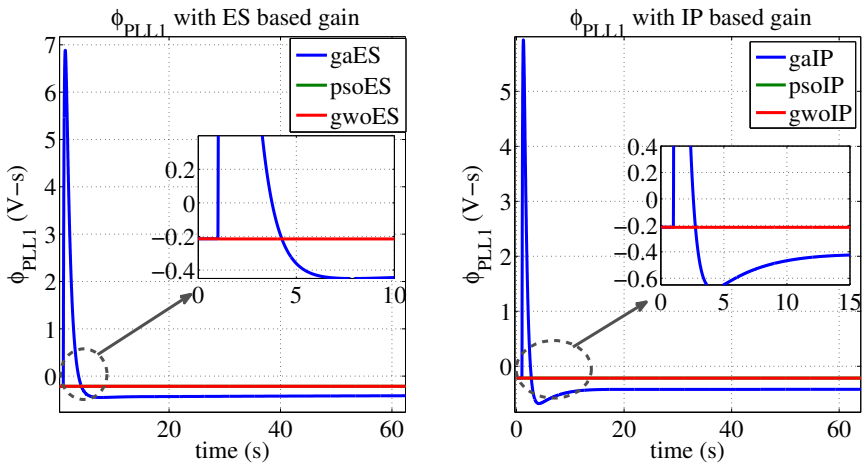

Figure 4.36: Response of , ϕ_{PLL1}

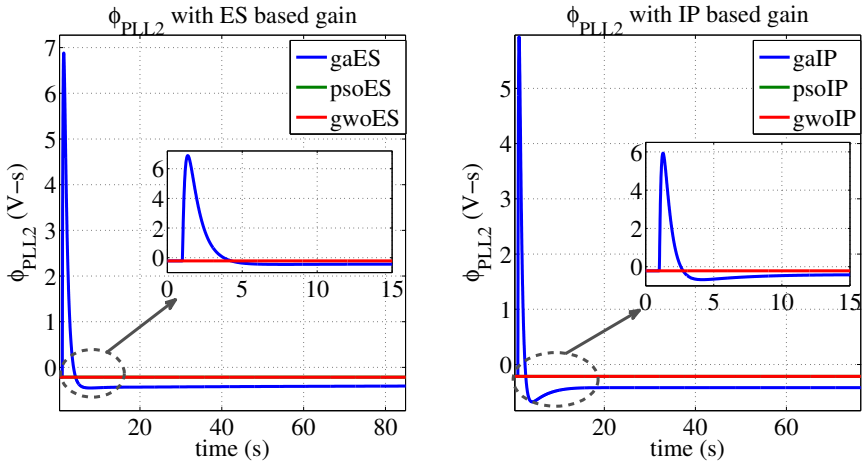

Figure 4.37: Response of , ϕ_{PLL2}

GWOIP and PSOIP gains. The settling time is minimum (1.8101 sec (for ϕ_{PLL1}) and 1.8233 sec (for ϕ_{PLL2})) with GWOES gain and maximum (12.449 sec (for ϕ_{PLL1}) and 13.0355 sec (for ϕ_{PLL2})) with GWOIP gains. The maximum and minimum overshoot for both ϕ_{PLL1} and ϕ_{PLL2} is obtained with GAIP and GWOIP gains respectively.

4.2.3 Statistical analysis

For further validation of obtained results, non-parametric statistical analysis has been carried out for the data obtained from 30 individual runs using IBM SPSS statistics software. Specifically, the One- sample Kolmogorov-Smirnov test is performed to determine the distribution of the data. During this test, the null hypothesis, H_0 is assumed as the data sample fits the normal distribution and the alternative hypothesis, H_1 is assumed as the data sample does not fit normal distribution with 5%. significance level. The result obtained from Kolmogorov-Smirnov has been summarized in table 4.16. From the table it is seen that the standard deviation of GAES

Table 4.16: Kolmogorov-Smirnov test result

		GAES	PSOES	GWOES
Kolmogorov-Smirnov test	Asymp. sig. (2-tailed)	0	0	0.2
	Std. deviation	$6.7\text{x}10^{-4}$	$1.25\text{x}10^{-2}$	$7.15\text{x}10^{-3}$

$(6.7x10-4)$ is the minimum among the three algorithms. However, as the analysis of table 4.4 revealed that the performance of GAES is the worst considering fitness value and execution time, whereas the performance of PSOES and GWOES were competitive, here the focus is to find out the statistical significant differences between the last two algorithms. Hence, upon comparison of PSOES and GWOES, from table 4.16 it is revealed that the standard deviation of GWOES is smaller than the standard deviation of PSOES by an order of 10. This reveals that for the conducted 30 individual runs, the optimum point achieved by GWOES is far closer to its mean fitness value than that obtained by the PSOES. Moreover, since the asymp. sigma value for GWOES is greater than 0.05, with 95% confidence level it can be concluded that the GWOES data sample fits the normal distribution. On the contrary, for the other two algorithms PSOES and GAES, the asymp. sigma value is less than 0.05 which is significant enough to reject the null hypothesis, H_0 and accept the alternate hypothesis, H_1 which signifies that that the data of PSOES and GAES do not follow normal distribution. Since PSOES is not normal distributed whereas GWOES follows normal distribution, permutation test [76] is suggested [77]. Here, the null hypothesis, H_0 is assumed as there is no difference in mean with fitness value obtained from 30 individual runs of PSOES and GWOES and the alternative hypothesis, H_1 is assumed as there is difference in mean with the fitness value obtained from PSOES and GWOES with 5% significant level. From the test with 10000 permutation, the p value observed is $0.79 > 0.05$ which is sufficient enough to accept the null hypothesis with 95% confidence level that there is no significant difference in mean with the fitness value obtained from PSOES and GWOES.

Chapter 5

Conclusion and Future Work

5.1 Conclusion

In this work, a detailed linearized small signal model of droop control based islanded microgrid system has been developed including the inverter, filter, phase lock loop (PLL), network and load dynamics. Through eigenvalue, participation factor and root locus analysis, it has been found that, the gains associated with voltage, current and PLL controllers are very sensitive for the stability of the system. These gains of current, voltage and PLL controllers of the studied islanded microgrid system have been optimized using a two-step optimization process. In this optimization process, GA, PSO, GWO algorithms are adopted in an unbounded search space to determine the upper and lower bound of the gains in the first stage and ES, IP algorithms are adopted to find the ultimate gain values in the second stage. Performance of the adopted two-stage algorithms are compared by observing minimum value of fitness function, execution time, time domain specifications, such as, rise time, settling time and percent overshoot and statistical analysis, such as, Kolmogorov-Smirnov test and permutation test. Upon comparing the performance of the algorithms it has been found that

- The performance of GA is relatively poor in comparison to GWO, PSO and GWO provides better optimization in comparatively less amount of time than PSO in the first stage.
- In the second stage, there is a variation in the fitness value obtained with ES algorithm but not with IP algorithm and on an average, IP provides better optimization than ES.
- Upon combining the two stages, PSOIP yields better optimization than GWOIP on an average but PSOIP takes significantly larger amount of time than GWOIP.
- For ultimate optimization, PSOES and GWOES provide almost similar result but GWOES is normally distributed and less divergent than PSOES.

Thus, it could be concluded that as the first stage algorithm GWO performs better compared

to the other two, while IP algorithm works better in the second stage. Hence, upon combining, GWOIP should be the final choice of optimization algorithm for this work.

5.2 Future work

Although the presented two-step tuning methodology should assist microgrid system engineers in designing controllers in more optimized manner, there exist some improvements that can still be accomplished. The algorithm developed for this work is based on offline tuning of the controller parameters and the results presented are based on MATLAB simulation. So, researchers could think about developing online tuning of the controller parameters along with the practical implementation of the work in the laboratory prototype. Besides, in this work proportional integral controller has been used. So, prospective researchers could think about other control strategies including non linear control design of microgrid system. Apart from that, the researchers could also ponder upon improvement of power quality and harmonic.

References

[1] J. A. Baroudi, V. Dinavahi, and A. M. Knight, "A review of power converter topologies for wind generators," *Renewable energy*, vol. 32, no. 14, pp. 2369–2385, 2007.

[2] Y. W. Li and C.-N. Kao, "An accurate power control strategy for power-electronics-interfaced distributed generation units operating in a low-voltage multibus microgrid," *IEEE Transactions on Power Electronics*, vol. 24, no. 12, pp. 2977–2988, 2009.

[3] E. Barklund, N. Pogaku, M. Prodanovic, C. Hernandez-Aramburo, and T. C. Green, "Energy management in autonomous microgrid using stability-constrained droop control of inverters," *IEEE Transactions on Power Electronics*, vol. 23, no. 5, pp. 2346–2352, 2008.

[4] N. Pogaku, M. Prodanovic, and T. C. Green, "Modeling, analysis and testing of autonomous operation of an inverter-based microgrid," *IEEE Transactions on power electronics*, vol. 22, no. 2, pp. 613–625, 2007.

[5] R.-F. Yuan, Q. Ai, and X. He, "Research on dynamic load modelling based on power quality monitoring system," *IET Generation, Transmission & Distribution*, vol. 7, no. 1, pp. 46–51, 2013.

[6] Y. Li and Y. W. Li, "Power management of inverter interfaced autonomous microgrid based on virtual frequency-voltage frame," *IEEE Transactions on Smart Grid*, vol. 2, no. 1, pp. 30–40, 2011.

[7] T. L. Vandoorn, J. C. Vasquez, J. De Kooning, J. M. Guerrero, and L. Vandevelde, "Microgrids: Hierarchical control and an overview of the control and reserve management strategies," *IEEE industrial electronics magazine*, vol. 7, no. 4, pp. 42–55, 2013.

[8] P. Tian, X. Xiao, K. Wang, and R. Ding, "A hierarchical energy management system based on hierarchical optimization for microgrid community economic operation," *IEEE Transactions on Smart Grid*, vol. 7, no. 5, pp. 2230–2241, 2015.

[9] Y. Yang, H.-G. Yeh, and S. Doan, "Optimal control methods for photovoltaic enabled grid with abnormal power loads," *IEEE Systems Journal*, 2019.

[10] T. Jain *et al.*, "Impact of load dynamics and load sharing among distributed generations on stability and dynamic performance of islanded ac microgrids," *Electric Power Systems Research*, vol. 157, pp. 200–210, 2018.

[11] K. Rajesh, S. Dash, R. Rajagopal, and R. Sridhar, "A review on control of ac microgrid," *Renewable and sustainable energy reviews*, vol. 71, pp. 814–819, 2017.

[12] U. B. Tayab, M. A. B. Roslan, L. J. Hwai, and M. Kashif, "A review of droop control techniques for microgrid," *Renewable and Sustainable Energy Reviews*, vol. 76, pp. 717–727, 2017.

[13] J. M. Guerrero, L. G. De Vicuna, J. Matas, M. Castilla, and J. Miret, "A wireless controller to enhance dynamic performance of parallel inverters in distributed generation systems," *IEEE Transactions on power electronics*, vol. 19, no. 5, pp. 1205–1213, 2004.

[14] B. Bahrani, S. Kenzelmann, and A. Rufer, "Multivariable-pi-based *dq* current control of voltage source converters with superior axis decoupling capability," *IEEE Transactions on Industrial Electronics*, vol. 58, no. 7, pp. 3016–3026, 2010.

[15] A. Mehrizi-Sani and R. Iravani, "Online set point modulation to enhance microgrid dynamic response: Theoretical foundation," *IEEE Transactions on Power Systems*, vol. 27, no. 4, pp. 2167–2174, 2012.

[16] A. Alzahrani, M. Ferdowsi, P. Shamsi, and C. H. Dagli, "Modeling and simulation of microgrid," *Procedia Computer Science*, vol. 114, pp. 392–400, 2017.

[17] M. Gheisarnejad and M. H. Khooban, "Secondary load frequency control for multi-microgrids: Hil real-time simulation," *Soft Computing*, vol. 23, no. 14, pp. 5785–5798, 2019.

[18] S. Wang, Z. Liu, J. Liu, D. Boroyevich, and R. Burgos, "Small-signal modeling and stability prediction of parallel droop-controlled inverters based on terminal characteristics of individual inverters," *IEEE Transactions on Power Electronics*, 2019.

[19] S. Tabatabaee, H. R. Karshenas, A. Bakhshai, and P. Jain, "Investigation of droop characteristics and x/r ratio on small-signal stability of autonomous microgrid," in *2011 2nd Power Electronics, Drive Systems and Technologies Conference*. IEEE, 2011, pp. 223–228.

[20] F. Katiraei, M. Iravani, and P. Lehn, "Small-signal dynamic model of a micro-grid including conventional and electronically interfaced distributed resources," *IET generation, transmission & distribution*, vol. 1, no. 3, pp. 369–378, 2007.

[21] Y. Zhang, Z. Jiang, and X. Yu, "Small-signal modeling and analysis of parallel-connected voltage source inverters," in *2009 IEEE 6th International Power Electronics and Motion Control Conference*. IEEE, 2009, pp. 377–383.

[22] E. A. A. Coelho, P. C. Cortizo, and P. F. D. Garcia, "Small-signal stability for parallel-connected inverters in stand-alone ac supply systems," *IEEE Transactions on Industry Applications*, vol. 38, no. 2, pp. 533–542, 2002.

[23] Y. A.-R. I. Mohamed and E. F. El-Saadany, "Adaptive decentralized droop controller to preserve power sharing stability of paralleled inverters in distributed generation microgrids," *IEEE Transactions on Power Electronics*, vol. 23, no. 6, pp. 2806–2816, 2008.

[24] M. Hassan and M. Abido, "Optimal design of microgrids in autonomous and grid-connected modes using particle swarm optimization," *IEEE Transactions on Power Electronics*, vol. 26, no. 3, p. 755, 2011.

[25] D. E. Olivares, A. Mehrizi-Sani, A. H. Etemadi, C. A. Cañizares, R. Iravani, M. Kazerani, A. H. Hajimiragha, O. Gomis-Bellmunt, M. Saeedifard, R. Palma-Behnke *et al.*, "Trends in microgrid control," *IEEE Transactions on smart grid*, vol. 5, no. 4, pp. 1905–1919, 2014.

[26] H. Karimi, H. Nikkhajoei, and R. Iravani, "Control of an electronically-coupled distributed resource unit subsequent to an islanding event," *IEEE Transactions on Power Delivery*, vol. 23, no. 1, pp. 493–501, 2007.

[27] J. Lai, H. Zhou, X. Lu, X. Yu, and W. Hu, "Droop-based distributed cooperative control for microgrids with time-varying delays," *IEEE Transactions on Smart Grid*, vol. 7, no. 4, pp. 1775–1789, 2016.

[28] N. Vazquez, S. S. Yu, T. Fernando, and H. H. C. Iu, "Control techniques and the mathematical model of microgrids," in *Microgrids: Design, Applications and Control*. Nova Science Publishers Inc, 2018, pp. 151–185.

[29] Y. Mi, H. Zhang, Y. Fu, C. Wang, P. C. Loh, and P. Wang, "Intelligent power sharing of dc isolated microgrid based on fuzzy sliding mode droop control," *IEEE Transactions on Smart Grid*, vol. 10, no. 3, pp. 2396–2406, 2018.

[30] J. Fattahi, H. Schriemer, B. Bacque, R. Orr, K. Hinzer, and J. E. Haysom, "High stability adaptive microgrid control method using fuzzy logic," *Sustainable Cities and Society*, vol. 25, pp. 57–64, 2016.

[31] M. R. B. Khan, R. Jidin, and J. Pasupuleti, "Multi-agent based distributed control architecture for microgrid energy management and optimization," *Energy Conversion and Management*, vol. 112, pp. 288–307, 2016.

[32] A. Khorshidi, T. Niknam, and B. Bahmani, "Robust multi-agent asynchronously compensated decentralized frequency synchronization control scheme for microgrids," *Journal of Electrical Engineering & Technology*, pp. 1–10, 2019.

[33] B. Hong and Z. Zheng, "Stochastic multi-objective dynamic optimal dispatch for combined heat and power microgrid," in *2016 IEEE PES Asia-Pacific Power and Energy Engineering Conference (APPEEC)*. IEEE, 2016, pp. 2369–2373.

[34] P. Basak, S. Chowdhury, S. H. nee Dey, and S. Chowdhury, "A literature review on integration of distributed energy resources in the perspective of control, protection and stability of microgrid," *Renewable and Sustainable Energy Reviews*, vol. 16, no. 8, pp. 5545–5556, 2012.

[35] Z. Shuai, Y. Sun, Z. J. Shen, W. Tian, C. Tu, Y. Li, and X. Yin, "Microgrid stability: Classification and a review," *Renewable and Sustainable Energy Reviews*, vol. 58, pp. 167–179, 2016.

[36] Y. Zhang, L. Xie, and Q. Ding, "Interactive control of coupled microgrids for guaranteed system-wide small signal stability," *IEEE transactions on smart grid*, vol. 7, no. 2, pp. 1088–1096, 2015.

[37] V. Mariani, F. Vasca, J. C. Vásquez, and J. M. Guerrero, "Model order reductions for stability analysis of islanded microgrids with droop control," *IEEE Transactions on Industrial Electronics*, vol. 62, no. 7, pp. 4344–4354, 2014.

[38] M. B. Delghavi and A. Yazdani, "An adaptive feedforward compensation for stability enhancement in droop-controlled inverter-based microgrids," *IEEE Transactions on Power Delivery*, vol. 26, no. 3, pp. 1764–1773, 2011.

[39] R. Majumder, B. Chaudhuri, A. Ghosh, R. Majumder, and G. F. Ledwich, "Improvement of stability and load sharing in an autonomous microgrid using supplementary droop control loop," *IEEE transactions on power systems*, 2010.

[40] X. Zhao-Xia and F. Hong-Wei, "Impacts of pf & qv droop control on microgrids transient stability," *physics procedia*, vol. 24, pp. 276–282, 2012.

[41] Y. Guo, L. Chen, X. Lu, J. Wang, T. Zheng, and S. Mei, "Region based stability analysis for active dampers in ac microgrids," *IEEE Transactions on Industry Applications*, 2019.

[42] S. Leitner, M. Yazdanian, A. Mehrizi-Sani, and A. Muetze, "Small-signal stability analysis of an inverter-based microgrid with internal model-based controllers," *IEEE Transactions on Smart Grid*, vol. 9, no. 5, pp. 5393–5402, 2017.

[43] K. Yu, Q. Ai, S. Wang, J. Ni, and T. Lv, "Analysis and optimization of droop controller for microgrid system based on small-signal dynamic model," *IEEE Transactions on Smart Grid*, vol. 7, no. 2, pp. 695–705, 2015.

[44] Z. XIAO, C. WANG, and S. WANG, "Small-signal stability analysis of microgrid containing multiple micro sources [j]," *Automation of Electric Power Systems*, vol. 6, p. 022, 2009.

[45] S. V. Iyer, M. N. Belur, and M. C. Chandorkar, "A generalized computational method to determine stability of a multi-inverter microgrid," *IEEE Transactions on Power Electronics*, vol. 25, no. 9, pp. 2420–2432, 2010.

[46] C. K. Sao and P. W. Lehn, "Control and power management of converter fed microgrids," *IEEE Transactions on Power Systems*, vol. 23, no. 3, pp. 1088–1098, 2008.

[47] A. Abraham and S. Das, *Computational intelligence in power engineering*. Springer, 2010, vol. 302.

[48] K. Yu, Q. Ai, S. Wang, J. Ni, and T. Lv, "Analysis and optimization of droop controller for microgrid system based on small-signal dynamic model." *IEEE Trans. Smart Grid*, vol. 7, no. 2, pp. 695–705, 2016.

[49] I.-Y. Chung, W. Liu, D. A. Cartes, E. G. Collins, and S.-I. Moon, "Control methods of inverter-interfaced distributed generators in a microgrid system," *IEEE Trans. Ind. Appl*, vol. 46, no. 3, pp. 1078–1088, 2010.

[50] J. Alipoor, Y. Miura, and T. Ise, "Stability assessment and optimization methods for microgrid with multiple vsg units," *IEEE Transactions on Smart Grid*, vol. 9, no. 2, pp. 1462–1471, 2018.

[51] M. S. Shahriar, M. Shafiullah, M. A. Asif, M. M. Hasan, A. Ishaque, and I. Rajgir, "Comparison of invasive weed optimization (iwo) and particle swarm optimization (pso) in improving power system stability by upfc controller employing a multi-objective approach," in *1st International Conference on Advanced Information and Communication Technology 2016 (ICAICT 2016)*, 2016, pp. 1–7.

[52] A. Ahmed, M. M. H. Galib, S. M. K. Zaman, and G. Sarowar, "An optimization methodology of susceptance variation using lead-lag controller for grid connected fsig based wind generator system," *Journal of the Franklin Institute*, vol. 355, no. 1, pp. 197–217, 2018.

[53] M. Rasheduzzaman, J. A. Mueller, and J. W. Kimball, "An accurate small-signal model of inverter-dominated islanded microgrids using *dq* reference frame," *IEEE Journal of Emerging and Selected Topics in Power Electronics*, vol. 2, no. 4, pp. 1070–1080, 2014.

[54] N. M. Dehkordi, N. Sadati, and M. Hamzeh, "Distributed robust finite-time secondary voltage and frequency control of islanded microgrids," *IEEE Transactions on Power Systems*, vol. 32, no. 5, pp. 3648–3659, 2016.

[55] D. Photovoltaics and E. Storage, "Ieee standard for interconnection and interoperability of distributed energy resources with associated electric power systems interfaces," *IEEE Std*, pp. 1547–2018, 2018.

[56] Q. Sun, Q. Sun, and D. Qin, "Adaptive fuzzy droop control for optimized power sharing in an islanded microgrid," *Energies*, vol. 12, no. 1, p. 45, 2019.

[57] J. Ögren, "Pll design for inverter grid connection: Simulations for ideal and non-ideal grid conditions," 2010.

[58] H. Wang and W. Du, *Analysis and damping control of power system low-frequency oscillations*. Springer, 2016.

[59] T. Moller, R. Machiraju, K. Mueller, and R. Yagel, "Evaluation and design of filters using a taylor series expansion," *IEEE transactions on Visualization and Computer Graphics*, vol. 3, no. 2, pp. 184–199, 1997.

[60] K. Ogata, "Modern control engineering," *Instructor*, vol. 201709, 2017.

[61] J. A. Mueller and J. W. Kimball, "An efficient method of determining operating points of droop-controlled microgrids," *IEEE Transactions on Energy Conversion*, vol. 32, no. 4, pp. 1432–1446, 2017.

[62] P. Kundur, N. J. Balu, and M. G. Lauby, *Power system stability and control*. McGraw-hill New York, 1994, vol. 7.

[63] J. Machowski, J. Bialek, and J. Bumby, *Power system dynamics: stability and control*. John Wiley & Sons, 2011.

[64] Z.-F. Fu and J. He, *Modal analysis*. Elsevier, 2001.

[65] L. Davis, "Handbook of genetic algorithms," 1991.

[66] T. Zeugmann, P. Poupart, J. Kennedy, X. Jin, J. Han, L. Saitta, M. Sebag, J. Peters, J. Bagnell, W. Daelemans *et al.*, "Particle swarm optimization," pp. 760–766, 2011.

[67] C. Muro, R. Escobedo, L. Spector, and R. Coppinger, "Wolf-pack (canis lupus) hunting strategies emerge from simple rules in computational simulations," *Behavioural processes*, vol. 88, no. 3, pp. 192–197, 2011.

[68] A. Askarzadeh and A. Rezazadeh, "A new heuristic optimization algorithm for modeling of proton exchange membrane fuel cell: bird mating optimizer," *International Journal of Energy Research*, vol. 37, no. 10, pp. 1196–1204, 2013.

[69] E. K. Burke, G. Kendall *et al.*, *Search methodologies*. Springer, 2005.

[70] S. J. Wright, *Primal-dual interior-point methods*. Siam, 1997, vol. 54.

[71] F. Milano, "Psat: Power system analysis toolbox, version 2.0. 0-beta," 2007.

[72] A. Lipowski and D. Lipowska, "Roulette-wheel selection via stochastic acceptance," *Physica A: Statistical Mechanics and its Applications*, vol. 391, no. 6, pp. 2193–2196, 2012.

[73] C. Reeves, "Handbook of metaheuristics," pp. 55–82, 2003.

[74] A. R. Jordehi and J. Jasni, "Parameter selection in particle swarm optimisation: a survey," *Experimental and Theoretical Artificial Intelligence*, vol. 25, no. 4, pp. 527–542, 2013.

[75] S. Mirjalili, S. M. Mirjalili, and A. Lewis, "Grey wolf optimizer," *Advaces in Engineering Software*, vol. 69, no. 1, pp. 46–61, 2014.

[76] P. Good, *Permutation tests: a practical guide to resampling methods for testing hypotheses*. Springer Science & Business Media, 2013.

[77] J. A. Barber and S. G. Thompson, "Analysis of cost data in randomized trials: an application of the non-parametric bootstrap," *Statistics in medicine*, vol. 19, no. 23, pp. 3219–3236, 2000.

Appendix A

Matrices and Tables

A.1 Matrix expansion

$$\left[B_{filter}\right] = \begin{bmatrix} 0 & I_{Ld2_i} & 0 & I_{Ld4_i} & 0 & I_{Ld6_i} & 0 & I_{Ld14_i} & I_{Ld15_i}\cdots & \\ & 0 & 0 & 0 & 0 & & & & & \\ 0 & 0 & I_{Lq3_i} & 0 & I_{Lq5_i} & 0 & I_{Lq7_i} & I_{Lq14_i} & I_{Lq15_i}\cdots & \\ & 0 & 0 & 0 & 0 & & & & & \\ I_{od1_i} & 0 & 0 & 0 & 0 & 0 & 0 & I_{od14_i} & I_{od15_i} & I_{od16_i}\cdots \\ & I_{od17_i} & I_{od35_i} & I_{od36_i} & & & & & & \\ I_{oq1_i} & 0 & 0 & 0 & 0 & 0 & 0 & I_{oq14_i} & I_{oq15_i} & I_{oq16_i}\cdots \\ & I_{oq17_i} & I_{oq35_i} & I_{oq36_i} & & & & & & \\ V_{od1_i} & V_{od2_i} & 0 & V_{od4_i} & 0 & V_{od6_i} & 0 & V_{od14_i} & V_{od15_i} & V_{od16_i}\cdots \\ & V_{od17_i} & V_{od35_i} & V_{od36_i} & & & & & & \\ V_{oq1_i} & 0 & V_{oq3_i} & 0 & V_{oq5_i} & 0 & V_{oq7_i} & V_{oq14_i} & V_{oq15_i} & V_{oq16_i}\cdots \\ & V_{oq17_i} & V_{oq35_i} & V_{oq36_i} & & & & & & \end{bmatrix}$$

$I_{Ld2_i} = \frac{mK_{pcd}K_{pvd}}{L_f}$; $I_{Ld4_i} = \frac{K_{pcd}K_{ivd}}{L_f}$
$I_{Ld6_i} = \frac{K_{icd}}{L_f}$; $I_{Ld14_i} = K_{i,PLL}i_{lqi_0} + \frac{K_{pcd}K_{pvd}K_{i,PLL}}{L_f}$
$I_{Ld15_i} = -K_{p,PLL}i_{lqi_0} - \frac{K_{pcd}K_{pvd}K_{p,PLL}}{L_f}$; $I_{Lq3_i} = \frac{-nK_{pcq}K_{pvq}}{L_f}$
$I_{Lq5_i} = \frac{K_{pcq}K_{ivq}}{L_f}$; $I_{Lq7_i} = \frac{K_{icq}}{L_f}$
$I_{Lq14_i} = -K_{i,PLL}i_{ldi_0}$; $I_{Lq15_i} = K_{p,PLL}i_{ldi_0}$
$I_{od1_i} = \frac{V_{bD_0}\sin\delta_{i0} + V_{bQ_0}\cos\delta_{i0}}{L_c} - \frac{2r_N i_{oqi_0}}{L_c}$
$I_{od14_i} = K_{i,PLL}i_{oqi_0}$; $I_{od15_i} = -i_{oqi_0}K_{p,PLL}$; $I_{od16_i} = \frac{\cos\delta_{i0}r_N}{L_c}$
$I_{od17_i} = -\frac{\sin\delta_{i0}r_N}{L_c}$; $I_{od35_i} = -\frac{\cos\delta_{i0}r_N}{L_c}$; $I_{od36_i} = \frac{\sin\delta_{i0}r_N}{L_c}$
$I_{oq1_i} = \frac{-V_{bD_0}\cos\delta_{i0} - V_{bQ_0}\sin\delta_{i0}}{L_c} + \frac{2r_N i_{odi_0}}{L_c}$
$I_{oq14_i} = -K_{i,PLL}i_{odi_0}$; $I_{oq15_i} = i_{odi_0}K_{p,PLL}$; $I_{oq16_i} = \frac{\sin\delta_{i0}r_N}{L_c}$
$I_{oq17_i} = \frac{\cos\delta_{i0}r_N}{L_c}$; $I_{oq35_i} = -\frac{\sin\delta_{i0}r_N}{L_c}$; $I_{oq36_i} = -\frac{\cos\delta_{i0}r_N}{L_c}$

$V_{od1_i} = -R_d I_{od1_i};$
$V_{od2_i} = R_d I_{Ld2_i}; \quad V_{od4_i} = R_d I_{Ld4_i}$
$V_{od6_i} = R_d I_{Ld6_i}; \ V_{od8_i} = \frac{1}{C_f} + R_d I_{Ld8_i}; \ V_{od9_i} = R_d I_{Ld9_i}$
$V_{od10_i} = R_d(I_{Ld10_i} - I_{od10_i}); \quad V_{od11_i} = \omega_{PLL}; \quad V_{od12_i} = -\frac{1}{C_f} - R_d I_{od12_i}$
$V_{od13_i} = -R_d I_{od13_i}; \ V_{od14_i} = R_d(I_{Ld14_i} - I_{od14_i}) + V_{oq_i} K_{i,PLL}$
$V_{od15_i} = R_d(I_{Ld15_i} - I_{od15_i}) - V_{oq_i} K_{p,PLL}; \quad V_{od16_i} = -R_d I_{od16_i}$
$V_{od17_i} = -R_d I_{od17_i}; \ V_{od35_i} = -R_d I_{od35_i}; \quad V_{od36_i} = -R_d I_{od36_i}$
$V_{oq1_i} = -R_d I_{oq1_i}; \quad V_{oq3_i} = R_d I_{Lq3_i}; \quad V_{oq5_i} = R_d I_{Lq5_i}$
$V_{oq7_i} = R_d I_{Lq7_i}; \quad V_{oq8_i} = R_d I_{Lq8_i}; \quad V_{oq9_i} = \frac{1}{C_f} + R_d I_{Lq9_i}$
$V_{oq10_i} = -\omega_{PLL} \ ; V_{oq11_i} = R_d(I_{Lq11_i} - I_{oq11_i}); \quad V_{oq12_i} = -R_d I_{oq12_i}$
$V_{oq13_i} = -\frac{1}{C_f} - R_d I_{oq13_i}; \quad V_{oq14_i} = R_d(I_{Lq14_i} - I_{oq14_i}) - V_{od_i} K_{i,PLL}$
$V_{oq15_i} = R_d(I_{Lq15_i} - I_{oq15_i}) + V_{od_i} K_{p,PLL}; \quad V_{oq16_i} = -R_d I_{oq16_i}$
$V_{oq17_i} = -R_d I_{oq17_i}; \quad V_{oq35_i} = -R_d I_{oq35_i}; \ V_{oq36_i} = -R_d I_{oq36_i}$

$$\left[B_{line}\right] \quad = \quad \begin{bmatrix} IND1 & IND2 & IND3 & IND4 & IND5 & IND6 & IND7 & IND8... \\ & IND9 & 0 & IND11 & 0 & & & \\ INQ1 & INQ2 & INQ3 & INQ4 & INQ5 & INQ6 & INQ7 & INQ8... \\ & 0 & INQ10 & 0 & INQ12 & & & \end{bmatrix}$$

$IND1 = -\frac{r_N(i_{odi_0}\sin\delta_{i0} + i_{oqi_0}\cos\delta_{i0})}{L_{line,ij}}$
$IND2 = -\frac{r_N(i_{odj_0}\sin\delta_{j0} - i_{oqj_0}\cos\delta_{j0})}{L_{line,ij}}$
$IND3 = \frac{r_N\cos\delta_{i0}}{L_{line,ij}}; \quad IND4 = \frac{r_N\sin\delta_{i0}}{L_{line,ij}}$
$IND5 = -\frac{r_N\cos\delta_{j0}}{L_{line,ij}}; \quad IND6 = -\frac{r_N\sin\delta_{j0}}{L_{line,ij}}$
$IND7 = K_{i,PLL} i_{lineQ,ij_0}; \quad IND8 = -K_{p,PLL} i_{lineQ,ij_0}$
$IND9 = -\frac{r_N}{L_{line,ij}} \ ; \quad IND11 = \frac{r_N}{L_{line,ij}}$
$INQ1 = -\frac{r_N(i_{odi_0}\cos\delta_{i0} + i_{oqi_0}\sin\delta_{i0})}{L_{line,ij}}$
$INQ2 = \frac{r_N(i_{odj_0}\cos\delta_{j0} + i_{oqj_0}\sin\delta_{j0})}{L_{line,ij}}$
$INQ3 = -\frac{r_N\sin\delta_{i0}}{L_{line,ij}}; \ INQ4 = \frac{r_N\cos\delta_{i0}}{L_{line,ij}}$
$INQ5 = \frac{r_N\sin\delta_{j0}}{L_{line,ij}}; \ INQ6 = -\frac{r_N\cos\delta_{j0}}{L_{line,ij}}$
$INQ7 = -K_{i,PLL} i_{lineD,ij_0}; \quad INQ8 = K_{p,PLL} i_{lineD,ij_0}$
$INQ10 = -\frac{r_N}{L_{line,ij}}; \quad INQ12 = \frac{r_N}{L_{line,ij}}$

A.1.1 A_{system} Expansion

Combined system model:

$$A_{System} = \begin{bmatrix} A_{Inverter} + B_{Inverter}A_{rN}C_{Inverterc} & B_{Inverter}C_{rN} & B_{Inverter}B_{rN} \\ B_{load}A_{rN}C_{Inverterc} + C_{load}D_{Inverter\omega} & B_{load}C_{rN} + A_{load} & B_{rN} \\ B_{line}A_{rN}C_{Inverterc} + C_{line}D_{Inverter\omega} & B_{line}C_{rN} & A_{line} + B_{line}B_{rN} \end{bmatrix}_{36x36}$$

$$A_{Inverter} = \begin{bmatrix} A_{Inv1} & 0 \\ C_{delta1} & A_{Inv2} - C_{delta2} \end{bmatrix}_{30x30}; B_{Inverter} = \begin{bmatrix} B_{Inv1} & 0 \\ 0 & B_{Inv2} \end{bmatrix}_{30x4}$$

$$C_{Inverterc} = \begin{bmatrix} D_{Invc1} & 0 \\ 0 & D_{Invc2} \end{bmatrix}_{4x30}; D_{Inverter\omega} = \begin{bmatrix} E_{Inv\omega1} & E_{Inv\omega2} \end{bmatrix}_{1x30}$$

Inverter:

$$A_{Invi} = \begin{bmatrix} 0 & 0 & 0 & 0... & \\ & 0 & 0 & & \\ 0 & A_{POi} & 0 & 0... & \\ & B_{PQi} & 0 & & \\ 0 & A_{vci}A_{droopi} & 0 & 0... & \\ & B_{vci} & C_{vci}B_{\omega plli} & & \\ 0 & A_{cci}E_{vci}A_{vci}A_{droopi} & A_{cci}D_{vci} & 0... & \\ & A_{cci}E_{vci}B_{vci} + B_{cci} & A_{cci}E_{vci}C_{vci}B_{\omega plli} & & \\ C_{LCL}T_v & B_{LCLi}D_{cci}A_{cci}E_{vci}A_{vci}A_{droopi} & B_{LCLi}D_{cci}A_{cci}D_{vci} & B_{LCLi}C_{cci}... & \\ & A_{LCLi} + B_{LCLi}E_{cci} + B_{LCLi} & D_{LCLi}B_{\omega plli} + B_{LCLi} & & \\ & D_{cci}(A_{cci}E_{cci}B_{vci} + B_{cci}) & D_{cci}A_{cci}E_{vci}C_{vci}B_{\omega plli} & & \\ 0 & 0 & 0 & 0 & ... \\ A_{PLLi} & B_{PLLi} & & & \end{bmatrix}_{15x15}$$

$$B_{Invi} = \begin{bmatrix} 0 & 0 \\ . & . \\ . & . \\ C_{LCLi}T_S^{-1} & \\ 0 & 0 \\ 0 & 0 \end{bmatrix}_{15x2} ; C_{deltai} = \begin{bmatrix} 0 & . & . & . & k_{i,PLL} & -k_{p,PLL} \\ . & . & . & . & . & 0 \\ . & . & . & . & . & 0 \\ 0 & . & . & . & . & 0 \end{bmatrix}_{15x15}$$

$$D_{Invci} = \begin{bmatrix} T_C & 0 & . & T_S & 0 & 0 \\ 0 & . & . & . & . & 0 \end{bmatrix}_{2x15} ; E_{Inv\omega i} = \begin{bmatrix} 0 & . & . & B_{\omega plli} \end{bmatrix}_{1x15} for \text{i} = 1$$

$$\text{and} E_{Inv\omega i} = \begin{bmatrix} 0 & . & . & 0 \end{bmatrix}_{1x15} \text{fori} \neq 1$$

Virtual resistor:

$$A_{rN} = \begin{bmatrix} r_N & 0 & 0 & 0 \\ 0 & r_N & 0 & 0 \\ 0 & 0 & r_N & 0 \\ 0 & 0 & 0 & r_N \end{bmatrix} ; B_{rN} = \begin{bmatrix} r_N & 0 \\ 0 & r_N \end{bmatrix} ; C_{rN} = \begin{bmatrix} -r_N & 0 & 0 & 0 \\ 0 & -r_N & 0 & 0 \\ 0 & 0 & -r_N & 0 \\ 0 & 0 & 0 & -r_N \end{bmatrix}$$

Line:

$$A_{line} = \begin{bmatrix} \frac{r_{line}}{L_{line}} & \omega_{PLL} \\ -\omega_{PLL} & \frac{r_{line}}{L_{line}} \end{bmatrix} ; B_{line} = \begin{bmatrix} 1 & 0 & -1 & 0 \\ 0 & 1 & 0 & -1 \end{bmatrix} ; C_{line} = \begin{bmatrix} I_{lineQij} \\ -I_{lineDij} \end{bmatrix}$$

Load:

$$A_{load} = \begin{bmatrix} -\frac{R_{load1}}{L_{load1}} & \omega_{PLL} & 0 & 0 \\ -\omega_{PLL} & -\frac{R_{load1}}{L_{load1}} & 0 & 0 \\ 0 & 0 & -\frac{R_{load2}}{L_{load2}} & \omega_{PLL} \\ 0 & 0 & -\omega_{PLL} & -\frac{R_{load2}}{L_{load2}} \end{bmatrix} ;$$

$$B_{load} = \begin{bmatrix} \frac{1}{L_{load1}} & 0 & 0 & 0 \\ 0 & \frac{1}{L_{load1}} & 0 & 0 \\ 0 & 0 & \frac{1}{L_{load2}} & 0 \\ 0 & 0 & 0 & \frac{1}{L_{load2}} \end{bmatrix} ; C_{load} = \begin{bmatrix} I_{loadQ1} \\ -I_{loadD2} \\ I_{loadQ2} \\ -I_{loadD2} \end{bmatrix}$$

Reference frame transformation:

$$T_S = \begin{bmatrix} \cos\theta & \sin\theta \\ -\sin\theta & \cos\theta \end{bmatrix}; T_C = \begin{bmatrix} -I_{od}\sin\theta + I_{oq}\cos\theta \\ -I_{od}\cos\theta - I_{oq}\sin\theta \end{bmatrix}; T_V = \begin{bmatrix} -V_{bD}\sin\theta - V_{bQ}\cos\theta \\ V_{bD}\cos\theta - V_{bQ}\sin\theta \end{bmatrix}$$

Filter:

$$A_{LCL} = \begin{bmatrix} -\frac{r_f}{L_f} & \omega_{PLL} & 0 & 0 & -\frac{1}{L_f} & 0 \\ -\omega_{PLL} & -\frac{r_f}{L_f} & 0 & 0 & 0 & -\frac{1}{L_f} \\ 0 & 0 & -\frac{r_c}{L_c} & \omega_{PLL} & \frac{1}{L_c} & 0 \\ 0 & 0 & -\omega_{PLL} & -\frac{r_c}{L_c} & 0 & \frac{1}{L_c} \\ \frac{1}{C_f} - \frac{r_f R_d}{L_f} & R_d\omega_{PLL} & -\frac{1}{C_f} + \frac{r_c R_d}{L_C} & R_d\omega_{PLL} & -R_d(\frac{1}{L_c} + \frac{1}{L_f}) & \omega_{PLL} \\ -R_d\omega_{PLL} & \frac{1}{C_f} - \frac{r_f R_d}{L_f} & R_d\omega_{PLL} & -\frac{1}{C_f} + \frac{r_c R_d}{L_C} & -\omega_{PLL} & -R_d(\frac{1}{L_c} + \frac{1}{L_f}) \end{bmatrix};$$

$$B_{LCL} = \begin{bmatrix} \frac{1}{L_f} & 0 \\ 0 & \frac{1}{L_f} \\ 0 & 0 \\ 0 & 0 \\ \frac{R_d}{L_f} & 0 \\ 0 & \frac{R_d}{L_f} \end{bmatrix}; D_{LCL} = \begin{bmatrix} i_{lqi} \\ -i_{ldi} \\ i_{oqi} \\ -i_{odi} \\ v_{oqi} + R_d i_{lqi} - R_d i_{oqi} \\ -v_{odi} - R_d i_{ldi} + R_d i_{odi} \end{bmatrix}; C_{LCL} = \begin{bmatrix} 0 & 0 \\ 0 & 0 \\ -\frac{1}{L_c} & 0 \\ 0 & -\frac{1}{L_c} \\ \frac{R_d}{L_c} & 0 \\ 0 & \frac{R_d}{L_c} \end{bmatrix};$$

Current Controller:

$$A_{CC} = \begin{bmatrix} 1 & 0 \\ 0 & 1 \end{bmatrix}; B_{CC} = \begin{bmatrix} -1 & 0 & 0 & 0 & 0 & 0 \\ 0 & -1 & 0 & 0 & 0 & 0 \end{bmatrix}$$

$$C_{CC} = \begin{bmatrix} k_{ic,d} & 0 \\ 0 & k_{ic,q} \end{bmatrix}; D_{CC} = \begin{bmatrix} k_{pc,d} & 0 \\ 0 & k_{pc,q} \end{bmatrix}; E_{CC} = \begin{bmatrix} 0 & -\omega_n L_f & 0 & 0 & 0 & 0 \\ \omega_n L_f & 0 & 0 & 0 & 0 & 0 \end{bmatrix}$$

Voltage Controller:

$$A_{VC} = \begin{bmatrix} -1 & 0 & 0 \\ 0 & 0 & -1 \end{bmatrix}; B_{VC} = \begin{bmatrix} 0 & 0 & 0 & 0 & 0 & 0 \\ 0 & 0 & 0 & 0 & 0 & -1 \end{bmatrix}; C_{VC} = \begin{bmatrix} 1 \\ 0 \end{bmatrix}$$

$$D_{VC} = \begin{bmatrix} k_{iv,d} & 0 \\ 0 & k_{iv,q} \end{bmatrix}; E_{VC} = \begin{bmatrix} k_{pv,d} & 0 \\ 0 & k_{pv,q} \end{bmatrix}$$

Phase locked loop:

$$A_{PLL} = \begin{bmatrix} 0 & 0 & 0 & 0 & 0 & 0 \\ 0 & 0 & 0 & 0 & \omega_{c,PLL} & 0 \end{bmatrix}; B_{PLL} = \begin{bmatrix} 0 & -1 \\ 0 & -\omega_{c,PLL} \end{bmatrix}; B_{\omega pll} = \begin{bmatrix} k_{i,PLL} & -k_{p,PLL} \end{bmatrix}$$

Power controller:

$$A_{PQi} = \begin{bmatrix} -\omega_c & 0 \\ 0 & -\omega_c \end{bmatrix}; B_{PQi} = 1.5\omega_c \begin{bmatrix} 0 & 0 & v_{odi} & v_{oqi} & i_{odi} & i_{oqi} \\ 0 & 0 & v_{oqi} & -v_{odi} & -i_{oqi} & i_{odi} \end{bmatrix}$$

Droop equations:

$$A_{\omega i} = \begin{bmatrix} -m & 0 \end{bmatrix}; B_{vi} = \begin{bmatrix} 0 & 0 \\ 0 & -n \end{bmatrix}; A_{droop} = \begin{bmatrix} -m & 0 \\ 0 & 0 \\ 0 & -n \end{bmatrix}$$

A.2 System parameters and operating point

Table A.1: System parameters

Parameter	value	Parameter	value
ω_c	50.26 rad/s	ω_n	377 rad/s
$\omega_{c,PLL}$	7853.98 rad/s	ω_{PLL}	377 rad/s
$V_{oq,n}$	85 V	r_n	1000 Ω
m	0.001	n	0.001
L_c	0.5 mH	r_c	0.09 Ω
C_f	15 μF	R_d	2.025 Ω
L_f	4.20 mH	r_f	0.5 Ω
r_{line}	0.15 Ω	L_{line}	0.4 mH
R_{load1}	25 Ω	L_{load1}	15 mH
R_{load2}	25 Ω	L_{load2}	15 mH
$k_{pv,d}$	0.5	$k_{pv,q}$	0.5
$k_{iv,d}$	25	$k_{iv,q}$	25
$k_{pc,d}$	1	$k_{pc,q}$	1
$k_{ic,d}$	100	$k_{ic,q}$	100
$k_{p,PLL}$	0.25	$k_{i,PLL}$	2

Table A.2: Steady state operating point

Parameter	value	Parameter	value
δ_1	0 rad	δ_2	0.0003 rad
P_1	427.9548 W	P_2	427.9548 W
Q_1	75.9562 VAR	Q_2	7.5445 VAR
ϕ_{d1}	0.0047 rad-s	ϕ_{d2}	0.0030 rad-s
ϕ_{q1}	0.1344 V-s	ϕ_{q2}	0.1344 V-s
γ_{d1}	0.0006 A-s	γ_{d2}	0.0004 A-s
γ_{q1}	0.8660 A-s	γ_{q2}	0.8661 A-s
i_{ld1}	0.1166 A	i_{ld2}	0.074 A
i_{lq1}	3.3595 A	i_{lq2}	3.3593 A
i_{od1}	0.5963 A	i_{od2}	0.5537 A
i_{oq1}	3.3595 A	i_{oq2}	3.3593 A
v_{od1}	0 V	v_{od2}	0 V
v_{oq1}	84.924 V	v_{oq2}	84.9295 V